

FIGURE 4.4.15

THIS FIGURE INTENTIONALLY DELETED.

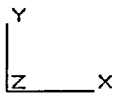
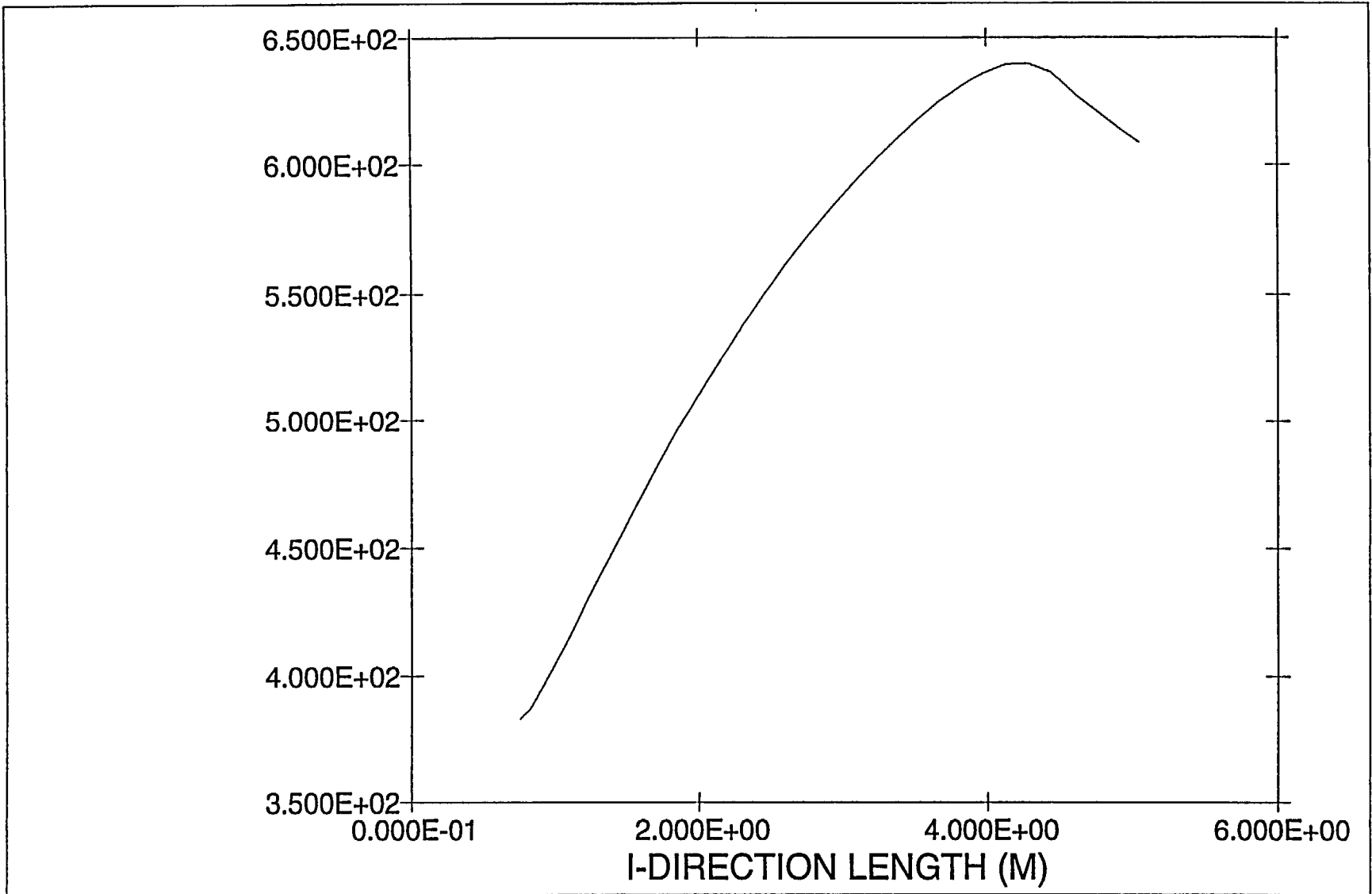


FIGURE 4.4.16: MPC-24 Peak Rod Axial Temperature Profile

Aug 22 2000
Fluent 4.48
Fluent Inc.

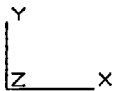
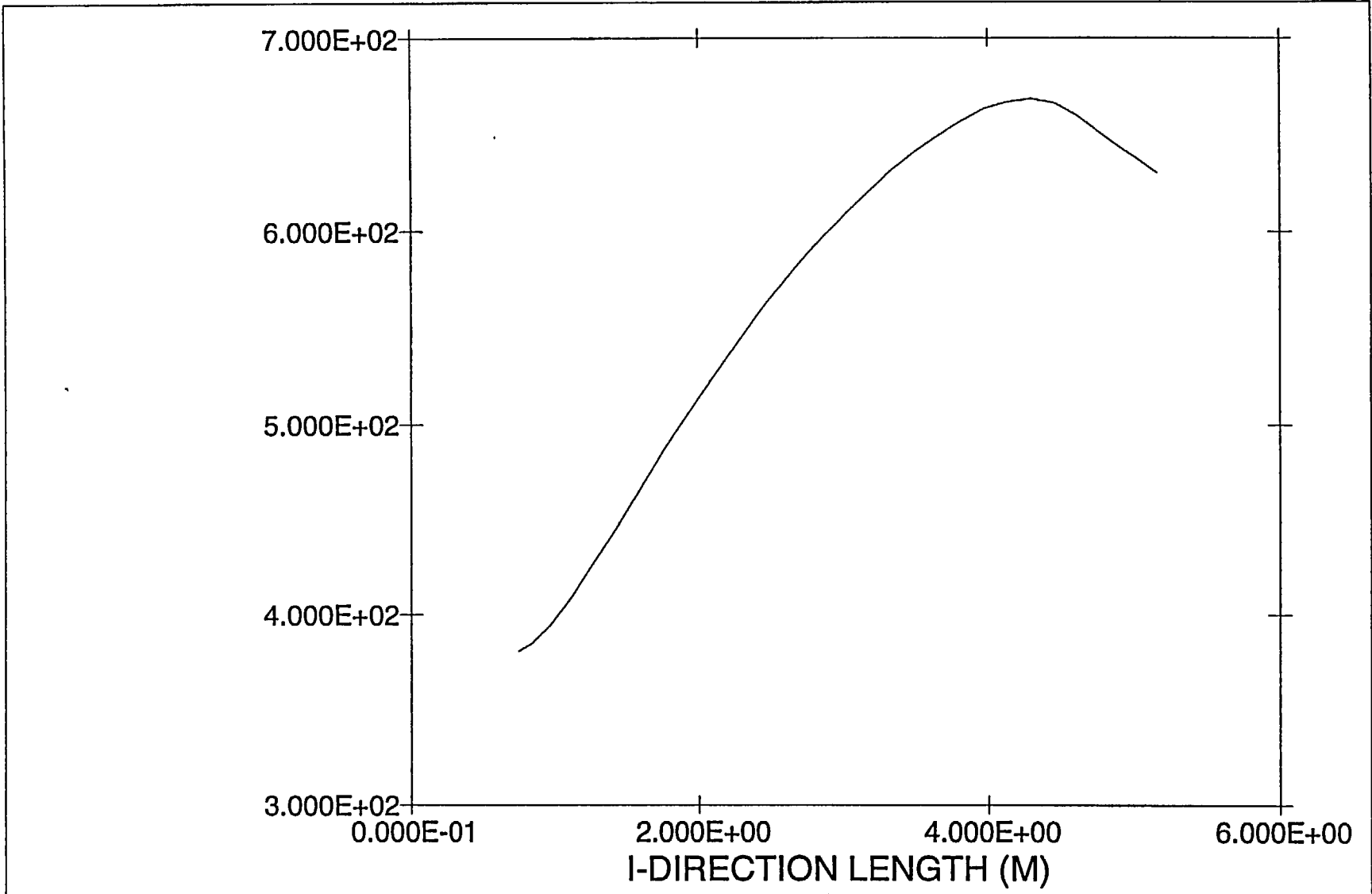


FIGURE 4.4.17: MPC-68 Peak Rod Axial Temperature Profile

Aug 22 2000

Fluent 4.48

Fluent Inc.

FIGURE 4.4.18

THIS FIGURE INTENTIONALLY DELETED.

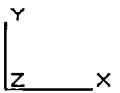
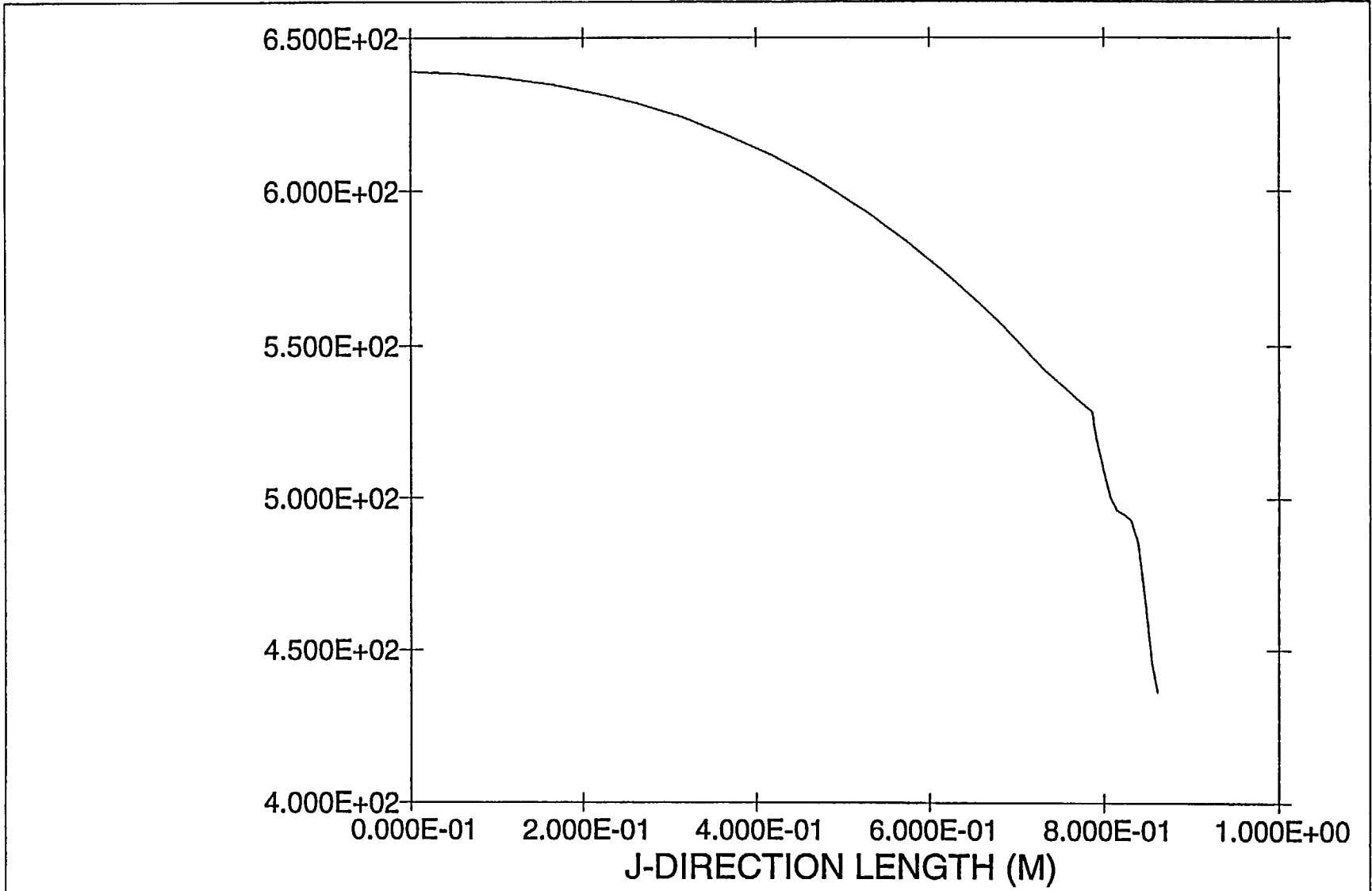


FIGURE 4.4.19: MPC-24 Radial Temperature Profile
(Hottest Basket Cross-Section)

Aug 23 2000
Fluent 4.48
Fluent Inc.

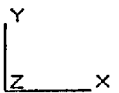
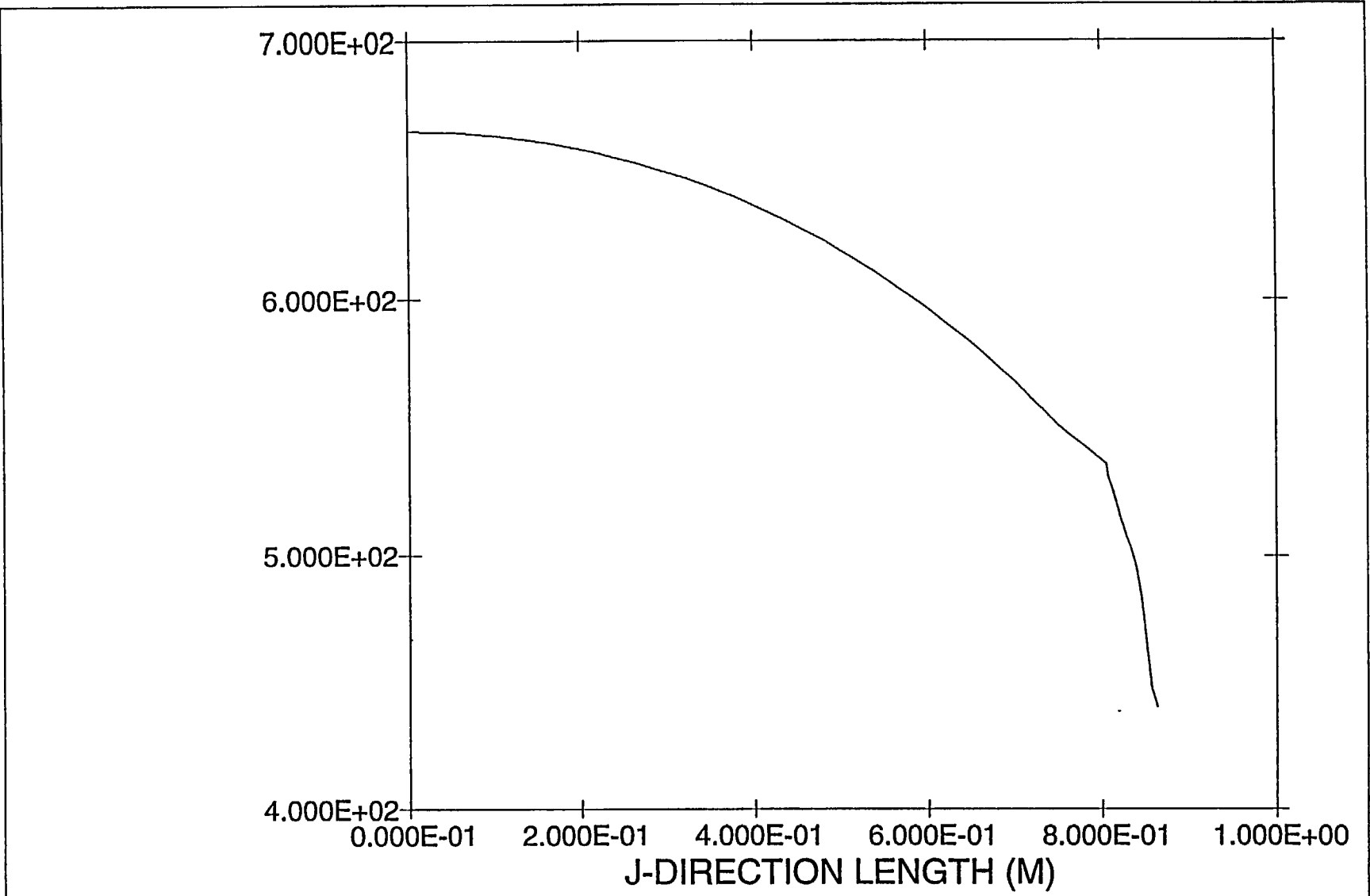


FIGURE 4.4.20: MPC-68 Radial Temperature Profile
(Hottest Basket Cross-section)

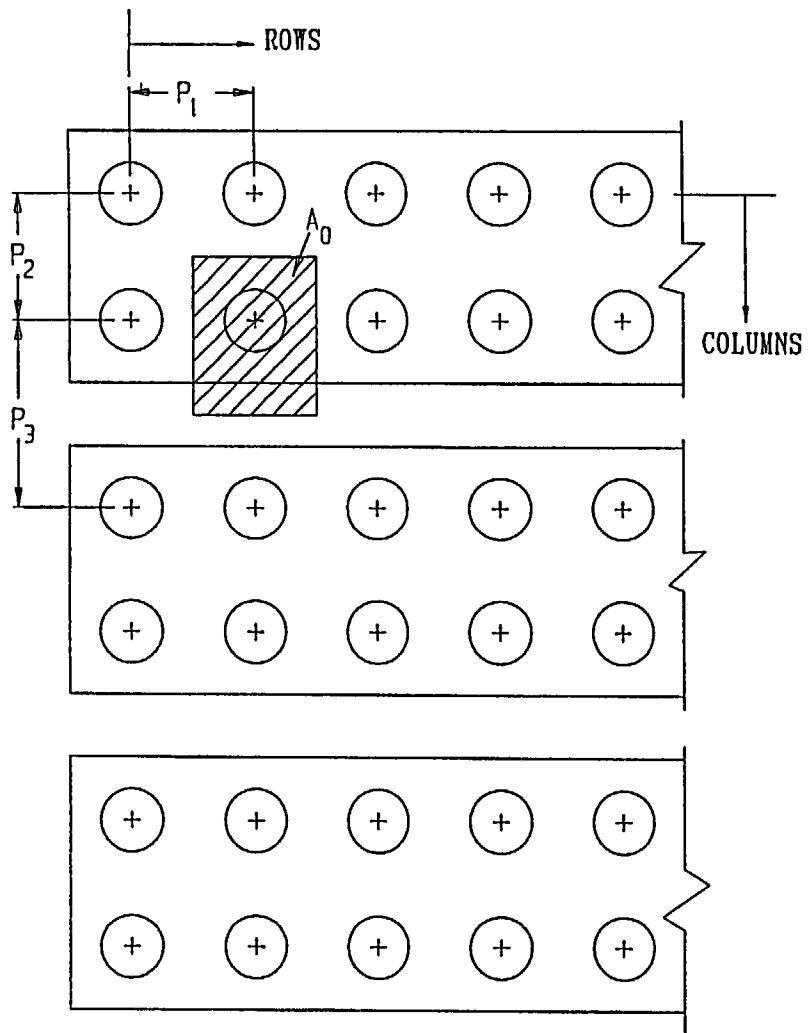
Aug 23 2000
Fluent 4.48
Fluent Inc.

FIGURE 4.4.21

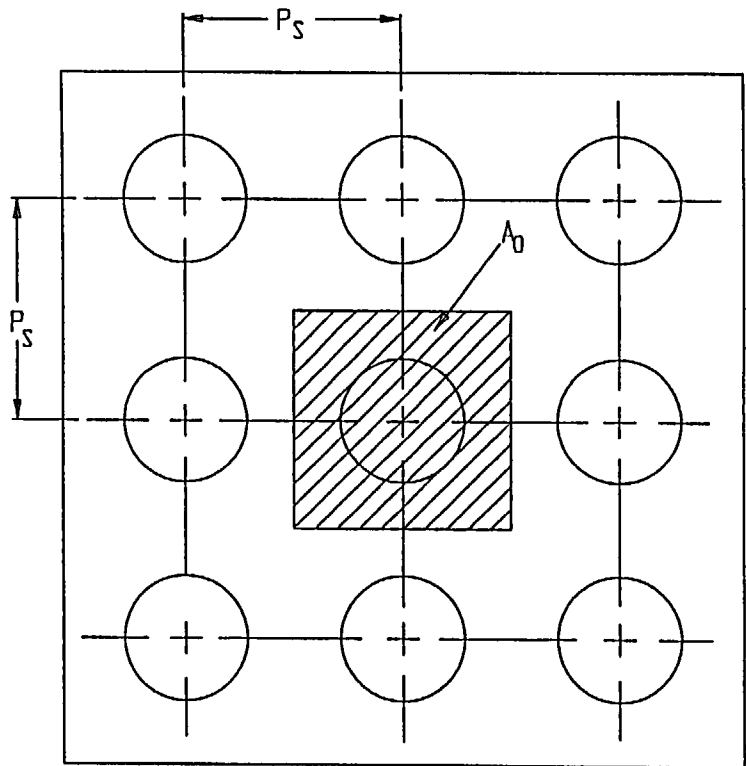
THIS FIGURE INTENTIONALLY DELETED.

FIGURE 4.4.22
INTENTIONALLY DELETED

FIGURE 4.4.23
INTENTIONALLY DELETED



CASE (i) LAYOUT ON A RECTANGULAR PITCH



CASE (ii) LAYOUT ON A SQUARE PITCH

LEGEND:
 $A_0 = P_1 \times (P_2 + P_3) / 2$ CASE (i)
 $A_0 = P_s \times P_s$ CASE (ii)

FIGURE 4.4.24; ILLUSTRATION OF MINIMUM AVAILABLE PLANAR AREA PER HI-STORM MODULE AT AN ISFSI.

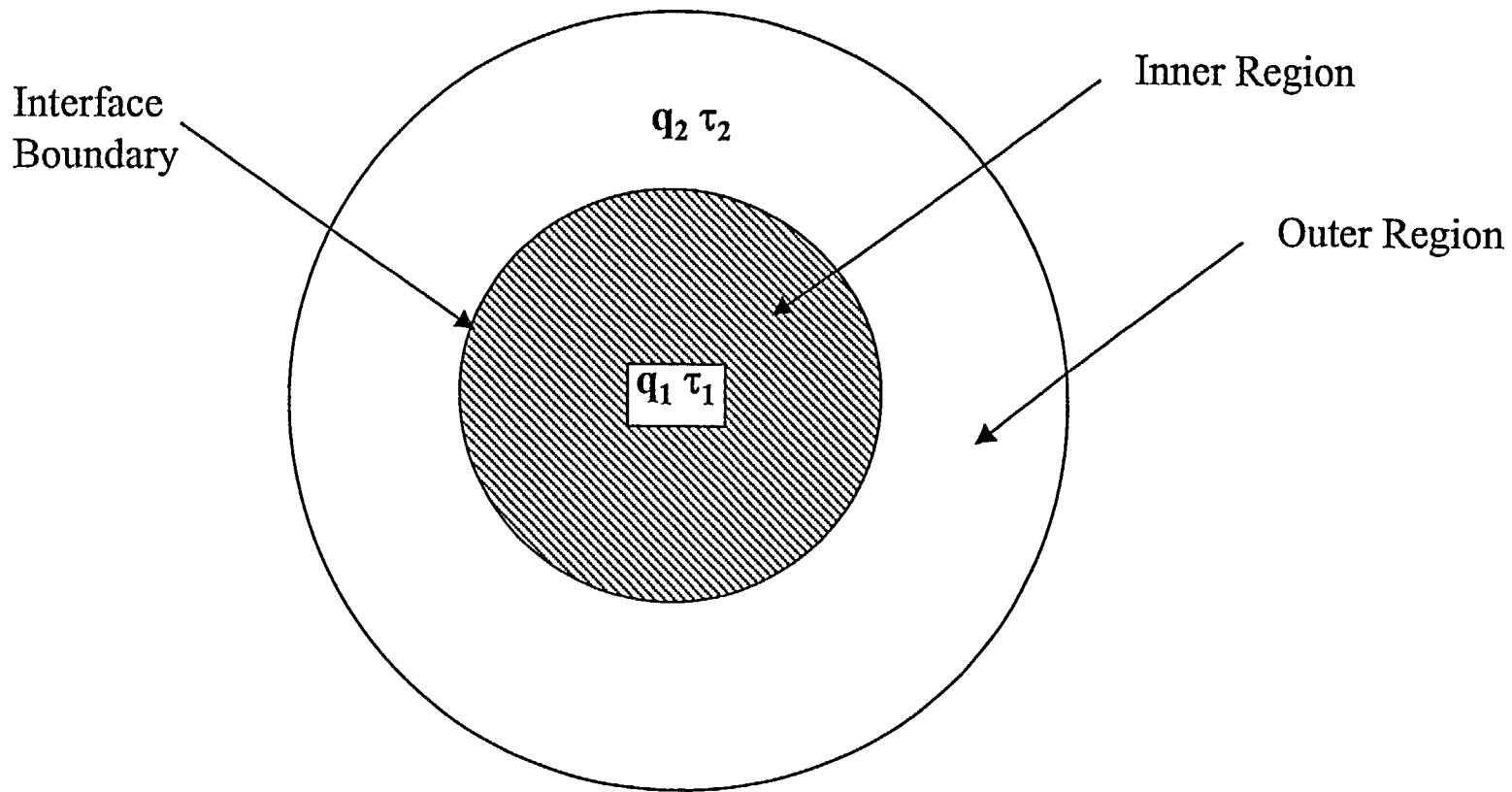


FIGURE 4.4.25: FUEL BASKET REGIONALIZED LOADING SCENARIO

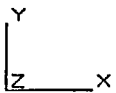
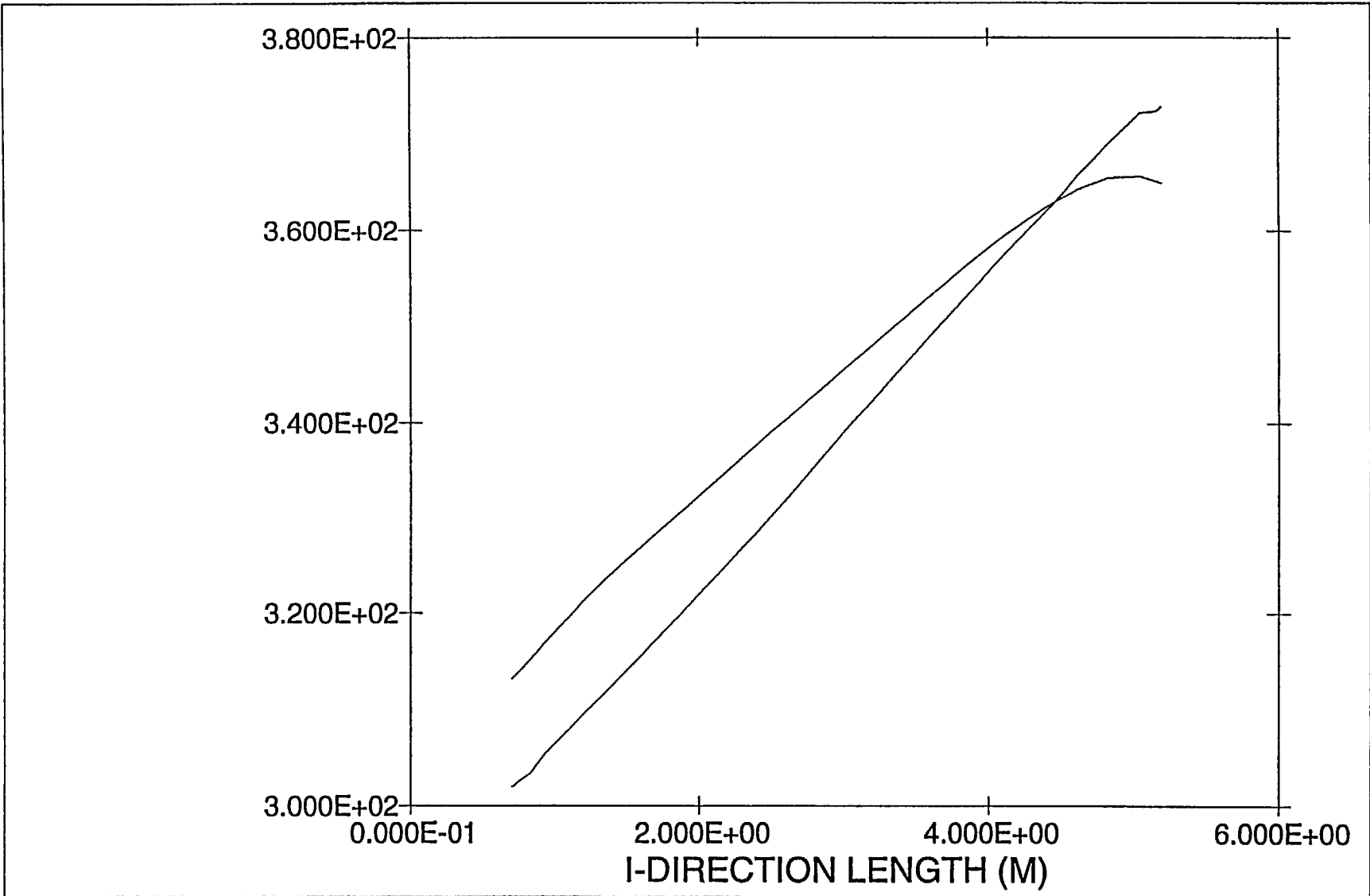


FIGURE 4.4.26: Bounding Overpack Annulus Axial Profiles

Aug 23 2000
Fluent 4.48
Fluent Inc.

4.5 THERMAL EVALUATION FOR NORMAL HANDLING AND ONSITE TRANSPORT

Prior to placement in a HI-STORM overpack, an MPC must be loaded with fuel, outfitted with closures, dewatered, vacuum dried, backfilled with helium and transported to the HI-STORM module. In the unlikely event that the fuel needs to be returned to the spent fuel pool, these steps must be performed in reverse. Finally, if required, transfer of a loaded MPC between HI-STORM overpacks or between a HI-STAR transport overpack and a HI-STORM storage overpack must be carried out in an assuredly safe manner. All of the above operations are short duration events that would likely occur no more than once or twice for an individual MPC.

The device central to all of the above operations is the HI-TRAC transfer cask that, as stated in Chapter 1, is available in two anatomically identical weight ratings (100- and 125-ton). The HI-TRAC transfer cask is a short-term host for the MPC; therefore it is necessary to establish that, during all thermally challenging operation events involving either the 100-ton or 125-ton HI-TRAC, the permissible temperature limits presented in Section 4.3 are not exceeded. The following discrete thermal scenarios, all of short duration, involving the HI-TRAC transfer cask have been identified as warranting thermal analysis.

- i. Normal Onsite Transport
- ii. MPC Cavity Vacuum Drying
- iii. Post-Loading Wet Transfer Operations
- iv. MPC Cooldown and Reflood for Unloading Operations

The above listed conditions are described and evaluated in the following subsections. Subsection 4.5.1 describes the individual analytical models used to evaluate these conditions. Due to the simplicity of the conservative evaluation of wet transfer operations, Subsection 4.5.1.1.5 includes both the analysis model and analysis results discussions. The maximum temperature analyses for onsite transport and vacuum drying are discussed in Subsection 4.5.2. Subsections 4.5.3, 4.5.4 and 4.5.5, respectively, discuss minimum temperature, MPC maximum internal pressure and thermal data for stress analyses during onsite transport.

4.5.1 Thermal Model

The HI-TRAC transfer cask is used to load and unload the HI-STORM concrete storage overpack, including onsite transport of the MPCs from the loading facility to an ISFSI pad. Section views of the HI-TRAC have been presented in Chapter 1. Within a loaded HI-TRAC, heat generated in the MPC is transported from the contained fuel assemblies to the MPC shell in the manner described in Section 4.4. From the outer surface of the MPC to the ambient air, heat is transported by a combination of conduction, thermal radiation and natural convection. It has been demonstrated in Section 4.3 that from a thermal standpoint, storage of stainless steel clad fuel assemblies is bounded by storage of zircaloy clad fuel assemblies. Thus, only zircaloy clad fuel assemblies shall be considered in the HI-TRAC thermal performance evaluations. Analytical modeling details of all the various thermal transport mechanisms are provided in the following subsection.

Two HI-TRAC transfer cask designs, namely, the 125-ton and the 100-ton versions, are developed for onsite handling and transport, as discussed in Chapter 1. The two designs are principally different in terms of lead thickness and the thickness of radial connectors in the water jacket region. The analytical model developed for HI-TRAC thermal characterization conservatively accounts for these differences by applying the higher shell thickness and thinner radial connectors' thickness to the model. In this manner, the HI-TRAC overpack resistance to heat transfer is overestimated, resulting in higher predicted MPC internals and fuel cladding temperature levels.

4.5.1.1 Analytical Model

From the outer surface of the MPC to the ambient atmosphere, heat is transported within HI-TRAC through multiple concentric layers of air, steel and shielding materials. Heat must be transported across a total of six concentric layers, representing the air gap, the HI-TRAC inner shell, the lead shielding, the HI-TRAC outer shell, the water jacket and the enclosure shell. From the surface of the enclosure shell heat is rejected to the atmosphere by natural convection and radiation.

A small diametral air gap exists between the outer surface of the MPC and the inner surface of the HI-TRAC overpack. Heat is transported across this gap by the parallel mechanisms of conduction and thermal radiation. Assuming that the MPC is centered and does not contact the transfer overpack walls conservatively minimizes heat transport across this gap. Additionally, thermal expansion that would minimize the gap is conservatively neglected. Heat is transported through the cylindrical wall of the HI-TRAC transfer overpack by conduction through successive layers of steel, lead and steel. A water jacket, which provides neutron shielding for the HI-TRAC overpack, surrounds the cylindrical steel wall. The water jacket is composed of carbon steel channels with welded, connecting enclosure plates. Conduction heat transfer occurs through both the water cavities and the channels. While the water jacket channels are sufficiently large for natural convection loops to form, this mechanism is conservatively neglected. Heat is passively rejected to the ambient from the outer surface of the HI-TRAC transfer overpack by natural convection and thermal radiation.

In the vertical position, the bottom face of the HI-TRAC is in contact with a supporting surface. This face is conservatively modeled as an insulated surface. Because the HI-TRAC is not used for long-term storage in an array, radiative blocking does not need to be considered. The HI-TRAC top lid is modeled as a surface with convection, radiative heat exchange with air and a constant maximum incident solar heat flux load. Insolation on cylindrical surfaces is conservatively based on 12-hour levels prescribed in 10CFR71 averaged on a 24-hour basis. Concise descriptions of these models are given below.

4.5.1.1.1 Effective Thermal Conductivity of Water Jacket

The 125-ton HI-TRAC water jacket is composed of fourteen formed channels equispaced along the circumference of the HI-TRAC and welded along their length to the HI-TRAC outer shell. Enclosure plates are welded to these channels, creating twenty-eight water compartments. The 100-ton HI-TRAC water jacket has 15 formed channels and enclosure plates creating thirty compartments. Holes in the channel legs connect all the individual compartments in the water jacket. Thus, the annular region between the HI-TRAC outer shell and the enclosure shell can be considered as an array of steel ribs and water spaces.

The effective radial thermal conductivity of this array of steel ribs and water spaces is determined by combining the heat transfer resistance of individual components in a parallel network. A bounding calculation is assured by using the minimum number of channels and channel thickness as input values. The thermal conductivity of the parallel steel ribs and water spaces is given by the following formula:

$$K_{ne} = \frac{K_r N_r t_r \ln \left(\frac{r_o}{r_i} \right)}{2\pi L_R} + \frac{K_w N_r t_w \ln \left(\frac{r_o}{r_i} \right)}{2\pi L_R}$$

where:

- K_{ne} = effective radial thermal conductivity of water jacket
- r_i = inner radius of water spaces
- r_o = outer radius of water spaces
- K_r = thermal conductivity of carbon steel ribs
- N_r = minimum number of channel legs (equal to number of water spaces)
- t_r = minimum (nominal) rib thickness (lower of 125-ton and 100-ton designs)
- L_R = effective radial heat transport length through water spaces
- K_w = thermal conductivity of water
- t_w = water space width (between two carbon steel ribs)

Figure 4.5.1 depicts the resistance network to combine the resistances to determine an effective conductivity of the water jacket. The effective thermal conductivity is computed in the manner of the foregoing, and is provided in Table 4.5.1.

4.5.1.1.2 Heat Rejection from Overpack Exterior Surfaces

The following relationship for the surface heat flux from the outer surface of an isolated cask to the environment applied to the thermal model:

$$q_s = 0.19 (T_s - T_A)^{4/3} + 0.1714 \left[\left(\frac{T_s + 460}{100} \right)^4 - \left(\frac{T_A + 460}{100} \right)^4 \right]$$

where:

- T_S = cask surface temperatures ($^{\circ}\text{F}$)
- T_A = ambient atmospheric temperature ($^{\circ}\text{F}$)
- q_s = surface heat flux ($\text{Btu}/\text{ft}^2 \times \text{hr}$)
- ϵ = surface emissivity

The second term in this equation is the Stefan-Boltzmann formula for thermal radiation from an exposed surface to ambient. The first term is the natural convection heat transfer correlation recommended by Jacob and Hawkins [4.2.9]. This correlation is appropriate for turbulent natural convection from vertical surfaces, such as the vertical overpack wall. Although the ambient air is conservatively assumed to be quiescent, the natural convection is nevertheless turbulent.

Turbulent natural convection correlations are suitable for use when the product of the Grashof and Prandtl ($\text{Gr} \times \text{Pr}$) numbers exceeds 10^9 . This product can be expressed as $L^3 \times \Delta T \times Z$, where L is the characteristic length, ΔT is the surface-to-ambient temperature difference, and Z is a function of the surface temperature. The characteristic length of a vertically oriented HI-TRAC is its height of approximately 17 feet. The value of Z , conservatively taken at a surface temperature of 340°F , is 2.6×10^5 . Solving for the value of ΔT that satisfies the equivalence $L^3 \times \Delta T \times Z = 10^9$ yields $\Delta T = 0.78^{\circ}\text{F}$. For a horizontally oriented HI-TRAC the characteristic length is the diameter of approximately 7.6 feet (minimum of 100- and 125-ton designs), yielding $\Delta T = 8.76^{\circ}\text{F}$. The natural convection will be turbulent, therefore, provided the surface to air temperature difference is greater than or equal to 0.78°F for a vertical orientation and 8.76°F for a horizontal orientation.

4.5.1.1.3 Determination of Solar Heat Input

As discussed in Section 4.4.1.1.8, the intensity of solar radiation incident on an exposed surface depends on a number of time varying terms. A twelve-hour averaged insolation level is prescribed in 10CFR71 for curved surfaces. The HI-TRAC cask, however, possesses a considerable thermal inertia. This large thermal inertia precludes the HI-TRAC from reaching a steady-state thermal condition during a twelve-hour period. Thus, it is considered appropriate to use the 24-hour averaged insolation level.

4.5.1.1.4 MPC Temperatures During Moisture Removal Operations

4.5.1.1.4.1 Vacuum Drying

The initial loading of SNF in the MPC requires that the water within the MPC be drained and replaced with helium. For MPCs containing moderate burnup fuel assemblies only, this operation may be carried out using the conventional vacuum drying approach. In this method, removal of the last traces of residual moisture from the MPC cavity is accomplished by evacuating the MPC for a short time after draining the MPC. As stipulated in the Technical Specifications, vacuum drying may not be performed on MPCs containing high

burnup fuel assemblies. High burnup fuel drying is performed by a forced flow helium drying process as described in Section 4.5.1.1.4.2 and Appendix 2.B.

Prior to the start of the MPC draining operation, both the HI-TRAC annulus and the MPC are full of water. The presence of water in the MPC ensures that the fuel cladding temperatures are lower than design basis limits by large margins. As the heat generating active fuel length is uncovered during the draining operation, the fuel and basket mass will undergo a gradual heat up from the initially cold conditions when the heated surfaces were submerged under water.

The vacuum condition effective fuel assembly conductivity is determined by procedures discussed earlier (Subsection 4.4.1.1.2) after setting the thermal conductivity of the gaseous medium to a small fraction (one part in one thousand) of helium conductivity. The MPC basket cross sectional effective conductivity is determined for vacuum conditions according to the procedure discussed in 4.4.1.1.4. Basket periphery-to-MPC shell heat transfer occurs through conduction and radiation.

For total decay heat loads up to and including 20.88 kW for the MPC-24 and 21.52 kW for the MPC-68, vacuum drying of the MPC is performed with the annular gap between the MPC and the HI-TRAC filled with water. The presence of water in this annular gap will maintain the MPC shell temperature approximately equal to the saturation temperature of the annulus water. Thus, the thermal analysis of the MPC during vacuum drying for these conditions is performed with cooling of the MPC shell with water at a bounding maximum temperature of 232°F.

For higher total decay heat loads in the MPC-24 and MPC-68 or for any decay heat load in an MPC-24E or MPC-32, vacuum drying of the MPC is performed with the annular gap between the MPC and the HI-TRAC continuously flushed with water. The water movement in this annular gap will maintain the MPC shell temperature at about the temperature of flowing water. Thus, the thermal analysis of the MPC during vacuum drying for these conditions is performed with cooling of the MPC shell with water at a bounding maximum temperature of 125°F.

An axisymmetric FLUENT thermal model of the MPC is constructed, employing the MPC in-plane conductivity as an isotropic fuel basket conductivity (i.e. conductivity in the the basket radial and axial directions is equal), to determine peak cladding temperature at design basis heat loads. To avoid excessive conservatism in the computed FLUENT solution, partial recognition for higher axial heat dissipation is adopted in the peak cladding calculations. The boundary conditions applied to this evaluation are:

- i. A bounding steady-state analysis is performed with the MPC decay heat load set equal to the largest design-basis decay heat load. As discussed above, there are two different ranges for the MPC-24 and MPC-68 designs.
- ii. The entire outer surface of the MPC shell is postulated to be at a bounding maximum temperature of 232°F or 125°F, as discussed above.

- iii. The top and bottom surfaces of the MPC are adiabatic.

Results of vacuum condition analyses are provided in Subsection 4.5.2.2.

4.5.1.1.4.2 Forced Helium Recirculation

To reduce moisture to trace levels in the MPC using a Forced Helium Dehydration (FHD) system, a conventional, closed loop dehumidification system consisting of a condenser, a demister, a compressor, and a pre-heater is utilized to extract moisture from the MPC cavity through repeated displacement of its contained helium, accompanied by vigorous flow turbulence. A vapor pressure of 3 torr or less is assured by verifying that the helium temperature exiting the demister is maintained at or below the psychrometric threshold of 21°F for a minimum of 30 minutes. See Appendix 2.B for detailed discussion of the design criteria and operation of the FHD system.

The FHD system provides concurrent fuel cooling during the moisture removal process through forced convective heat transfer. The attendant forced convection-aided heat transfer occurring during operation of the FHD system ensures that the fuel cladding temperature will remain below the applicable peak cladding temperature limit for normal conditions of storage, which is well below the high burnup cladding temperature limit 752°F (400°C) for all combinations of SNF type, burnup, decay heat, and cooling time. Because the FHD operation induces a state of forced convection heat transfer in the MPC, (in contrast to the quiescent mode of natural convection in long term storage), it is readily concluded that the peak fuel cladding temperature under the latter condition will be greater than that during the FHD operation phase. In the event that the FHD system malfunctions, the forced convection state will degenerate to natural convection, which corresponds to the conditions of normal storage. As a result, the peak fuel cladding temperatures will approximate the values reached during normal storage as described elsewhere in this chapter.

4.5.1.1.5 Maximum Time Limit During Wet Transfer Operations

In accordance with NUREG-1536, water inside the MPC cavity during wet transfer operations is not permitted to boil. Consequently, uncontrolled pressures in the de-watering, purging, and recharging system that may result from two-phase conditions are completely avoided. This requirement is accomplished by imposing a limit on the maximum allowable time duration for fuel to be submerged in water after a loaded HI-TRAC cask is removed from the pool and prior to the start of vacuum drying operations.

When the HI-TRAC transfer cask and the loaded MPC under water-flooded conditions are removed from the pool, the combined water, fuel mass, MPC, and HI-TRAC metal will absorb the decay heat emitted by the fuel assemblies. This results in a slow temperature rise of the entire system with time, starting from an initial temperature of the contents. The rate of temperature rise is limited by the thermal inertia of the HI-TRAC system. To enable a bounding heat-up rate determination for the HI-TRAC system, the following conservative assumptions are imposed:

- i. Heat loss by natural convection and radiation from the exposed HI-TRAC surfaces to the pool building ambient air is neglected (i.e., an adiabatic temperature rise calculation is performed).
- ii. Design-basis maximum decay heat input from the loaded fuel assemblies is imposed on the HI-TRAC transfer cask.
- iii. The smaller of the two (i.e., 100-ton and 125-ton) HI-TRAC transfer cask designs is credited in the analysis. The 100-ton design has a significantly smaller quantity of metal mass, which will result in a higher rate of temperature rise.
- iv. The smallest of the minimum MPC cavity-free volumes among the two MPC types is considered for flooded water mass determination.
- v. Only fifty percent of the water mass in the MPC cavity is credited towards water thermal inertia evaluation.

Table 4.5.5 summarizes the weights and thermal inertias of several components in the loaded HI-TRAC transfer cask. The rate of temperature rise of the HI-TRAC transfer cask and contents during an adiabatic heat-up is governed by the following equation:

$$\frac{dT}{dt} = \frac{Q}{C_h}$$

where:

- Q = decay heat load (Btu/hr) [Design Basis maximum 28.74 kW = 98,205 Btu/hr]
 C_h = combined thermal inertia of the loaded HI-TRAC transfer cask (Btu/°F)
 T = temperature of the contents (°F)
 t = time after HI-TRAC transfer cask is removed from the pool (hr)

A bounding heat-up rate for the HI-TRAC transfer cask contents is determined to be equal to 3.77 °F/hr. From this adiabatic rate of temperature rise estimate, the maximum allowable time duration (t_{max}) for fuel to be submerged in water is determined as follows:

$$t_{\max} = \frac{T_{\text{boil}} - T_{\text{initial}}}{(dT/dt)}$$

where:

- T_{boil} = boiling temperature of water (equal to 212°F at the water surface in the MPC cavity)
 T_{initial} = initial temperature of the HI-TRAC contents when the transfer cask is removed from the pool

Table 4.5.6 provides a summary of t_{\max} at several representative HI-TRAC contents starting temperature.

As set forth in the HI-STORM operating procedures, in the unlikely event that the maximum allowable time provided in Table 4.5.6 is found to be insufficient to complete all wet transfer operations, a forced water circulation shall be initiated and maintained to remove the decay heat from the MPC cavity. In this case, relatively cooler water will enter via the MPC lid drain port connection and heated water will exit from the vent port. The minimum water flow rate required to maintain the MPC cavity water temperature below boiling with an adequate subcooling margin is determined as follows:

$$M_w = \frac{Q}{C_{pw}(T_{\max} - T_{in})}$$

where:

M_w = minimum water flow rate (lb/hr)

C_{pw} = water heat capacity (Btu/lb-°F)

T_{\max} = maximum MPC cavity water mass temperature

T_{in} = temperature of pool water supply to MPC

With the MPC cavity water temperature limited to 150°F, MPC inlet water maximum temperature equal to 125°F and at the design basis maximum heat load, the water flow rate is determined to be 3928 lb/hr (7.9 gpm).

4.5.1.1.6 Cask Cooldown and Reflood Analysis During Fuel Unloading Operation

NUREG-1536 requires an evaluation of cask cooldown and reflood procedures to support fuel unloading from a dry condition. Past industry experience generally supports cooldown of cask internals and fuel from hot storage conditions by direct water quenching. The extremely rapid cooldown rates to which the hot MPC internals and the fuel cladding are subjected during water injection may, however, result in uncontrolled thermal stresses and failure in the structural members. Moreover, water injection results in large amounts of steam generation and unpredictable transient two-phase flow conditions inside the MPC cavity, which may result in overpressurization of the confinement boundary. To avoid potential safety concerns related to rapid cask cooldown by direct water quenching, the HI-STORM MPCs will be cooled in a gradual manner, thereby eliminating thermal shock loads on the MPC internals and fuel cladding.

In the unlikely event that a HI-STORM storage system is required to be unloaded, the MPC will be transported on-site via the HI-TRAC transfer cask back to the fuel handling building. Prior to reflooding the MPC cavity with water[†], a forced flow helium recirculation system with adequate flow capacity shall be operated to remove the decay heat and initiate a slow cask cooldown lasting for several days. The operating

[†] Prior to helium circulation, the HI-TRAC annulus is flooded with water to substantially lower the MPC shell temperature (approximately 100°F). For low decay heat MPCs (~10 kW or less) the annulus cooling is adequate to lower the MPC cavity temperature below the boiling temperature of water.

procedures in Chapter 8 (Section 8.3) provide a detailed description of the steps involved in the cask unloading. An analytical method that provides a basis for determining the required helium flow rate as a function of the desired cooldown time is presented below, to meet the objective of eliminating thermal shock when the MPC cavity is eventually flooded with water.

Under a closed-loop forced helium circulation condition, the helium gas is cooled, via an external chiller, down to 100°F. The chilled helium is then introduced into the MPC cavity, near the MPC baseplate, through the drain line. The helium gas enters the MPC basket from the bottom oversized flow holes and moves upward through the hot fuel assemblies, removing heat and cooling the MPC internals. The heated helium gas exits from the top of the basket and collects in the top plenum, from where it is expelled through the MPC lid vent connection to the helium recirculation and cooling system. The MPC contents bulk average temperature reduction as a function of time is principally dependent upon the rate of helium circulation. The temperature transient is governed by the following heat balance equation:

$$C_h \frac{dT}{dt} = Q_D - m C_p (T - T_i) - Q_c$$

Initial Condition: $T = T_o$ at $t = 0$

where:

- T = MPC bulk average temperature (°F)
- T_o = initial MPC bulk average temperature in the HI-TRAC transfer cask (equal to 586°F)
- t = time after start of forced circulation (hrs)
- Q_D = decay heat load (Btu/hr)
(equal to Design Basis maximum 28.74kW (i.e., 98,205 Btu/hr) m = helium circulation rate (lb/hr)
- C_p = helium heat capacity (Btu/lb-°F)
(equal to 1.24 Btu/lb-°F)
- Q_c = heat rejection from cask exposed surfaces to ambient (Btu/hr) (conservatively neglected)
- C_h = thermal capacity of the loaded MPC (Btu/°F)
(For a bounding upper bound 100,000 lb loaded MPC weight and heat capacity of Alloy X equal to 0.12 Btu/lb-°F, the heat capacity is equal to 12,000 Btu/°F.)
- T_i = MPC helium inlet temperature (°F)

The differential equation is analytically solved, yielding the following expression for time-dependent MPC bulk temperature:

$$T(t) = \left(T_i + \frac{Q_D}{m C_p} \right) \left(1 - e^{-\frac{m C_p}{C_h} t} \right) + T_o e^{-\frac{m C_p}{C_h} t}$$

This equation is used to determine the minimum helium mass flow rate that would cool the MPC cavity down from initially hot conditions to less than 200°F (i.e., with a subcooling margin for normal boiling

temperature of water[†] (212°F)). For example, to cool the MPC to less than 200°F in 72 hours using 0°F helium would require a helium mass flow rate of 432 lb/hr (i.e., 647 SCFM).

Once the helium gas circulation has cooled the MPC internals to less than 200°F, water can be injected to the MPC without risk of boiling and the associated thermal stress concerns. Because of the relatively long cooldown period, the thermal stress contribution to the total cladding stress would be negligible, and the total stress would therefore be bounded by the normal (dry) condition. The elimination of boiling eliminates any concern of overpressurization due to steam production.

4.5.1.1.7 Study of Lead-to-Steel Gaps on Predicted Temperatures

Lead, poured between the inner and outer shells, is utilized as a gamma shield material in the HI-TRAC on-site transfer cask designs. Lead shrinks during solidification requiring the specification and implementation of appropriate steps in the lead installation process so that the annular space is free of gaps. Fortunately, the lead pouring process is a mature technology and proven methods to insure that radial gaps do not develop are widely available. This subsection outlines such a method to achieve a zero-gap lead installation in the annular cavity of the HI-TRAC casks.

The 100-ton and 125-ton HI-TRAC designs incorporate 2.5 inch and 4.5 inch annular spaces, respectively, formed between a 3/4-inch thick steel inner shell and a 1-inch thick steel outer shell. The interior steel surfaces are cleaned, sandblasted and fluxed in preparation for the molten lead that will be poured in the annular cavity. The appropriate surface preparation technique is essential to ensure that molten lead sticks to the steel surfaces, which will form a metal to lead bond upon solidification. The molten lead is poured to fill the annular cavity. The molten lead in the immediate vicinity of the steel surfaces, upon cooling by the inner and outer shells, solidifies forming a melt-solid interface. The initial formation of a gap-free interfacial bond between the solidified lead and steel surfaces initiates a process of lead crystallization from the molten pool onto the solid surfaces. Static pressure from the column of molten lead further aids in retaining the solidified lead layer to the steel surfaces. The melt-solid interface growth occurs by freezing of successive layers of molten lead as the heat of fusion is dissipated by the solidified metal and steel structure enclosing it. This growth stops when all the molten lead is used up and the annulus is filled with a solid lead plug. The shop fabrication procedures, being developed in conjunction with the designated manufacturer of the HI-TRAC transfer casks, shall contain detailed step-by-step instructions devised to eliminate the incidence of annular gaps in the lead space of the HI-TRAC.

In the spirit of a defense-in-depth approach, however, a conservatively bounding lead-to-steel gap is assumed herein and the resultant peak cladding temperature under design basis heat load is computed. It is noted that in a non-bonding lead pour scenario, the lead shrinkage resulting from phase transformation related density changes introduces a tendency to form small gaps. This tendency is counteracted by gravity

[†] Certain fuel configurations in PWR MPCs are required to be flooded with borated water, which has a higher boiling temperature. Thus, greater subcooling margins are present in this case.

induced slump, which tends to push the heavy mass of lead against the steel surfaces. If the annular molten mass of lead is assumed to contract as a solid, in the absence of gravity, then a bounding lead-to-steel gap is readily computed from density changes. This calculation is performed for the 125-ton HI-TRAC transfer cask, which has a larger volume of lead and is thus subject to larger volume shrinkage relative to the 100-ton design, and is presented below.

The densities of molten (ρ_l) and solid (ρ_s) lead are given on page 3-96 of Perry's Handbook (6th Edition) as 10,430 kg/m³ and 11,010 kg/m³, respectively. The fractional volume contraction during solidification ($\delta v/v$) is calculated as:

$$\frac{\delta v}{v} = \frac{(\bar{n}_s - \bar{n}_l)}{\bar{n}_l} = \frac{(11,010 - 10,430)}{10,430} = 0.0556$$

and the corresponding fractional linear contraction during solidification is calculated as:

$$\frac{\delta L}{L} = \left[1 + \frac{\delta v}{v} \right]^{1/3} - 1 = 1.0556^{1/3} - 1 = 0.0182$$

The bounding lead-to-steel gap, which is assumed filled with air, is calculated by multiplying the nominal annulus radial dimension (4.5 inches in the 125-ton HI-TRAC) by the fractional linear contraction as:

$$\delta = 4.5 \times \frac{\delta L}{L} = 4.5 \times 0.0182 = 0.082 \text{ inches}$$

In this hypothetical lead shrinkage process, the annular lead cylinder will contract towards the inner steel shell, eliminating gaps and tightly compressing the two surfaces together. Near the outer steel cylinder, a steel-to-lead air gap will develop as a result of volume reduction in the liquid to solid phase transformation. The air gap is conservatively postulated to occur between the inner steel shell and the lead, where the heat flux is higher relative to the outer steel shell, and hence the computed temperature gradient is greater. The combined resistance of an annular lead cylinder with an air gap (R_{cyl}) is computed by the following formula:

$$R_{cyl} = \frac{\ln(R_o/R_i)}{2\delta\delta_{pb}} + \frac{\delta}{2\delta\delta_i[K_{air} + K_r]}$$

where:

- R_i = inner radius (equal to 35.125 inches)
- R_o = outer radius (equal to 39.625 inches)
- K_{pb} = bounding minimum lead conductivity (equal to 16.9 Btu/ft-hr-°F, from Table 4.2.2)
- δ = lead-to-steel air gap, computed above
- K_{air} = temperature dependent air conductivity (see Table 4.2.2)
- K_r = effective thermal conductivity contribution from radiation heat transfer across air gap

The effective thermal conductivity contribution from radiation heat transfer (K_r) is defined by the following equation:

$$K_r = 4 \times \sigma \times F_z \times T^3 \times \bar{\alpha}$$

where:

- σ = Stefan-Boltzmann constant
- $F_\epsilon = (1/\epsilon_{cs} + 1/\epsilon_{pb} - 1)^{-1}$
- ϵ_{cs} = carbon steel emissivity (equal to 0.66, HI-STORM FSAR Table 4.2.4)
- ϵ_{pb} = lead emissivity (equal to 0.63 for oxidized surfaces at 300°F from McAdams, Heat Transmission, 3rd Ed.)
- T = absolute temperature

Based on the total annular region resistance (R_{cyl}) computed above, an equivalent annulus conductivity is readily computed. This effective temperature-dependent conductivity results are tabulated below:

Temperature (°F)	Effective Annulus Conductivity (Btu/ft-hr-°F)
200	1.142
450	1.809

The results tabulated above confirm that the assumption of a bounding annular air gap grossly penalizes the heat dissipation characteristics of lead filled regions. Indeed, the effective conductivity computed above is an order of magnitude lower than that of the base lead material. To confirm the heat dissipation adequacy of HI-TRAC casks under the assumed overly pessimistic annular gaps, the HI-TRAC thermal model described earlier is altered to include the effective annulus conductivity computed above for the annular lead region. The peak cladding temperature results are tabulated below:

Annular Gap Assumption	Peak Cladding Temperature (°F)	Cladding Temperature Limit (°F)
None	872	1058
Bounding Maximum	924	1058

From these results, it is readily apparent that the stored fuel shall be maintained within safe temperature limits by a substantial margin of safety (in excess of 100°F).

4.5.1.2 Test Model

A detailed analytical model for thermal design of the HI-TRAC transfer cask was developed using the FLUENT CFD code, the industry standard ANSYS modeling package and conservative adiabatic calculations, as discussed in Subsection 4.5.1.1. Furthermore, the analyses incorporate many conservative

assumptions in order to demonstrate compliance to the specified short-term limits with adequate margins. In view of these considerations, the HI-TRAC transfer cask thermal design complies with the thermal criteria established for short-term handling and onsite transport. Additional experimental verification of the thermal design is therefore not required.

4.5.2 Maximum Temperatures

4.5.2.1 Maximum Temperatures Under Onsite Transport Conditions

An axisymmetric FLUENT thermal model of an MPC inside a HI-TRAC transfer cask was developed to evaluate temperature distributions for onsite transport conditions. A bounding steady-state analysis of the HI-TRAC transfer cask has been performed using the hottest MPC, the highest design-basis decay heat load (Table 2.1.6), and design-basis insulation levels. While the duration of onsite transport may be short enough to preclude the MPC and HI-TRAC from obtaining a steady-state, a steady-state analysis is conservative. Information listing all other thermal analyses pertaining to the HI-TRAC cask and associated subsection of the FSAR summarizing obtained results is provided in Table 4.5.8.

A converged temperature contour plot is provided in Figure 4.5.2. Maximum fuel clad temperatures are listed in Table 4.5.2, which also summarizes maximum calculated temperatures in different parts of the HI-TRAC transfer cask and MPC. As described in Subsection 4.4.2, the FLUENT calculated peak temperature in Table 4.5.2 is actually the peak pellet centerline temperature, which bounds the peak cladding temperature. We conservatively assume that the peak clad temperature is equal to the peak pellet centerline temperature.

The maximum computed temperatures listed in Table 4.5.2 are based on the HI-TRAC cask at Design Basis Maximum heat load, passively rejecting heat by natural convection and radiation to a hot ambient environment at 100°F in still air in a vertical orientation. In this orientation, there is apt to be a less of metal-to-metal contact between the physically distinct entities, viz., fuel, fuel basket, MPC shell and HI-TRAC cask. For this reason, the gaps resistance between these parts is higher than in a horizontally oriented HI-TRAC. To bound gaps resistance, the various parts are postulated to be in a centered configuration. MPC internal convection at a postulated low cavity pressure of 5 atm is included in the thermal model. The peak cladding temperature computed under these adverse Ultimate Heat Sink (UHS) assumptions is 872°F which is substantially lower than the short-term temperature limit of 1058°F. Consequently, cladding integrity assurance is provided by large safety margins (in excess of 100°F) during onsite transfer of an MPC emplaced in a HI-TRAC cask.

As a defense-in-depth measure, cladding integrity is demonstrated for a theoretical bounding scenario. For this scenario, all means of convective heat dissipation within the canister are neglected in addition to the bounding relative configuration for the fuel, basket, MPC shell and HI-TRAC overpack assumption stated earlier for the vertical orientation. This means that the fuel is centered in the basket cells, the basket is centered in the MPC shell and the MPC shell is centered in the HI-TRAC overpack to maximize gaps

thermal resistance. The peak cladding temperature computed for this scenario (1025°F) is below the short-term limit of 1058°F.

As discussed in Sub-section 4.5.1.1.6, MPC fuel unloading operations are performed with the MPC inside the HI-TRAC cask. For this operation, a helium cooldown system is engaged to the MPC via lid access ports and a forced helium cooling of the fuel and MPC is initiated. With the HI-TRAC cask external surfaces dissipating heat to a UHS in a manner in which the ambient air access is not restricted by bounding surfaces or large objects in the immediate vicinity of the cask, the temperatures reported in Table 4.5.2 will remain bounding during fuel unloading operations. Under a scenario in which the cask is emplaced in a area with ambient air access restrictions (for example in a cask pit area), additional means shall be devised to limit the cladding temperature rise arising from such restrictions to less than 100°F. These means are discussed next.

The time duration allowed for the cask to be emplaced in a ambient air restricted area with the helium cooling system non-operational shall be limited to 22 hours. Conservatively postulating that the rate of passive cooling is substantially degraded by 90% (i.e., 10% of decay heat is dissipated to ambient), cladding integrity is demonstrated based on cask heating considerations from the undissipated heat. At a bounding heat load of 28.74kW, the HI-TRAC cask system thermal inertia (19,532 Btu/°F, Table 4.5.5), limits the temperature rise to 4.52°F/hr. Thus, the computed cladding temperature rise during this time period will be less than 100°F.

A forced supply of ambient air near the bottom of the cask pit to aid heat dissipation by the natural convection process is another adequate means to maintain the fuel cladding within safe operating limits. Conservatively assuming this column of moving air as the UHS (i.e. to which all heat dissipation occurs) with no credit for enhanced cooling as a result of forced convection heat transfer, a nominal air supply of 1000 SCFM (4850 lbs/hr) adequately meets the cooling requirement. At this flow rate, the temperature rise of the UHS resulting from cask decay heat input to the airflow will be less than 100°F. The cladding temperature elevation will consequently be bounded by this temperature rise.

4.5.2.2 Maximum MPC Basket Temperature Under Vacuum Conditions

As stated in Subsection 4.5.1.1.4, above, an axisymmetric FLUENT thermal model of the MPC is developed for the vacuum condition. For the MPC-24E and MPC-32 designs, and for the higher heat load ranges in the MPC-24 and MPC-68 designs, the model also includes an isotropic fuel basket thermal conductivity. Each MPC is analyzed at its respective design maximum heat load. The steady-state peak cladding results, with partial recognition for higher axial heat dissipation where included, are summarized in Table 4.5.9. The peak fuel clad temperatures during short-term vacuum drying operations with design-basis maximum heat loads are calculated to be less than 1058°F for all MPC baskets by a significant margin..

4.5.3 Minimum Temperatures

In Table 2.2.2 and Chapter 12, the minimum ambient temperature condition required to be considered for the HI-TRAC design is specified as 0°F. If, conservatively, a zero decay heat load (with no solar input) is applied to the stored fuel assemblies then every component of the system at steady state would be at this outside minimum temperature. Provided an antifreeze is added to the water jacket (required by Technical Specification for ambient temperatures below 32°F), all HI-TRAC materials will satisfactorily perform their intended functions at this minimum postulated temperature condition. Fuel transfer operations are controlled by Technical Specifications in Chapter 12 to ensure that onsite transport operations are not performed at an ambient temperature less than 0°F.

4.5.4 Maximum Internal Pressure

After fuel loading and vacuum drying, but prior to installing the MPC closure ring, the MPC is initially filled with helium. During handling in the HI-TRAC transfer cask, the gas temperature within the MPC rises to its maximum operating temperature as determined based on the thermal analysis methodology described previously. The gas pressure inside the MPC will also increase with rising temperature. The pressure rise is determined based on the ideal gas law, which states that the absolute pressure of a fixed volume of gas is proportional to its absolute temperature. The net free volumes of the four MPC designs are determined in Section 4.4.

The maximum MPC internal pressure is determined for normal onsite transport conditions, as well as off-normal conditions of a postulated accidental release of fission product gases caused by fuel rod rupture. Based on NUREG-1536 [4.4.10] recommended fission gases release fraction data, net free volume and initial fill gas pressure, the bounding maximum gas pressures with 1% and 10% rod rupture are given in Table 4.5.3. The MPC maximum gas pressures listed in Table 4.5.3 are all below the MPC design internal pressure listed in Table 2.2.1.

4.5.5 Maximum Thermal Stresses

Thermal expansion induced mechanical stresses due to non-uniform temperature distributions are reported in Chapter 3. Tables 4.5.2 and 4.5.4 provide a summary of MPC and HI-TRAC transfer cask component temperatures for structural evaluation.

4.5.6 Evaluation of System Performance for Normal Conditions of Handling and Onsite Transport

The HI-TRAC transfer cask thermal analysis is based on a detailed heat transfer model that conservatively accounts for all modes of heat transfer in various portions of the MPC and HI-TRAC. The thermal model incorporates several conservative features, which are listed below:

- i. The most severe levels of environmental factors - bounding ambient temperature (100°F) and constant solar flux - were coincidentally imposed on the thermal design. A bounding solar absorptivity of 1.0 is applied to all insolation surfaces.
- ii. The HI-TRAC cask-to-MPC annular gap is analyzed based on the nominal design dimensions. No credit is considered for the significant reduction in this radial gap that would occur as a result of differential thermal expansion with design basis fuel at hot conditions. The MPC is considered to be concentrically aligned with the cask cavity. This is a worst-case scenario since any eccentricity will improve conductive heat transport in this region.
- iii. No credit is considered for cooling of the HI-TRAC baseplate while in contact with a supporting surface. An insulated boundary condition is applied in the thermal model on the bottom baseplate face.

Temperature distribution results (Tables 4.5.2 and 4.5.4, and Figure 4.5.2) obtained from this highly conservative thermal model show that the short-term fuel cladding and cask component temperature limits are met with adequate margins. Expected margins during normal HI-TRAC use will be larger due to the many conservative assumptions incorporated in the analysis. Corresponding MPC internal pressure results (Table 4.5.3) show that the MPC confinement boundary remains well below the short-term condition design pressure. Stresses induced due to imposed temperature gradients are within ASME Code limits (Chapter 3). The maximum local axial neutron shield temperature is lower than design limits. Therefore, it is concluded that the HI-TRAC transfer cask thermal design is adequate to maintain fuel cladding integrity for short-term onsite handling and transfer operations.

The water in the water jacket of the HI-TRAC provides necessary neutron shielding. During normal handling and onsite transfer operations this shielding water is contained within the water jacket, which is designed for an elevated internal pressure. It is recalled that the water jacket is equipped with pressure relief valves set at 60 psig and 65 psig. This set pressure elevates the saturation pressure and temperature inside the water jacket, thereby precluding boiling in the water jacket under normal conditions. Under normal handling and onsite transfer operations, the bulk temperature inside the water jacket reported in Table 4.5.2 is less than the coincident saturation temperature at 60 psig (307°F), so the shielding water remains in its liquid state. The bulk temperature is determined via a conservative analysis, presented earlier, with design-basis maximum decay heat load. One of the assumptions that render the computed temperatures extremely conservative is the stipulation of a 100°F steady-state ambient temperature. In view of the large thermal inertia of the HI-TRAC, an appropriate ambient temperature is the "time-averaged" temperature, formally referred to in this FSAR as the normal temperature.

Note that during hypothetical fire accident conditions (see Section 11.2) these relief valves allow venting of any steam generated by the extreme fire flux, to prevent overpressurizing the water jacket. In this manner, a portion of the fire heat flux input to the HI-TRAC outer surfaces is expended in vaporizing a portion of the water in the water jacket, thereby mitigating the magnitude of the heat input to the MPC during the fire.

During vacuum drying operations, the annular gap between the MPC and the HI-TRAC is filled with water. The saturation temperature of the annulus water bounds the maximum temperatures of all HI-TRAC components, which are located radially outside the water-filled annulus. As previously stated (see Subsection 4.5.1.1.4) the maximum annulus water temperature is only 125°F, so the HI-TRAC water jacket temperature will be less than the 307°F saturation temperature.

Table 4.5.1

EFFECTIVE RADIAL THERMAL CONDUCTIVITY OF THE WATER JACKET

Temperature (°F)	Thermal Conductivity (Btu/ft-hr-°F)
200	1.376
450	1.408
700	1.411

Table 4.5.2

HI-TRAC TRANSFER CASK STEADY-STATE
MAXIMUM TEMPERATURES

Component	Temperature [°F]
Fuel Cladding	872
MPC Basket	852
Basket Periphery	600
MPC Outer Shell Surface	455
HI-TRAC Overpack Inner Surface	322
Water Jacket Inner Surface	314
Enclosure Shell Outer Surface	224
Water Jacket Bulk Water	258
Axial Neutron Shield [†]	258

[†] Local neutron shield section temperature.

Table 4.5.3

SUMMARY OF MPC CONFINEMENT BOUNDARY PRESSURES[†] FOR
NORMAL HANDLING AND ONSITE TRANSPORT

Condition	Pressure (psig)
MPC-24:	
Initial backfill (at 70°F)	31.3
Normal condition	76.0
With 1% rod rupture	76.8
With 10% rod rupture	83.7
MPC-68:	
Initial backfill (at 70°F)	31.3
Normal condition	76.0
With 1% rods rupture	76.5
With 10% rod rupture	80.6
MPC-32:	
Initial backfill (at 70°F)	31.3
Normal condition	76.0
With 1% rods rupture	77.1
With 10% rod rupture	86.7
MPC-24E:	
Initial backfill (at 70°F)	31.3
Normal condition	76.0
With 1% rods rupture	76.8
With 10% rod rupture	83.7

[†] Includes gas from BPRA rods for PWR MPCs

Table 4.5.4

SUMMARY OF HI-TRAC TRANSFER CASK AND MPC COMPONENTS
NORMAL HANDLING AND ONSITE TRANSPORT TEMPERATURES

Location	Temperature (°F)
MPC Basket Top:	
Basket periphery	590
MPC shell	445
O/P [†] inner shell	280
O/P enclosure shell	196
MPC Basket Bottom:	
Basket periphery	334
MPC shell	302
O/P inner shell	244
O/P enclosure shell	199

[†] O/P is an abbreviation for HI-TRAC overpack.

Table 4.5.5

SUMMARY OF LOADED 100-TON HI-TRAC TRANSFER CASK
 BOUNDING COMPONENT
 WEIGHTS AND THERMAL INERTIAS

Component	Weight (lbs)	Heat Capacity (Btu/lb-°F)	Thermal Inertia (Btu/°F)
Water Jacket	7,000	1.0	7,000
Lead	52,000	0.031	1,612
Carbon Steel	40,000	0.1	4,000
Alloy-X MPC (empty)	39,000	0.12	4,680
Fuel	40,000	0.056	2,240
MPC Cavity Water [†]	6,500	1.0	6,500
			26,032 (Total)

[†] Conservative lower bound water mass.

Table 4.5.6

MAXIMUM ALLOWABLE TIME DURATION FOR WET
TRANSFER OPERATIONS

Initial Temperature (°F)	Time Duration (hr)
115	25.7
120	24.4
125	23.1
130	21.7
135	20.4
140	19.1
145	17.8
150	16.4

Table 4.5.7

INTENTIONALLY DELETED

Table 4.5.8
MATRIX OF HI-TRAC TRANSFER CASK THERMAL EVALUATIONS

Scenario	Description	Ultimate Heat Sink	Analysis Type	Principal Input Parameters	Results in FSAR Subsection
1	Onsite Transport	Ambient	SS(B)	O _T , Q _D , ST, SC	4.5.2.1
2	Lead Gaps	Ambient	SS(B)	O _T , Q _D , ST, SC	4.5.1.1.7
3	Vacuum	HI-TRAC annulus water	SS(B)	Q _D	4.5.2.2
4	Wet Transfer Operation	Cavity water and Cask Internals	AH	Q _D	4.5.1.1.5
5	Fuel Unloading	Helium Circulation	TA	Q _D	4.5.1.1.6
6	Fire Accident	Jacket Water, Cask Internals	TA	Q _D , F	11.2.4
7	Jacket Water Loss Accident	Ambient	SS(B)	O _T , Q _D , ST, SC	11.2.1

Legend:

O_T - Off-Normal Temperature (100°F)

Q_D - Design Basis Maximum Heat Load

ST - Insolation Heating (Top)

SC - Insolation Heating (Curved)

F - Fire Heating (1475°F)

SS(B) - Bounding Steady State

TA - Transient Analysis

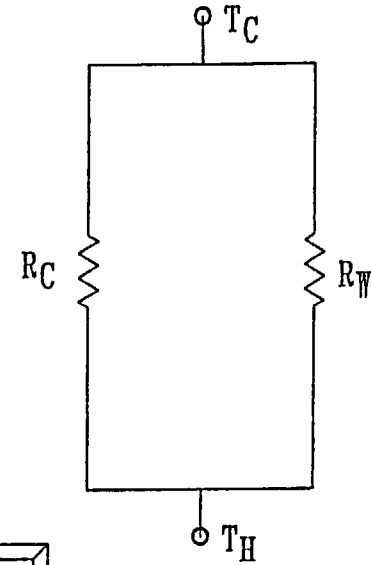
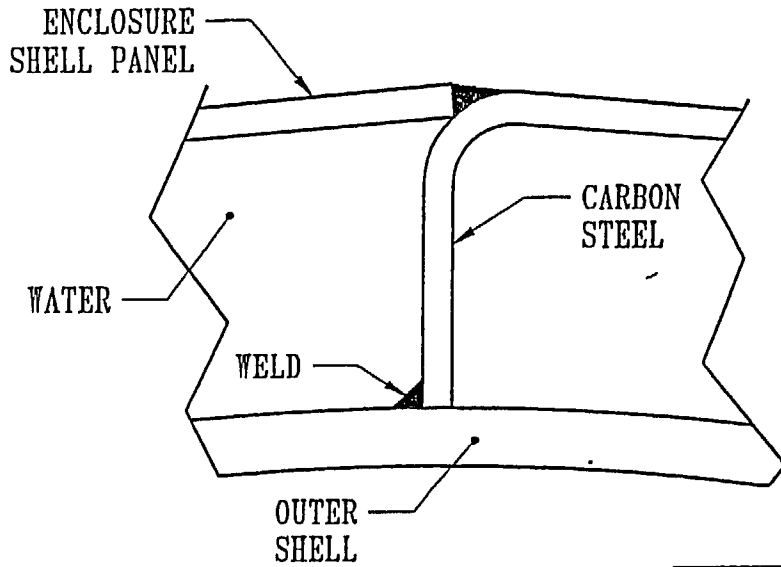
AH - Adiabatic Heating

Table 4.5.9

PEAK CLADDING TEMPERATURE IN VACUUM[†]

MPC	Lower Decay Heat Load Range Temperatures (°F)	Higher Decay Heat Load Range Temperature (°F)
MPC-24	827	960
MPC-68	822	1014
MPC-32	n/a	1040
MPC-24E	n/a	942

[†] Steady state temperatures at the MPC design maximum heat load reported.



R_C : CARBON STEEL RESISTANCE
R_W : WATER RESISTANCE
T_H : HOT TEMPERATURES
T_C : COLD TEMPERATURES

FIGURE 4.5.1; WATER JACKET RESISTANCE NETWORK ANALOGY FOR EFFECTIVE CONDUCTIVITY CALCULATION

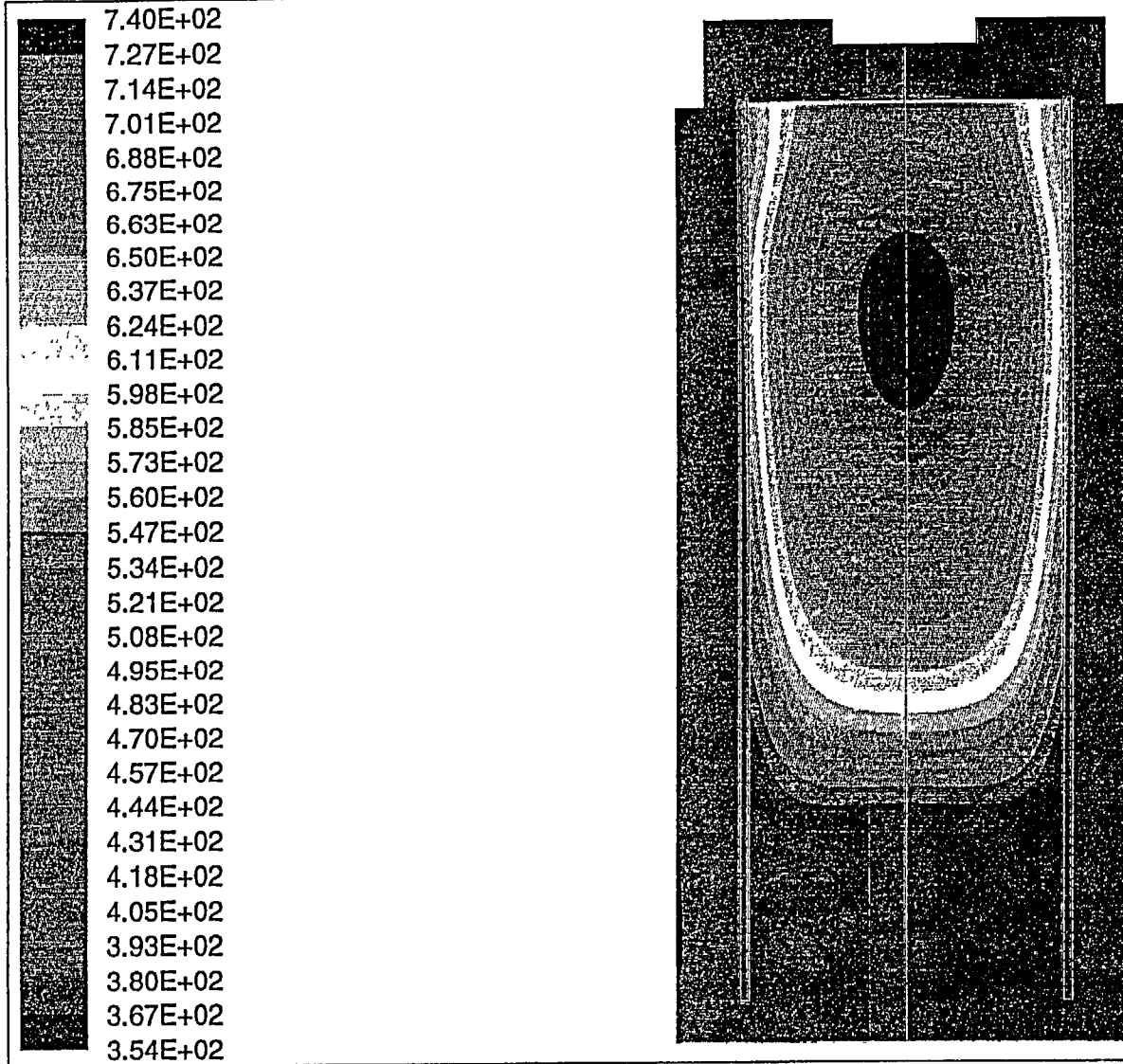


FIGURE 4.5.2: HI-TRAC Temperature Contours Plot
 Temperature (Degrees Kelvin)
 Max = 7.398E+02 Min = 3.540E+02

Aug 24 2000
 Fluent 4.48
 Fluent Inc.

FIGURE 4.5.3
INTENTIONALLY DELETED

4.6 REGULATORY COMPLIANCE

4.6.1 Normal Conditions of Storage

NUREG-1536 [4.4.10] defines several thermal acceptance criteria that must be applied to evaluations of normal conditions of storage. These items are addressed in Sections 4.1 through 4.4.5. Each of the pertinent criteria and the conclusion of the evaluations are summarized here.

As required by NUREG-1536 (4.0,IV,1), the fuel cladding temperature at the beginning of dry cask storage is maintained below the anticipated damage-threshold temperatures for normal conditions and a minimum of 20 years of cask storage. Maximum clad temperatures for long-term storage conditions are reported in Section 4.4.2. Anticipated damage-threshold temperatures, calculated as described in Section 4.3, are summarized in Table 2.2.3.

As required by NUREG-1536 (4.0,IV,3), the maximum internal pressure of the cask remains within its design pressure for normal, off-normal, and accident conditions, assuming rupture of 1 percent, 10 percent, and 100 percent of the fuel rods, respectively. Assumptions for pressure calculations include release of 100 percent of the fill gas and 30 percent of the significant radioactive gases in the fuel rods. Maximum internal pressures are reported in Section 4.4.4. Design pressures are summarized in Table 2.2.1.

As required by NUREG-1536 (4.0,IV,4), all cask and fuel materials are maintained within their minimum and maximum temperature for normal and off-normal conditions in order to enable components to perform their intended safety functions. Maximum and minimum temperatures for long-term storage conditions are reported in Sections 4.4.2 and 4.4.3, respectively. Design temperature limits are summarized in Table 2.2.3. HI-STORM System components defined as important to safety are listed in Table 2.2.6.

As required by NUREG-1536 (4.0,IV,5), the cask system ensures a very low probability of cladding breach during long-term storage. Further, NUREG-1536 (4.0,IV,6) requires that the fuel cladding damage resulting from creep cavitation should be limited to 15 percent of the original cladding cross section area during dry storage. The calculation methodology, described in Section 4.3, for determining initial dry storage fuel clad temperature limits, ensures that both of these requirements are satisfied. Maximum fuel clad temperature limits are summarized in Table 2.2.3.

As required by NUREG-1536 (4.0,IV,7), the cask system is passively cooled. All heat rejection mechanisms described in this chapter, including conduction, natural convection, and thermal radiation, are completely passive.

As required by NUREG-1536 (4.0,IV,8), the thermal performance of the cask is within the allowable design criteria specified in FSAR Chapters 2 and 3 for normal conditions. All thermal results

reported in Sections 4.4.2 through 4.4.5 are within the design criteria allowable ranges for all normal conditions of storage.

4.6.2 Normal Handling and Onsite Transfer

NUREG-1536 [4.4.10] defines several thermal acceptance criteria that are addressed in Sections 4.5.1 through 4.5.5. Each of the pertinent criteria is summarized here.

As required by NUREG-1536 (4.0,IV,2), the fuel cladding temperature is maintained below 570°C (1058°F) for fuel transfer operations. Maximum clad temperatures for normal on-site transfer conditions are reported in Section 4.5.2. Maximum clad temperatures for vacuum drying conditions are reported in Section 4.5.2.1 and comply within this limit by large conservative margins.

As required by NUREG-1536 (4.0,IV,3), the maximum internal pressure of the cask remains within its design pressure for normal and off-normal conditions, assuming rupture of 1 percent and 10 percent of the fuel rods, respectively. Assumptions for pressure calculations include release of 100 percent of the fill gas and 30 percent of the significant radioactive gases in the fuel rods. Maximum internal pressures are reported in Section 4.5.4. Design pressures are summarized in Table 2.2.1.

As required by NUREG-1536 (4.0,IV,4), all cask and fuel materials are maintained within their minimum and maximum temperature for normal (short-term) fuel handling operations in order to enable components to perform their intended safety functions. Maximum and minimum temperatures for fuel handling operations are reported in Sections 4.5.2 and 4.5.3, respectively. Design temperature limits are summarized in Table 2.2.3.

As required by NUREG-1536 (4.0,IV,7), the cask system is passively cooled. All heat rejection mechanisms described in this chapter, including conduction, natural convection, and thermal radiation, are completely passive.

As required by NUREG-1536 (4.0,IV,8), the thermal performance of the cask is within the allowable design criteria specified in FSAR Chapters 2 and 3 for normal (short-term) fuel handling operations. All thermal results reported in Sections 4.5.2 through 4.5.5 are within the design criteria allowable ranges for short-term conditions.

4.7 REFERENCES

- [4.1.1] ANSYS Finite Element Modeling Package, Swanson Analysis Systems, Inc., Houston, PA, 1993.
- [4.1.2] FLUENT Computational Fluid Dynamics Software, Fluent, Inc., Centerra Resource Park, 10 Cavendish Court, Lebanon, NH 03766.
- [4.1.3] "The TN-24P PWR Spent-Fuel Storage Cask: Testing and Analyses," EPRI NP-5128, (April 1987).
- [4.2.1] Baumeister, T., Avallone, E.A. and Baumeister III, T., "Marks' Standard Handbook for Mechanical Engineers," 8th Edition, McGraw Hill Book Company, (1978).
- [4.2.2] Rohsenow, W.M. and Hartnett, J.P., "Handbook of Heat Transfer," McGraw Hill Book Company, New York, (1973).
- [4.2.3] Creer et al., "The TN-24P Spent Fuel Storage Cask: Testing and Analyses," EPRI NP-5128, PNL-6054, UC-85, (April 1987).
- [4.2.4] Rust, J.H., "Nuclear Power Plant Engineering," Haralson Publishing Company, (1979).
- [4.2.5] Kern, D.Q., "Process Heat Transfer," McGraw Hill Kogakusha, (1950).
- [4.2.6] "A Handbook of Materials Properties for Use in the Analysis of Light Water Reactor Fuel Rod Behavior," NUREG/CR-0497, (August 1981).
- [4.2.7] "Safety Analysis Report for the NAC Storable Transport Cask," Docket No. 71-9235.
- [4.2.8] ASME Boiler and Pressure Vessel Code, Section II, Part D, (1995).
- [4.2.9] Jakob, M. and Hawkins, G.A., "Elements of Heat Transfer," John Wiley & Sons, New York, (1957).
- [4.2.10] ASME Steam Tables, 3rd Edition (1977).
- [4.3.1] Levy, I.S., et al., "Recommended Temperature Limits for Dry Storage of Spent Light Water Reactor Zircaloy-Clad Fuel Rods in Inert Gas," PNL-6189, (May 1987).

- [4.3.2] Johnson, Jr., A.B. and Gilbert, E.R., "Technical Basis for Storage of Zircaloy-Clad Spent Fuel in Inert Gases," PNL-4835, (September 1983).
- [4.3.3] "Spent Fuel Heat Generation in an Independent Spent Fuel Storage Installation," Regulatory Guide 3.54, Revision 1, (January 1999).
- [4.3.4] Cunningham et. al., "Evaluation of Expected Behavior of LWR Stainless Steel-Clad Fuel in Long-Term Dry Storage," EPRI TR-106440, (April 1996).
- [4.3.5] Schwartz, M.W., Witte, M.C., Lawrence Livermore National Laboratory, "Spent Fuel Cladding Integrity During Dry Storage," UCID-21181.
- [4.3.6] "Temperature Limit Determination for the Inert Dry Storage of Spent Nuclear Fuel," EPRI TR-103949, (May 1994).
- [4.3.7] Schemel, J.H., "ASTM Manual on Zirconium and Hafnium," STP 639, American Society for Testing and Materials, (December 1977).
- [4.4.1] Wooton, R.O. and Epstein, H.M., "Heat Transfer from a Parallel Rod Fuel Element in a Shipping Container," Battelle Memorial Institute, (1963).
- [4.4.2] Rapp, D., "Solar Energy," Prentice-Hall, Inc., Englewood Cliffs, NJ, (1981).
- [4.4.3] Siegel, R. and Howell, J.R., "Thermal Radiation Heat Transfer," 2nd Edition, McGraw Hill (1981).
- [4.4.4] Holman, J.P., "Heat Transfer," 6th ed., McGraw Hill Book Company, (1986).
- [4.4.5] Sanders et al., "A Method for Determining the Spent-Fuel Contribution to Transport Cask Containment Requirements," Sandia Report SAND90-2406, TTC-1019, UC-820, page II-127, (November 1992).
- [4.4.6] Hewitt, G.F., Shires, G.L. and Bott, T.R., "Process Heat Transfer," CRC Press, (1994).
- [4.4.7] Hagman, Reymann and Mason, "MATPRO-Version 11 (Revision 2) A Handbook of Materials Properties for Use in the Analysis of Light Water Reactor Fuel Rod Behavior," NUREG/CR-0497, Tree 1280, Rev. 2, EG&G Idaho, August 1981.
- [4.4.8] "Effective Thermal Conductivity and Edge Conductance Model for a Spent-Fuel Assembly," R. D. Manteufel & N. E. Todreas, Nuclear Technology, 105, 421- 440, (March 1994).

[4.4.9] "Spent Nuclear Fuel Effective Thermal Conductivity Report," US DOE Report BBA000000-01717-5705-00010 REV 0, (July 11, 1996).

[4.4.10] NUREG-1536, "Standard Review Plan for Dry Cask Storage Systems," USNRC, (January 1997).

[4.4.11] "Fuel Cladding Cladding Temperatures in Transport and Storage Casks Development and Validation of a Computation Method," S. Anton, Ph.D. Thesis (German) RWTH Aachen, Germany, 1997.

[4.4.12] "Topical Report on the HI-STAR/HI-STORM Thermal Model and its Benchmarking with Full-Size Cask Test Data", Holtec Report HI-992252, Rev. 1.

APPENDIX 4.A: CLAD TEMPERATURE LIMITS FOR HIGH-BURNUP FUEL

4.A.1 INTRODUCTION

The current revision of NUREG-1536 [4.A.1] for storage of spent fuel in dry storage casks essentially limits fuel burnup to 45 GWd/MTU. In light of the continuous improvements in fuel bundle design and manufacturing technologies and longer fuel cycles, the quantity of fuel assemblies with burnups in excess of 45 GWd/MTU stored in the spent fuel pools is expected to rise at a rapid pace. It is therefore necessary to address the storage of these high-burnup fuel assemblies in Holtec's storage system. This appendix presents a summary of the methodology developed by Holtec for determining suitable clad temperature limits consistent with the intent of the regulatory review guidelines presented in ISG-15 [4.A.2]. The governing mode for cladding failure, as specified in ISG-15, is assumed to be thermal creep, and the strain limit is set equal to 1% in spite of growing scientific evidence that supports a 2% minimum strain limit. Finally, an alternative criterion for categorizing a spent nuclear fuel (SNF) as "damaged" is proposed in lieu of the ISG-15 criterion which, based on recent data, would needlessly classify a large quantity of high burnup intact SNF as "damaged". This deviation from the guidance contained in ISG-15 has been added to the list of deviations from NUREG-1536 in Table 1.0.3.

4.A.2 REGULATORY GUIDANCE

NRC ISG-15 [4.A.2] presents the current regulatory position on storage and transport of high-burnup spent fuel assemblies. For the purpose of storage in the HI-STORM system, we define high-burnup spent fuel as any fuel assembly with an assembly average burnup greater than 45 GWd/MTU. This definition is consistent with ISG-15.

The mode of failure is postulated to be excessive hoop dilation of the pressurized tubes (fuel rods). Failure is postulated to occur when the cumulative strain reaches 1%. ISG-15 does not prescribe a mathematical model to compute the creep rate. It is incumbent on the certificate holder or licensee to propose an appropriate correlation. In this appendix, we present such a correlation along with the necessary justifications to substantiate its veracity.

ISG-15 also provides a set of fuel integrity criteria predicated on the extent of corrosion (oxidation) of the fuel cladding to define when a high burnup spent nuclear fuel should be treated as damaged. We discuss the ISG integrity criteria vis-à-vis our proposed criteria in a later section in this appendix.

4.A.3 CREEP DEFORMATION MECHANISM AND FAILURE STRAIN

Failure of the fuel cladding in dry storage is postulated to occur from the visco-elastic-plastic effect known as creep. The fuel cladding very gradually dilates in the manner of a pressurized tube under the influence of internal pressure of the contained gas. The predominant stress component in the cladding is the hoop stress, σ , which is readily computed by the classical Lamé's formula:

$$\sigma = pr/t \quad (1)$$

where p , r and t are, respectively, the net outward pressure acting on the cladding in dry storage, inside cladding radius and cladding wall thickness.

Classical creep mechanics instructs us that the magnitude of stress, σ , and the coincident metal temperature, T , are the most significant variables in determining the rate of creep for a given material. The development in predicting creep behavior of pure metals and alloys has traditionally followed the path of measuring the creep rate while holding the stress and temperatures constant and then developing a compact mathematical correlation that accords with the measured data. This process, quite logical in light of the absence of an identifiable fundamental constitutive relation for metal creep, has spawned numerous creep equations in the past ninety years. Lin, in his text on creep mechanics [4.A.7] published in 1968, cites eight general correlations: Many more have followed in the years since then. Attempts by the American Society of Metals to correlate the multitude of correlations [4.A.8], each purporting to represent the creep behavior of certain metals and alloys with precision, ended up in an essentially non-specific recommendation that recognizes creep rate as a complex and non-linear function of stress and temperature.

To propose a creep equation for irradiated Zircaloy, an appropriate relationship for strain as a function of stress, temperature and time must be defined. Then the available experimental data on irradiated Zircaloy must be used to correlate and benchmark the functional relationship.

Having developed an experimentally corroborated creep rate functional relationship, the next step in the analysis process is to determine the permissible peak cladding temperature at the start of dry storage that will limit the total creep strain accumulation in the hottest fuel rod in forty years of dry storage to 0.01.

Holtec International has proposed 1% uniform circumferential creep strain of the fuel cladding as a conservative limit for the purpose of establishing the permissible peak cladding temperature, T_p , in dry storage, even though independent work by EPRI [4.A.9], citing several references, including a recent experimental work by Goll [4.A.10], asserts that the 1% strain limit is "overly

The test creep experiments by Goll et al. [4.A.10] appear to have been expressly performed to establish the failure strain limit of high burnup SNF (54 to 64 GWD/MTU) with a heavy oxide layer (up to $\sim 100 \mu\text{m}$). To achieve circumferential strains in the range of 2% in a short period, the samples were subjected to a much higher stress (400 to 600 MPa) than would be obtained in dry storage of spent nuclear fuel (<150 MPa). The experiments included 21 creep tests on samples of two rods, none of which failed at 2% hoop strain. Ductility tests on cladding containing radially oriented hydrides also exhibited unbreached integrity at 100 MPa and 423°K, indicating that the increased vulnerability of the fuel cladding in the presence of radially oriented hydride lenses is not a cladding integrity limiting condition.

Oxidation of the cladding during reactor operations is an immutable fact. Oxidation leads to flaking or spalling of the cladding, resulting in a reduction of the tube wall, t , development of a rough external surface (stress raisers) and incursion of hydrogen into the cladding microstructure.

Spalling of the fuel cladding, associated with oxidation of zirconium, is a function of numerous variables, including reactor operation history, water chemistry, areal power density, coolant temperature, and burnup. Spalling or flaking introduces a local surface discontinuity on the cladding surface. However, burst test data on spalled cladding by Garde et al. [4.A.11], if interpreted properly, as shown by EPRI [4.A.9], support the conclusion that a 1% creep strain limit is conservative even for spalled cladding where the hydride lenses, formed as a byproduct of the oxidation process, have penetrated as far as the cladding mid-wall. EPRI [4.A.9] computes the Critical Strain Energy Density (CSED) [4.A.15, 4.A.16] corresponding to the Garde data to be 5 MPa, which corresponds to the fracture toughness value, K_{IC} , of $7.8 \text{ MPa}\sqrt{m}$. EPRI computes the K_{IC} for the heavily spalled cladding (up to 50% hydride penetration) at 1% creep to be $3.8 \text{ MPa}\sqrt{m}$, thus demonstrating that 1% creep strain limit is conservative. Recent work by Jarheiff, Manzel, and Ortlieb [4.A.17] corroborates EPRI's position by showing that at even up to 2,000 ppm hydride concentration (which will develop only under extremely high levels of burnup), the ductility of irradiated Zircaloy is essentially undiminished.

Failure strain under rapidly applied mechanical loading is a measure of the ductility of the material, which can be significantly lower than the creep strain limit. EPRI [4.A.9] suggests using the strain energy density at failure in burst tests as the invariant parameter to estimate the corresponding creep strain limit for the material. Using this method and typical temperatures and pressures attendant to dry storage, the creep strain limit may be as much as five to ten times the plastic failure strain under burst tests.

Burst tests on irradiated fuel cladding from commercial reactors (Calvert Cliffs Unit 1, ANO Unit 2, Ft. Calhoun) by Garde et al. [4.A.11] show that "ductility of Zircaloy-4 irradiated to fluence levels of $1.2 \times 10^{22} \text{ n/cm}^2$ ($E > 1 \text{ MeV}$) at LWR operating temperatures of roughly 600°K is about 3 to 4% and depends on the hydride precipitate local volume."

It is generally recognized that the tertiary creep stage [4.A.7, pp. 60-61] is essentially obviated if the material is subject to a constant stress (rather than a constant load, which is common in most engineering applications). Andrade explained the difference between constant load and constant stress creep in 1910: His classical curve [4.A.7, p. 61] is reproduced herein as Figure 4.A.1. The case of irradiated fuel cladding in dry storage, however, belongs to the special class of problems wherein the stress would decrease as the fuel rod containing a fixed quantity of gas at a constant temperature increases in diameter with passage of time due to creep. This is due to the fact that, based on the perfect gas law, the increase in the cladding diameter due to creep reduces the pressure exerted by the contained gas. The increase in diameter also causes a concomitant reduction in the cladding wall thickness. Since the hoop stress σ , governed by Lamé's formula (Equation 4.A.1) is proportional to the radius and internal pressure, and inversely proportional to

the wall thickness, it is shown in the following that the hoop stress will remain essentially constant as the cladding radius increases due to creep if the fuel rod were a hollow tube (no fuel pellets) and will decrease if the gas is contained in the annulus between the pellets and the rod.

To quantify the reduction in gas pressure, p , due to creep-induced increase in the rod diameter, let us consider a unit length of a fuel rod of inside radius, r , and initial wall thickness, t , containing a fuel pellet of radius a . The pellet is assumed to be rigid and the gas is assumed to be confined to the annular region defined by radii r and a . If the inner radius of the rod expands to $(r+\Delta r)$ due to creep, then the annular space will accordingly increase, reducing the gas pressure to say, p' . p' is related to p by the perfect gas law:

$$p' [(r + \Delta r)^2 - a^2] = p (r^2 - a^2)$$

Neglecting the terms of second order, we have

$$p' = \frac{p b^2}{b^2 + 2 r \Delta r} \quad (2)$$

where we have defined

$$b^2 = r^2 - a^2 \quad (3)$$

Since the increase in circumference of the rod due to increase in radius by Δr causes a corresponding decrease in the rod wall thickness by Δt to maintain a constant metal volume, we have

$$2\pi (r + \Delta r) (t - \Delta t) = 2\pi r t$$

or
$$r \Delta t = t \Delta r \quad (4)$$

The initial stress σ is given by Equation (1), the final stress σ' after creep to radius Δr is given by

$$\sigma' = \frac{p' (r + \Delta r)}{(t - \Delta t)} \quad (5)$$

Substituting for p' from Equation (2), utilizing Equation (4), and neglecting terms of higher order, we obtain

$$\sigma' = \frac{pr}{t} \left[1 - \frac{2\bar{A}\bar{A}a^2}{r \cdot b^2} \right] \quad (6)$$

The fractional decrease in stress is given by Eqs. (1) and (6); we have

$$\frac{\sigma - \sigma'}{\sigma} = \frac{\bar{A}\sigma}{\sigma} = 2c\bar{\nu}^2 \quad (7)$$

where

$$c = \frac{\bar{A}r}{r} \quad (8)$$

and:

$$\bar{\nu}^2 = \frac{a^2}{r^2 - a^2} \quad (9)$$

We note that in the case of a hollow tube (i.e., no pellets, $a = 0$), $\chi=0$ and $\Delta\sigma = 0$, i.e., the hoop stress will not change with creep. However, for the case of a fuel rod containing pellets (the real life case), the drop in the stress level with creep is a strong function of χ . If we assume that $a = .99r$, then $\bar{\nu}^2 = 49.25$. Using Equation (7), we find that the percentage reduction in stress is 98.5%, corresponding to 1% creep ($c=\Delta r/r = .01$). In a fuel rod, the gas is in the annulus as well as in the plenum. For a typical fuel rod, EPRI [4.A.9] estimates that the reduction in stress is 17% for 1% creep.

In view of the foregoing, the condition of rapid straining leading to gross rupture that characterizes failure in the tertiary creep domain can be ruled out for fuel cladding in dry storage (Figure 4.A.1). In fact the state of hoop stress in the fuel cladding suffers additional decrease as the heat emission rate from the fuel declines, resulting in the decrease of the gas temperature (and hence, pressure) inside the rods.

To summarize:

- The process of creep will result in a reduction in the cladding hoop stress even if the gas temperature were to remain constant.
- The continuous reduction in the heat emission rate from the fuel correspondingly reduces the gas temperature in the fuel rods, leading to an additional reduction in the hoop stress.
- Creep in fuel rods in dry storage belongs to the special class of problems where the actuating stress decreases with time, thus inoculating the fuel rod against tertiary creep (which is characterized by rapid deformation).

Finally, a fundamental characteristic of creep in metals is its relationship to the mechanical properties of the material. The rate of creep is known to decrease monotonically with the increase in yield strength. The creep strain limit also reduces as the ductility of the material

(measured by its "elongation" in the terminology of ASTM) is reduced. The effect of irradiation is to modify Zircaloy's microstructure resulting in an increase in the yield strength and reduction in the ductility. This would imply a reduced rate of creep and a lower creep limit for the irradiated cladding than its unirradiated counterpart. However, both the yield strength and elongation curves tend to flatten out at high burnup levels (fluence $\approx 10^{22}$ N/cm² (E > 1 MeV)) [4.A.12, 4.A.13], suggesting that the Holtec creep equation and 1% creep limit will remain conservative for burnups up to 68,400 MWD/MTU.

4.A.4 ZIRCALOY CREEP STRAIN MODELING: PRIOR WORK

An experimental program to compile creep data on internally pressurized irradiated Zircaloy fuel cladding has been carried out jointly by GNB and Siemens AG [4.A.3]. In this experimental study, internally pressurized Zircaloy samples were irradiated for 10,000 hours at a variety of temperatures and hoop stresses. Test temperatures for each sample were held constant over the entire irradiation period and ranged from 250°C to 400°C. Hoop stresses are temperature dependent and were also, therefore, held constant for each sample over the entire irradiation period and ranged from 80 MPa to 150 MPa. Creep was measured for up to 10,000 hours.

The GNB/Siemens researchers also proposed an empirical model that could be used to predict cladding creep as a function of the cladding hoop stress and temperature. Their model, which we henceforth refer to as the "Siemen's model", is fully described in Reference [4.A.3] and is, therefore, merely summarized in this subsection. The Siemen's creep equation is given as:

$$\dot{\epsilon} = At^m \quad (10)$$

where:

- ϵ = the total creep strain at time t (%)
- A = the so-called "initial creep strain" (%)
- t = the storage time (hr)

The exponent 'm' on the time value in Equation (10) is expressed as a high-order polynomial function as:

$$m = \sum_{i=1}^{11} c_i \times T_f^{i-1} \quad (11)$$

In Equation (11), the c_i values are constants and T_f is a function of hoop stress and the temperature. The constants are given as:

$c_1 = 0.361705 \times 10^{-13}$	$c_7 = -0.126131 \times 10^{-12}$
$c_2 = 0.500028 \times 10^{-3}$	$c_8 = 0.433320 \times 10^{-15}$
$c_3 = -0.555901 \times 10^{-6}$	$c_9 = -0.835848 \times 10^{-18}$
$c_4 = 0.715481 \times 10^{-7}$	$c_{10} = 0.842689 \times 10^{-21}$
$c_5 = -0.181897 \times 10^{-8}$	$c_{11} = -0.345181 \times 10^{-24}$
$c_6 = 0.207254 \times 10^{-10}$	

and T_f is given as:

$$T_f = T + (\sigma - 80) \times \frac{45}{70} \quad (12)$$

where:

T is the cladding temperature ($^{\circ}\text{C}$)

σ is the cladding hoop stress (MPa)

Equation (12) is held in the Siemen's formulation to be valid for temperatures between 100°C and 400°C and for hoop stresses between 80 MPa and 150 MPa.

As stated above, we refer to the modeling approach embodied in Equations (10) through (12) as the Siemen's model. This model does, however, have some shortcomings.

Figure 10 of a paper by Dr. Martin Peehs [4.A.4], using the recommended [4.A.3] initial creep strain (A) of 0.04% shows that the Siemen's model more closely approximates the creep behavior of unirradiated Zircaloy and is inordinately conservative for irradiated Zircaloy. As the model is intended for use in determining clad temperature limits for high-burnup fuel assemblies, this might result in erroneous low temperature limits.

The perceived over-conservatism in the Siemen's correlation was empirically remedied in the recent WESFLEX application [4.A.5] by dividing the cumulative creep predicted by the Siemen's model by a factor of two.

Unfortunately, the Siemen's model correlates poorly with the recent creep data published by Goll et al. [4.A.10]. Therefore, it was decided to develop a creep equation for irradiated Zircaloy, using standard procedures, that benchmarks satisfactorily with all publicly available data.

4.A.5 IRRADIATED ZIRCALLOY TEST DATA

In this section, we provide a listing of all test data that is utilized herein to benchmark the proposed Holtec creep model. The test data that we are seeking to utilize pertains to experimentally measured creep in irradiated Zircaloy. Although the published data in this area are admittedly sparse, cited bibliographies and public-domain documents have been reviewed to adequately cover the range of stress and temperature conditions in dry storage.

Five sources of creep data are identified for benchmarking the Holtec creep model. The first data source is from the published creep results by Spilker et al. [4.A.3]. The test conditions are:

Temperature: 400°C
Stress: 70 MPa
Time: 1,000-6,000 hrs.

The second data source is from the Kaspar et al. high temperature creep data reported in a docketed dry storage document [4.A.22]. The test conditions for this data are:

Stress: 86 MPa
Temperature: 380°C (0-1,000 hrs)
395°C (>1,000 hrs)
Time: 1,000-8,000 hrs

The third source of data is from the accelerated creep testing by Goll et al. [4.A.10]. The testing was done on samples of Zircaloy cladding from fuel rods of up to 64,000 MWD/MTU burnup. The test conditions are summarized below:

Stress: 320 MPa to 630 MPa
Temperature: 300°C to 370°C
Time: 2 to 189 hrs

The fourth source of data is from the low temperature creep testing by Einziger and Kohli [4.A.20] on irradiated Turkey Point fuel rods. A total of five pressurized rods were tested at 323°C for a time period of between 31 to 2,101 hrs, and stress of between 146 MPa to 157 MPa. Four of the rods lost their pressure because of an end cap brazing failure.

The test conditions for the rod (TPD04-H6) that retained its pressure are:

Temperature: 323°C
Stress: 146 MPa
Time: 2,101 hrs
Cladding Strain: 0.157%

The fifth data source is from the low temperature creep testing by Kaspar et al. [4.A.21] on irradiated KWO samples. The test conditions are:

Temperature: 350°C
Stress: 50 MPa
Time: 1,000 to 8,000 hrs

4.A.6 PROPOSED CORRELATION (HOLTEC MODEL)

The experimental data cited in the foregoing provides us with creep data for different stress levels up to about 600 MPa and for different temperatures (up to 400°C). While the database is admittedly not copious, it is adequate to provide the means to establish the coefficients in a creep equation of standard form, which, according to classical creep mechanics [4.A.7; 4.A.19, p. 95] should have the following key characteristics:

- i. The accumulated creep bears a hyperbolic function relationship to the hoop stress, σ , i.e.,

$$\epsilon \sim \sinh(\gamma\sigma)$$

- ii. The temperature dependence (T) of the accumulated creep follows the Arrhenius equation; $\epsilon \sim \exp\left(-\frac{\alpha\epsilon}{RT}\right)$

where ζ is the activation energy, R is the universal gas constant, and T is the absolute temperature.

- iii. Recognizing that the test data exhibits continuously decreasing creep rate (i.e., the slope of the creep-time curve is continuously decreasing), the correlation should be appropriate for primary creep of the form $\epsilon \sim \tau^\beta$ where $\beta < 1$, and τ is the time coordinate.

In other words, the Holtec creep model constructed from the above three functional elements is of the form:

$$\epsilon = \alpha \exp\left(-\frac{\zeta}{RT}\right) \sinh(\gamma\sigma) \tau^\beta \quad (13)$$

where α , $\alpha\epsilon$, γ , and β are creep constants with values suitably selected to bound all relevant irradiated cladding creep data and R is the Universal Gas constant (8.31 J/(g-mol^oK)). Differentiating ϵ with τ will give the rate of creep, ϕ , as a function of time.

$$\phi = \frac{d\epsilon}{d\tau} \quad (14)$$

The correlation provided in Equation (13) is applicable in the primary creep stage. Creep is assumed to transition into the secondary regime when ϵ reaches 0.5%.

Figures 4.A.2-4.A.5 show the creep rate predicted by the proposed Holtec creep model against the previously discussed test data. Five principal sources of creep data are identified for benchmarking the creep model. The first data source is shown plotted in Figure 4.A.2 from the Spilker et al. experiments on irradiated fuel rods. The second data source is the Kaspar et al. irradiated cladding creep strain results shown plotted in Figure 4.A.3. The third source of data is by Goll et al. [4.A.10]. The data from the first two sources was essentially at constant stress and temperature and strain was measured at several instants in time. The family of creep strain vs. time relationships are therefore amenable to a graphical representation in a single plot. In contrast, the Goll et al. data is a single creep strain measurement at the end of each experiment at a stress and temperature that was different in each experiment. The stress and temperature range

for the experiments covered a large band (320 to 630 MPa & 300 to 370°C). Therefore, to display the benchmark results from the collected data, a scatter plot of the experimental creep strain vs. Holtec model creep strain is provided in Figure 4.A.4. A straight line representing the ordinate equal to experimental creep strain is shown to aid the reader in confirming that in all cases the Holtec model correlates with the measured creep strain with suitable margins.

For the Einziger and Kohli [4.A.20] creep strain data on the intact TPD04-H6 rod sample, the Holtec Creep Model computes a creep strain of 0.191%. This bounds the measured creep strain of 0.157% by a respectable margin (21.6%). A comparison of the Holtec creep model predictions for the KWO creep testing conditions [Kaspar et al., 4.A.21] is shown in Figure 4.A.5. The Holtec predictions bound the KWO creep curve over the range of time (0 to 8,000 hrs). In the 4,000 to 8,000 hrs time interval, the Holtec model exhibits a diverging trend from the KWO creep curve in the conservative direction. In other words, the slope of the Holtec creep model is steeper than the Kaspar et al. creep curve. Thus, creep strain beyond 8,000 hrs is overestimated by the Holtec creep model.

It is quite obvious from the foregoing that the proposed correlation accords well with the available test data, bounding some with large margins. It is thus established that the proposed creep equation is suitable to bound (not predict) the rate of creep that high burnup fuel in dry storage will sustain with the passage of time.

4.A.7 APPLICATION TO STORAGE IN HI-STORM

Equation (13) provides an appropriate vehicle for computing the accumulated creep over a time, say τ^* , if the stress σ and metal temperature, T , are known. If σ and T are varying with time, then the accumulated creep ϵ will be calculated by integrating the rate of creep ϕ ($\phi = d\epsilon/d\tau$) over the time period in dry storage. Therefore, in the HI-STORM system, where σ and T decrease with time, the total creep ϵ is computed by

$$\dot{\epsilon} = \int_0^{\sigma} \ddot{\sigma} \, d\sigma \quad (15)$$

where $\ddot{\sigma} = \frac{d\dot{\sigma}}{d\sigma}$

ϵ is given by Equation (13). The creep rate, ϕ , like ϵ , is a function of σ and T .

Hoop stress is directly proportional to internal pressure, which itself is a function of the gas temperature. The fuel temperatures in dry storage casks like the HI-STORM system, however, are not constant but rather decrease over the duration of the dry storage period. To accurately predict the fuel cladding creep strain, this time-varying temperature behavior must be properly incorporated.

It is recognized that the stress σ in a fuel rod will depend on its radius to cladding thickness ratio and internal pressure. Referring to the table of SNF types (Tables 4.3.3 and 4.3.6), it is evident that the r/t ratio varies widely among the various SNF types. To establish a common peak cladding temperature (PCT) limit for all SNF of a given type, we select one upper bound r/t ratio for PWR fuel and one for BWR fuel so that all SNF types included in this FSAR are covered. We assume:

$$w = r/t = 10.5 \text{ (PWR fuel)} \quad (16a)$$

$$w = r/t = 9.5 \text{ (BWR fuel)} \quad (16b)$$

For a specific SNF, defined by cladding thickness t_g and internal radius r , Equations 16a and 16b imply that a certain amount of its wall thickness, Δ , is not recognized in the hoop stress computation. Δ is given by:

$$\text{For PWR fuel; } \Delta = t_g - \frac{r}{10.5} \quad (17a)$$

$$\text{For BWR fuel; } \Delta = t_g - \frac{r}{9.5} \quad (17b)$$

Δ represents the cladding unused thickness not accounted for in the creep analysis and, hence, can be viewed as the "corrosion reserve" in the specific SNF type. Having defined an upper bound r/t , we now need to use an upper bound internal pressure at the start of dry storage to establish the hoop stress, σ , at the beginning of dry storage. In Section 4.3.1, the upper bound of the internal pressure p is set at 2,000 psi and 1,000 psi, respectively, for PWR and BWR SNF at the reference temperature θ_r ($\theta_r = 387^\circ\text{C}$ (PWR), 311°C (BWR)). Both the PWR and BWR cladding internal pressure values, as discussed in Section 4.3.1, are quite conservative.

The stress in the fuel cladding is given by the Lamé's formula (Equation (1)).

Using the r/t value given by Equations (16a) and (16b) above, the hoop stress in the cladding at the gas temperature, θ_r , is given as:

$$\begin{aligned} \sigma &= (10.5) (2,000) = 20,500 \text{ psi or } 144.7 \text{ MPa (PWR)} \\ &= (9.5) (1,000) = 9,500 \text{ psi or } 65.5 \text{ MPa (BWR)} \end{aligned} \quad (18)$$

In the next step it is necessary to define the variation of hoop stress σ with time. The internal pressure, p , in the fuel rod (and, therefore, σ through Lamé's equation) will decrease with the passage of time due to two discrete effects: (i) creep-induced increase in the cladding diameter explained in Equation (7) and Subsection 4.A.3 above, and (ii) reduction in the bulk temperature of the contained gas due to the monotonic decline in the heat generated by the stored SNF.

For conservatism, the creep-induced pressure reduction is neglected completely. The reduction in the cladding internal pressure due to the continuing reduction in the heat emission rate is determined by ascertaining the rod bulk gas temperature, θ , as a function of time (in storage in HI-STORM).

The internal gas pressure p corresponding to gas temperature θ (in °C) is given by the perfect gas law

$$p = \frac{p_r (\dot{e} + 273)}{(\dot{e}_r + 273)} \quad (19)$$

where $p_r = 2,000$ psi and 1,000 psi for PWR and BWR SNF, respectively.

Using Equation (1), the corresponding stress σ is given by

$$\sigma = \frac{p_r (\dot{e} + 273)}{(\dot{e}_r + 273)} \frac{r}{t} \quad (20)$$

It is recognized that both the cladding temperature, T , and gas temperature, θ , depend on the system heat generation rate, Q , and the thermal characteristics of the storage system (HI-STORM). Because the HI-STORM system is certified to store a large array of PWR and BWR SNF types, it is necessary that the T and θ functions be defined in a conservative manner to bound all SNF types (a conservative T or θ function means one whose attenuation with time is "less steep" than all SNF types covered by the CoC.) For this purpose, we must first define the heat generation decay function (η) in a conservative manner. Recognizing that the $Q(\tau)$ function will attenuate least rapidly with time, τ , for bounding burnup (b) and uranium content in the SNF, we select $b=70$ GWD/MTU and the B&W 15x15 SNF (uranium content = 495 kg) as the reference PWR SNF. Henceforth, we will refer the SNF with the bounding burnup and uranium content simply as the "bounding SNF". For the same reason, we select GE 7x7 as the reference BWR SNF. The η functions for the reference PWR and BWR SNF are shown in Figure 4.A.6 and 4.A.7, respectively. In Figures 4.A.6 and 4.A.7, η is plotted as the ratio of heat generation of the "bounding SNF" to that at PCDT = 5 years.

In the next step, the HI-STORM 100 thermal model (described in Chapter 4) was used for discrete values of Q to determine T and θ as a function of Q . Strictly speaking, the T and θ functions will be very slightly different for the different MPC types (because of the small differences in their gross heat dissipation capacities). The analytical (curve fit) relationships developed for $T(Q)$ and $\theta(Q)$ are accordingly developed to bound the curves obtained by the HI-STORM thermal model analysis. Figure 4.A.8 shows the postulated $T(Q)$ curve and the computed $T(Q)$ curve using FLUENT for MPC-24 to illustrate the conservatism. Likewise, Figure 4.A.9 shows the postulated $\theta(Q)$ curve and the computed $\theta(Q)$ using FLUENT for hottest

PWR canister (MPC-24). T (Q) and $\theta(Q)$ plots for BWR fuel are provided in Figures 4.A.10 and 4.A.11.

These enveloping $\theta(Q)$ and T(Q) curves along with the appropriate $\eta(\tau)$ curve (Figure 4.A.6) for PWR SNF and Figure 4.A.7 for BWR SNF) are essential for utilizing the Holtec creep model. The T curve (cladding metal temperature), of course, is the direct input variable in the creep equation. The θ curve, through Equation (20), provides the means to compute the hoop stress, σ , as a function of the time coordinate.

The procedure to compute the peak cladding temperature (PCT) limit using the creep equation (Equation 13) for the HI-STORM system to store an MPC containing SNF of a certain age (post-core decay time (PCDT)) can now be outlined.

Let τ_0 denote the PCDT at which the SNF is placed in dry storage in HI-STORM. The object is to calculate the PCT, T_p , such that the accumulated creep in 40 years of storage is 1%.

In other words, the mathematical problem resolves to computing T at $\tau = \tau_0$ such that ϵ_s is 1%; i.e.,

Determine T at $\tau = \tau_0$ such that

$$\dot{a}_s = \int_{\delta_0}^{\delta_0 + \delta} \varphi(\delta\delta T) d\delta \leq 1\% \quad (21)$$

where τ_0 is the PCDT at which the SNF is placed in dry storage, $\tau^* =$ the design life of 40 years.

The problem of determining the permissible initial cladding temperature T_p when the fuel is placed in dry storage such that the value of the integral (in Equation 21) is equal to 1% requires an iterative analysis with assumed values of the initial fuel cladding temperature, T_0 . The computation proceeds as follows:

- i. Assume a value of the peak cladding temperature at τ_0 (say T_0). (τ_0 is the post-core decay time at which the SNF is placed into dry storage)
- ii. Use the T-Q curve (Figure 4.A.8 or 4.A.10, as applicable) to obtain the associated value of the heat generation rate, Q_0 .
- iii. From Figure 4.A.9 or 4.A.11 as applicable, obtain the associated value of the gas temperature, θ_0 . Equation (20) provides the associated hoop stress, σ_0 .
- iv. With T_0 and σ_0 defined, the rate of creep, φ , is provided by Equation (14).

- v. To compute the value of ϕ , at the next time step ($\tau_0 + \Delta\tau$), updated values of σ and T are required. For this purpose, the coincident heat generation rate Q is obtained by using Figure 4.A.6 or 4.A.7, as applicable, which provides Q at any time τ through the simple algebraic relationship

$$Q = \frac{Q_0 \eta}{\eta_0} \quad (22)$$

where η is the value of the dimensionless heat generation rate at the PCDT of interest, and η_0 is the corresponding value at τ_0 (PCDT at the initiation of dry storage). Figure 4.A.8 (or 4.A.10) and 4.A.9 (or 4.A.11), respectively, provide the associated T and θ . Equation (20) provides the associated σ . This process is repeated at incremental time steps. In this manner, time history of σ and T as a function of τ (starting at σ_0 and T_0 computed for $\tau = \tau_0$) is obtained for the 40-year duration.

- vi. Equation (21) is used to compute the total accumulated creep, ϵ_s , in 40 years ($\tau^* = 40$ years).
- vii. If the value of ϵ_s is greater than 1%, then the initial assumed value of the peak cladding temperature, T_0 , is appropriately adjusted and the calculation returns to Step (i) above.
- viii. The process is repeated until the computed ϵ_s is close to 1% within a small tolerance (set equal to 0.001) in the numerical analysis. The converged value of T_0 is the permissible cladding temperature (T_p) for fuel placed in dry storage at PCDT = τ_0 .

4.A.8 ALLOWABLE CLAD TEMPERATURE LIMITS

Using the Holtec creep model described in the preceding section, allowable peak clad temperature limits for high-burnup fuel assemblies have been determined. These calculated temperature limits are presented in Table 4.A.1, below.

Table 4.A.1
Allowable Peak Clad Temperature Limits for High Burnup Fuel from Holtec Creep Model

Fuel Age at Initial Loading	PWR Fuel Limit	BWR Fuel Limit
5 years	361.55°C [682.79°F]	397.63°C [747.73°F]
6 years	358.00°C [676.40°F]	393.49°C [740.28°F]
7 years	354.80°C [670.64°F]	390.26°C [734.47°F]
10 years	349.15°C [660.47°F]	384.49°C [724.08°F]
15 years	345.78°C [654.40°F]	380.95°C [717.71°F]

The temperature limits in Table 4.A.1, it should be recalled, are obtained using a most conservative equation of state for creep, a bounding value of internal gas pressure at the start of fuel storage, an upper bound value for cladding radius-to-thickness ratio (10.5 for PWR and 9.5 for BWR fuel), and a 1% limit on creep deformation in 40 years of storage. To build in even additional margins in the allowable heat load for the MPCs, the PCT limit is further reduced, as shown in Table 4.A.2. The values in Table 4.A.2 are the ones used in the thermal analysis in Chapter 4. The PCT limits in Table 4.A.2, as can be ascertained by direct comparison with Table 4.A.1, are as much as 39.85°C less. This additional margin in the PCT limits, admittedly not typical in dry storage applications, has been provided as a first step in addressing the issue of dry storage of high burnup fuel, and may be re-visited.

Table 4.A.2
High Burnup Fuel Allowable Peak Clad Temperature Limits Used in the Thermal Analysis in Chapter 4

Fuel Age at Initial Loading	PWR Fuel Limit	BWR Fuel Limit
5 years	359.7°C [679°F]	393.2°C [740°F]
6 years	348.7°C [660°F]	377.9°C [712°F]
7 years	335.0°C [635°F]	353.7°C [669°F]
10 years	327.2°C [621°F]	347.9°C [658°F]
15 years	321.9°C [611°F]	341.1°C [646°F]

4.A.9 INTACT AND DAMAGED FUEL

ISG-15 states that for a fuel assembly to be considered intact, the following criteria must be met:

- “A1. No more than 1% of the rods in the assembly have peak cladding oxide thicknesses greater than 80 micrometers.
- A2. No more than 3% of the rods in the assembly have peak cladding oxide thicknesses greater than 70 micrometers.”

ISG-15 provides the bases for the conditions and guidelines presented above. The limits on cladding oxide thickness are intended to ensure that the hydrogen concentration in the cladding micro-structure does not exceed 400 to 500 parts per million. The creep strain limit of 1%, along with hydrogen concentration limits, are intended to ensure that cladding perforation does not occur. Specifically, ISG-15 states:

“The staff believes that Zircaloy cladding can withstand uniform creep strains (i.e., creep prior to tertiary or accelerating creep strain rates) of about 1% before the cladding can become perforated if the average hydrogen concentration in the cladding is less than about 400 to 500 parts per million (ppm). This amount of hydrogen corresponds to an oxide thickness of approximately 70-80 micrometers using the recommended hydrogen pickup fraction of 0.15 from Lanning, et al, and Garde. The staff also believes that the strength and ductility of irradiated Zircaloy do not appear to be significantly affected by corrosion-induced hydrides at hydrogen concentrations up to approximately 400 ppm.

According to ISG-15, the thickness of the cladding oxide layer needs to be determined prior to loading for high burnup fuel. Only those high-burnup fuel assemblies that meet both of the oxidation conditions presented above may be stored as intact; all other assemblies must be treated as potentially damaged fuel. This, as we discuss below, is an overly restrictive requirement, which has prompted Holtec to propose an alternative criterion for damaged fuel as an approved deviation from this regulatory guidance.

Available cladding thickness measurement data on high burnup SNF is quite sparse. However, recent data collected by a Westinghouse PWR owner indicates that the oxidation-induced cladding metal loss can be well in excess of 80µm in a substantial fraction of the population of high burnup fuel. All fuel rods that had experienced a heavy oxide corrosion, however, were found to be intact, i.e., none exhibited loss of pressure boundary integrity. Corrosion data compiled in Japan [4.A.23] reproduced in Figures 4.A.12 and 13 show that the corrosion loss increases rapidly with increasing burnup. In view of the data in Figures 4.A.12 and 13, applying the ISG-15 criteria will a priori consign hundreds of undamaged, high burnup fuel assemblies already stored in the plant's fuel pool to the potentially damaged category. This experience is sure to be repeated at other plants when measurements are taken. Clearly, the oxidation threshold for defining damaged SNF warrants additional consideration.

To propose a technically sound cladding corrosion limit, we must consider two underlying facts, namely: (i) the collateral effect of cladding oxidation on its creep capacity and (ii) the increase in circumferential stress due to loss in the cladding wall thickness.

The effect of cladding oxidation on the creep limit of the cladding material has been assayed by EPRI [4.A.18]. EPRI recommends a 2% creep strain limit for high burnup fuel that may have sustained spallation in the reactor core. Our proposed strain limit of 1% quite clearly provides a significant additional margin over the EPRI/NEI recommendation.

If the 1% creep strain limit is accepted for the spalled cladding, then it is possible to define the acceptable metal loss (oxidation loss) using the hoop stress as the guiding parameter. It is recalled that the computation of the creep strain in Section 4.A.8 in the foregoing has been performed for $\sigma_o = 144.7$ MPa for PWR SNF and 65.5 MPa for BWR SNF, where σ_o = the hoop stress in the fuel cladding at the beginning of dry storage. Furthermore, the internal gas pressure in the cladding, at the beginning of dry storage, p_o , has been assumed to be equal to 2000 psi and 1000 psi for PWR and BWR SNF, respectively. Using Lamé's formula, the maximum cladding stress (σ_o) is computed as the product of p and cladding radius to thickness ratio, w . The value of w has been set as 10.5 and 9.5 for PWR and BWR fuel, respectively, in the calculation of accumulated creep (Section 4.A.8).

In other words, the initial stress σ_o used in the creep analysis in this appendix uses the limiting values of p and r/t as shown in Table 4.A.3.

Table 4.A.3

Assumed Pressure Geometry Parameters for Creep Analysis

	Internal Pressure at the Start of Storage	$w = r/t$	Stress σ_o Computed by Lamé Formula
PWR Fuel	2,000 psi	10.5	144.7 MPa
BWR Fuel	1,000 psi	9.5	65.5 MPa

PWR and BWR fuel assemblies used in commercial reactors in the U.S. have lower values of w than the number used in the creep analysis herein (Table 4.A.3). The metal wall in the as-fabricated fuel in excess of that implied by the value of w in the above table therefore is the available corrosion allowance, Δ . Tables 4.A.4 and 4.A.5 provide the values of Δ using Equation (17) for different PWR and BWR fuel classes using the thinnest cladding assembly type within each class (fuel assembly types in any one class have the same rod O.D. and pitch, but may have different cladding thicknesses). It is evident from these tables that the available Δ in all fuel assembly array/classes is well in excess of 100 μ m.

In view of the information presented in the foregoing, it is proposed that the permitted maximum cladding corrosion be specified so that the value of w in Table 4.A.3 for high burnup fuel is preserved.

Table 4.A.4

Available Corrosion Reserve in PWR Fuel Cladding

Holtec Fuel Assembly Array/Class*	Nominal Cladding Outer Diameter (in.)	Nominal Cladding Thickness (in.)	Available Corrosion* Reserve (μm), Δ
14x14A	0.4	0.0243	192
14x14B	0.417	0.0243	165
14x14C	0.44	0.026	191
15x15A	0.418	0.026	217
15x15B	0.42	0.024	159
15x15C	0.417	0.03	321
15x15D	0.43	0.025	175
15x15E	0.428	0.0245	163
15x15F	0.428	0.023	122
15x15H	0.414	0.022	111
16x16A	0.382	0.025	233
17x17A	0.36	0.0225	190
17x17B	0.372	0.0205	120
17x17C	0.377	0.022	156

* Fuel Assembly Array Classes are defined in Section 6.2

* Any form of corrosion that produces non-adherent (flaked or spalled) metal layers should be considered to be lost for load (pressure) bearing purposes.

Table 4.A.5

Available Corrosion Reserve in BWR Fuel Cladding

Holtec Fuel Assembly Array/Class*	Nominal Cladding Outer Diameter (in.)	Nominal Cladding Thickness (in.)	Available Corrosion* Reserve (μm), Δ
7x7B	0.563	0.032	145
8x8B	0.484	0.034	295
8x8C	0.483	0.032	252
8x8D	0.483	0.03	196
8x8E	0.493	0.034	295
9x9A	0.440	0.028	197
9x9B	0.433	0.026	151
9x9C	0.423	0.0295	262
9x9D	0.424	0.03	275
9x9E	0.417	0.0265	186
9x9F	0.417	0.0265	186
9x9G	0.424	0.03	275
10x10A	0.404	0.026	189
10x10B	0.3957	0.0239	141
10x10C	0.378	0.0243	176

* Fuel Assembly Array Classes are defined in Section 6.2

4.A.10 CLOSURE

A mathematical relationship to conservatively estimate the extent of primary creep in the irradiated Zircaloy cladding has been proposed. The form of proposed creep equation is consistent with the classical metal creep formulation wherein the two principal variables, stress and temperature, respectively, bear an exponential and Arrhenius-type relationship to creep accumulation. The creep equation has been validated against available irradiated cladding creep data and shown to correlated with the measured data in the temperature range (300 to 400°C) and stress range (70 MPa – 630 MPa) with considerable margins. This benchmarked creep equation is used to compute the PCT limits for SNF placed in dry storage after a given amount of time in

* Any form of corrosion that produces non-adherent (flaked or spalled) metal layers should be considered to be lost for load (pressure) bearing purposes.

wet storage (wet storage time is also referred to as "fuel age"). In computing the PCT limits, several assumptions have been made to render a conservative prediction. The key conservatisms (in addition to the use of a creep equation that overpredicts creep for a given stress and temperature) are:

- i. The maximum permissible creep is set at 1%.
- ii. The internal pressure (hence the hoop stress) in the cladding is assumed to remain unchanged due to the creep induced dilation of the rod radius (Equation 7 in Subsection 4.A.3).
- iii. The primary creep that is characterized by a monotonically decreasing creep rate with time is assumed to cease when 0.5% creep has been accumulated and the transition to secondary creep is assumed to begin. Thereafter, the creep rate is conservatively held constant for constant stress and temperature.
- iv. The bounding burnup of 70 GWD/MTU is used to construct the relationship for decay of heat generation from the stored spent nuclear fuel (Figure 4.A.6 and 4.A.7).
- v. The assumed internal rod pressure, which directly affects the level of hoop stress, has been set at a bounding high value for both PWR and BWR SNF.

4.A.11 NOMENCLATURE

- K_{IC} : Fracture Toughness
- p : Internal gas pressure in the fuel rod
- Q : The total heat generation in the HI-STORM 100 MPC.
- r : Inside radius of the fuel rod
- T : Peak cladding temperature
- t : Cladding wall thickness recognized in the hoop stress calculation
- t_g : Nominal thickness of the fuel cladding
- w : Ratio of r to t
- ϵ : Accumulated creep in dry storage (%)
- ϵ_s : Total accumulated creep in 40 years of storage (%)

- τ : Post Core Decay Time (PCTD), i.e., the time elapsed after reactor shutdown
- τ_0 : PCDT at the time the SNF is placed in dry storage (also known as "fuel age")
- θ : Bulk gas temperature in the fuel rod, °C
- ϕ : Rate of creep
- σ : Hoop stress in the fuel cladding
- η : Ratio of $Q(\tau)$ to Q_0

Subscripts

- o: Value of the variable at $\tau = \tau_0$
- a: Ambient
- r: Reference point

4.A.12 REFERENCES

- [4.A.1] "Standard Review Plan for Dry Cask Storage Systems," NUREG-1536, January 1997.
- [4.A.2] USNRC Interim Staff Guidance -15, "Materials Evaluation," Revision 0, January 10, 2001.
- [4.A.3] Spilker et al., "Spent LWR fuel dry storage in large transport and storage casks after extended burnup," Journal of Nuclear Materials 250 (1997) 63-74.
- [4.A.4] Peehs, Martin, "Assessment of Dry Storage Performance of Spent LWR Fuel Assemblies with Increasing Burn-Up," CRP on Spent Fuel Performance Assessment and Research (SPAR): 1st RCM in Washington D.C., April 20 through 24, 1998.
- [4.A.5] Gilbert et al., "Technical Evaluation Report of WCAP-15168 (Dry Storage of High Burnup Spent Nuclear Fuel)," PNNL, February 2000.
- [4.A.6] Levy et al., "Recommended Temperature Limits for Dry Storage of Spent Light Water Reactor Zircaloy-Clad Fuel Rods in Inert Gas," PNL-6189, May 1987.
- [4.A.7] Lin, T.H., "Theory of Inelastic Structures", Wiley (1968).
- [4.A.8] M.A. Meyers and K.K. Chawla, "Mechanical Metallurgy", Chapter 20, page 667, Prentice Hall (1984).

- [4.A.9] "Storage and Transportation of Spent LWR Fuel Having Burnup in Excess of 45 GWD/MTU", NEI submittal to the SFPO dated October 2, 2000 (L. Hendricks to E.W. Brach).
- [4.A.10] W. Goll et al., "Short-Time Creep and Rupture Tests on High Burnup Fuel Rod Cladding, Journal of Nuclear Materials", to be published.
- [4.A.11] Garde, A.M., Smith, G.P. and Pirek, R.C., "Effects of Hydride Precipitate Localization and Neutron Fluence on the Ductility of Irradiated Zircaloy-4", ASTM, STP 1295 (1996) pp 407-428.
- [4.A.12] J.H. Schemel, "ASTM Manual Zirconium and Hafnium", STP 639, ASTM (1977).
- [4.A.13] Zirconium in the Nuclear Industry, ASTM 1354, edited by G.P. Sabol and G.D. Moan (January 2000).
- [4.A.14] J.A.L. Robertson, "Learning from History: A Case Study in Nuclear Fuel", ASTM STP 1295, edited by E.R. Bradley and G.A. Sabol (1996).
- [4.A.15] Montgomery R.O. and Rashid Y.R., "Evaluation of Irradiated Fuel During RIA Simulation Tests", EPRI TR-106387, August 1996.
- [4.A.16] Rashid, Y.R., "Montgomery R.O. and Yang, R.L., "A Cladding Failure Model for Fuel Rods Subjected to Operational and Accident Transients", IAEA Specialists Meeting on Fuel Modeling, Windmere, U.K., June 2000.
- [4.A.17] J. Jarheiff, R., Manzel, and E. Ortlieb, "Influence of Hydrogen Content and Irradiation on the Mechanical Behavior of Fuel Assembly Structural Members Made of Zircaloy", 1993, Annual Nuclear Engineering Convention, Cologne, Germany, May 1993.
- [4.A.18] EPRI Report 1001207, "Creep As the Limiting Mechanism for Spent Fuel Dry Storage" (Progress Report, December, 2000).
- [4.A.19] Franklin, D.G., Lucas G.E. and Bement, A.L., "Creep of Zirconium Alloys in Nuclear Reactors", ASTM STP 815 (1985).
- [4.A.20] "Low-Temperature Rupture Behavior of Zircaloy-clad Pressurized Water Reactor Spent Fuel Rods Under Dry Storage Conditions," R.E. Einziger and R. Kohli, Nuclear Technology, Vol. 67, Oct. 1984, 107-123.

- [4.A.21] "Release of Fission Products and Post-Pile Creep Behavior of Irradiated Fuel Rods Stored Under Dry Conditions", Kaspar et al., BMFT-KWA 2100 BO, 1985, Erlangen, Germany.
- [4.A.22] "Dry Storage of High Burnup Spent Nuclear Fuel", (Wesflex Docket 72-1026), WCAP-15211, (page 4-20).
- [4.A.23] Inter Company Communication from T. Miyazaki, Manager Nuclear Fuel Cycle Group, Kansai Electric Power Co. to K. P. Singh, Holtec International, Dated December 26, 2000.

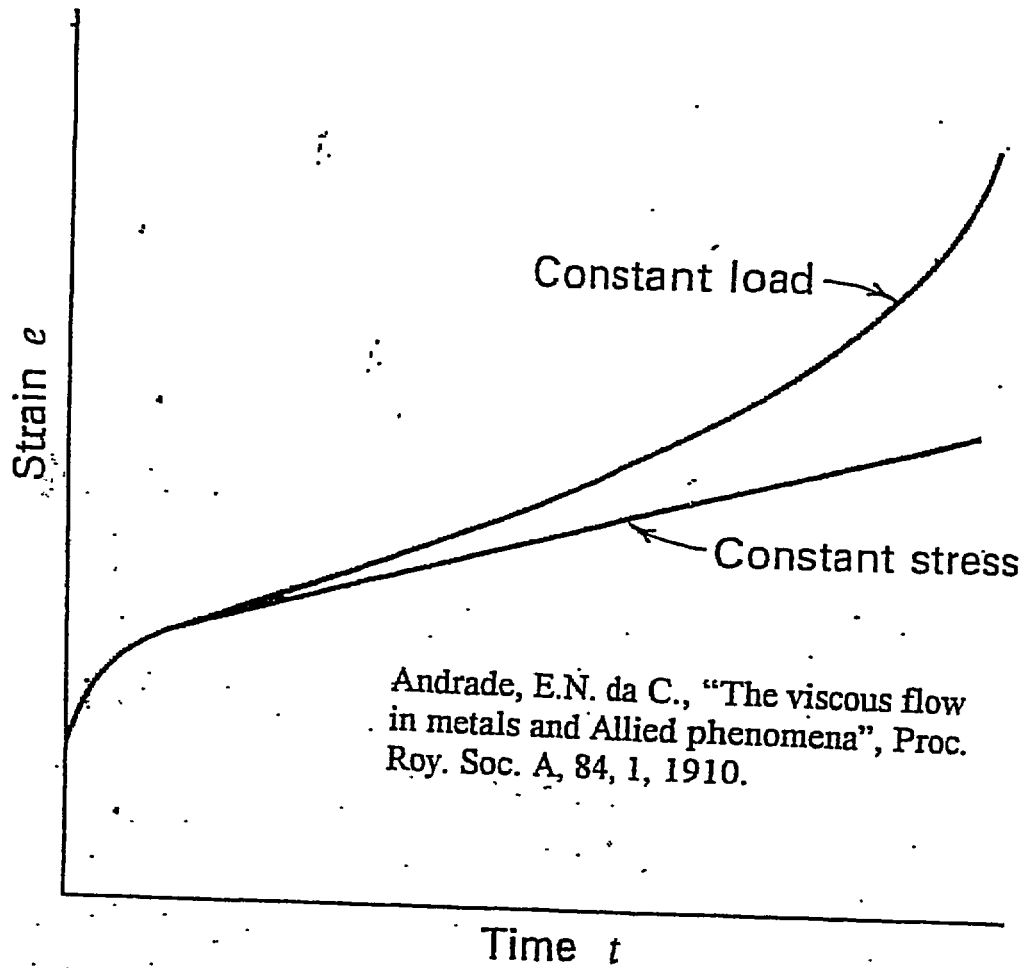


FIGURE 4.A.1: CREEP TESTS OF LEAD WIRE

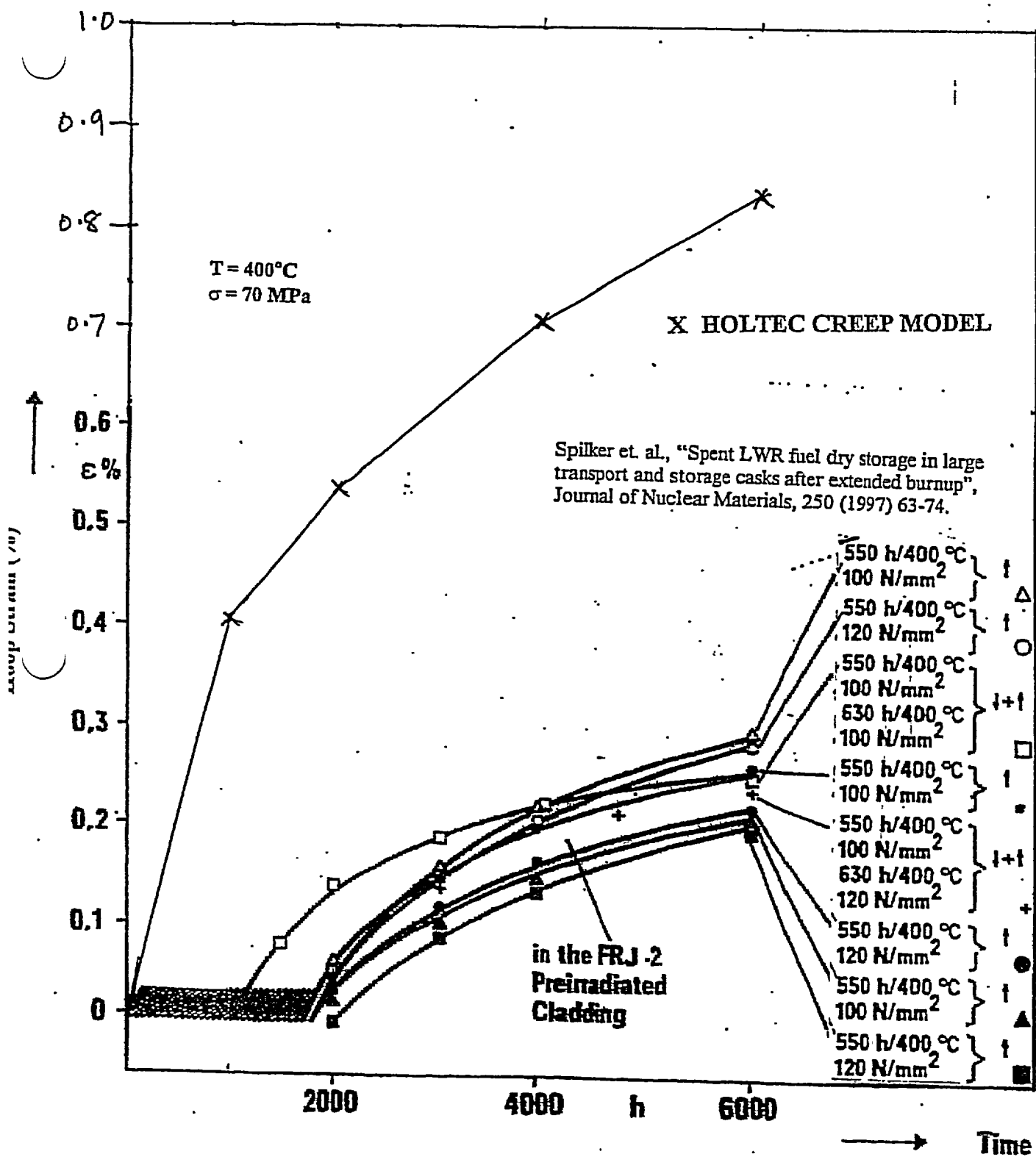


FIGURE 4.A.2: COMPARISON OF HOLTEC MODEL CREEP TO IRRADIATED CLADDING CREEP DATA

REVISION 1

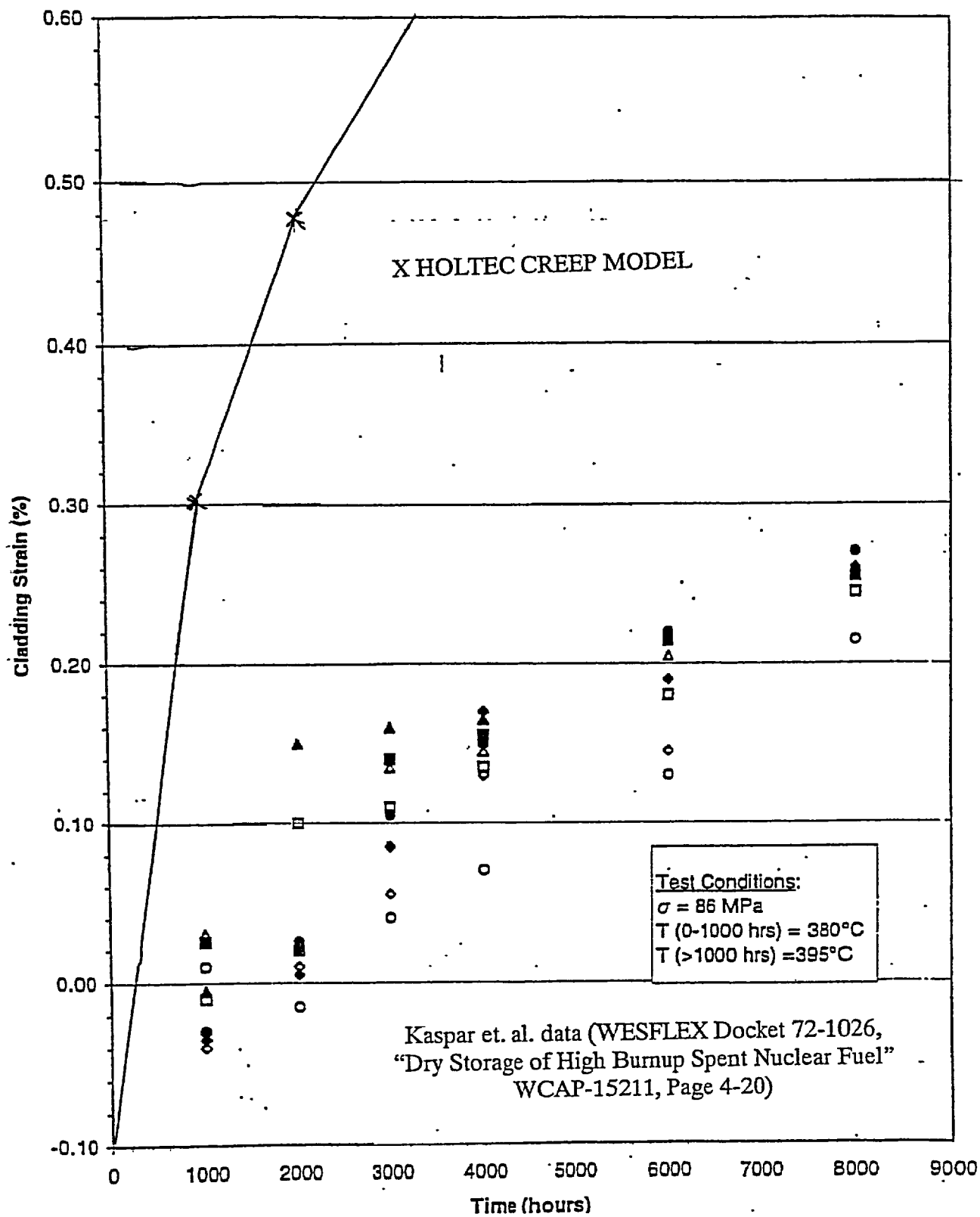


FIGURE 4.A.3: COMPARISON OF HOLTEC MODEL CREEP TO KASPAR ET. AL. IRRADIATED CLADDING CREEP DATA

REVISION 1

Goll et. al. Data, "Short-Time Creep and Rupture Tests on High Burnup Fuel Rod Cladding".
 Temperature = 300 - 370 Deg. C
 Stress = 320 - 630 MPa

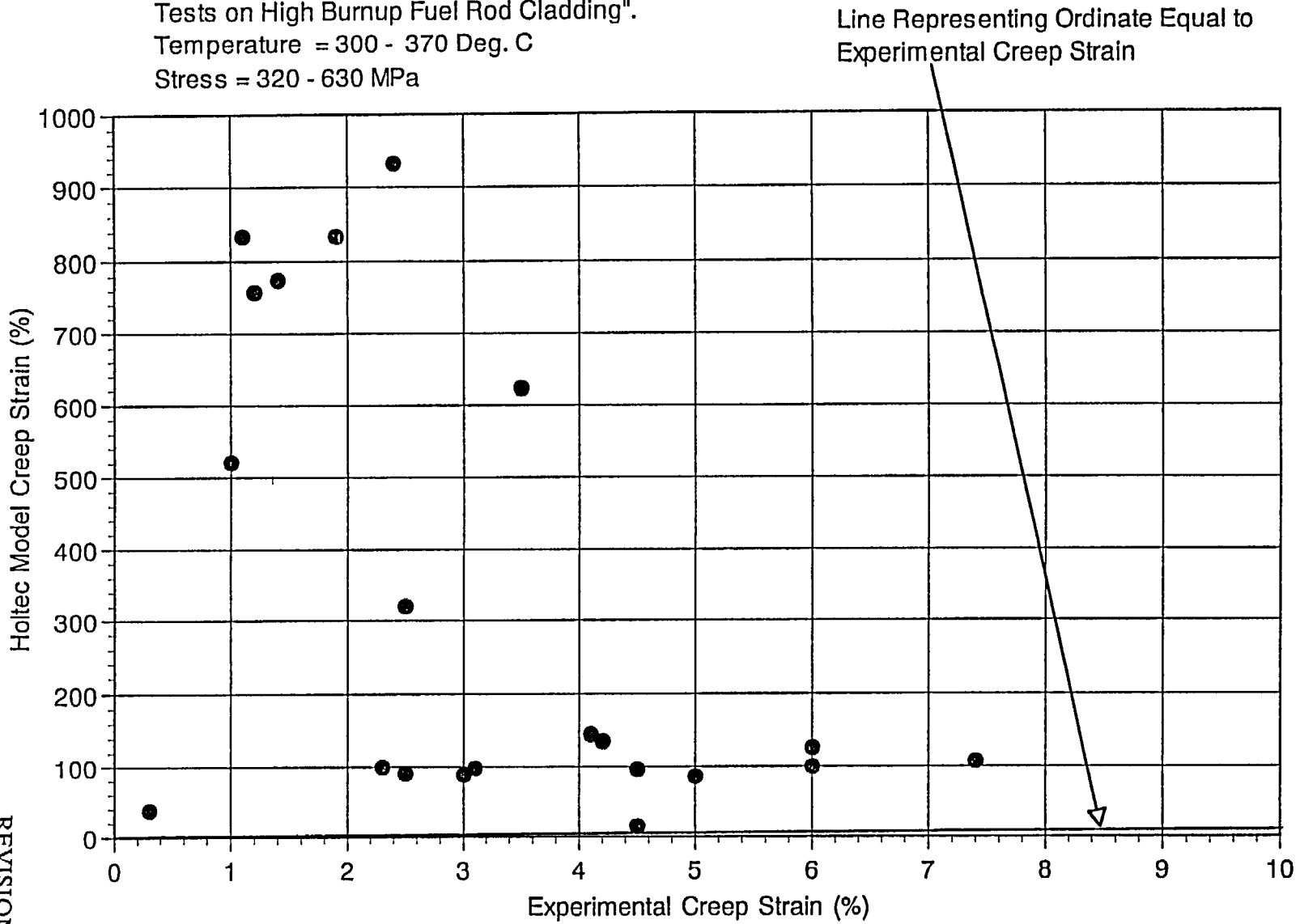


FIGURE 4.A.4: COMPARISON OF HOLTEC MODEL CREEP TO GOLL ET. AL. IRRADIATED CLADDING CREEP DATA - SCATTER PLOT

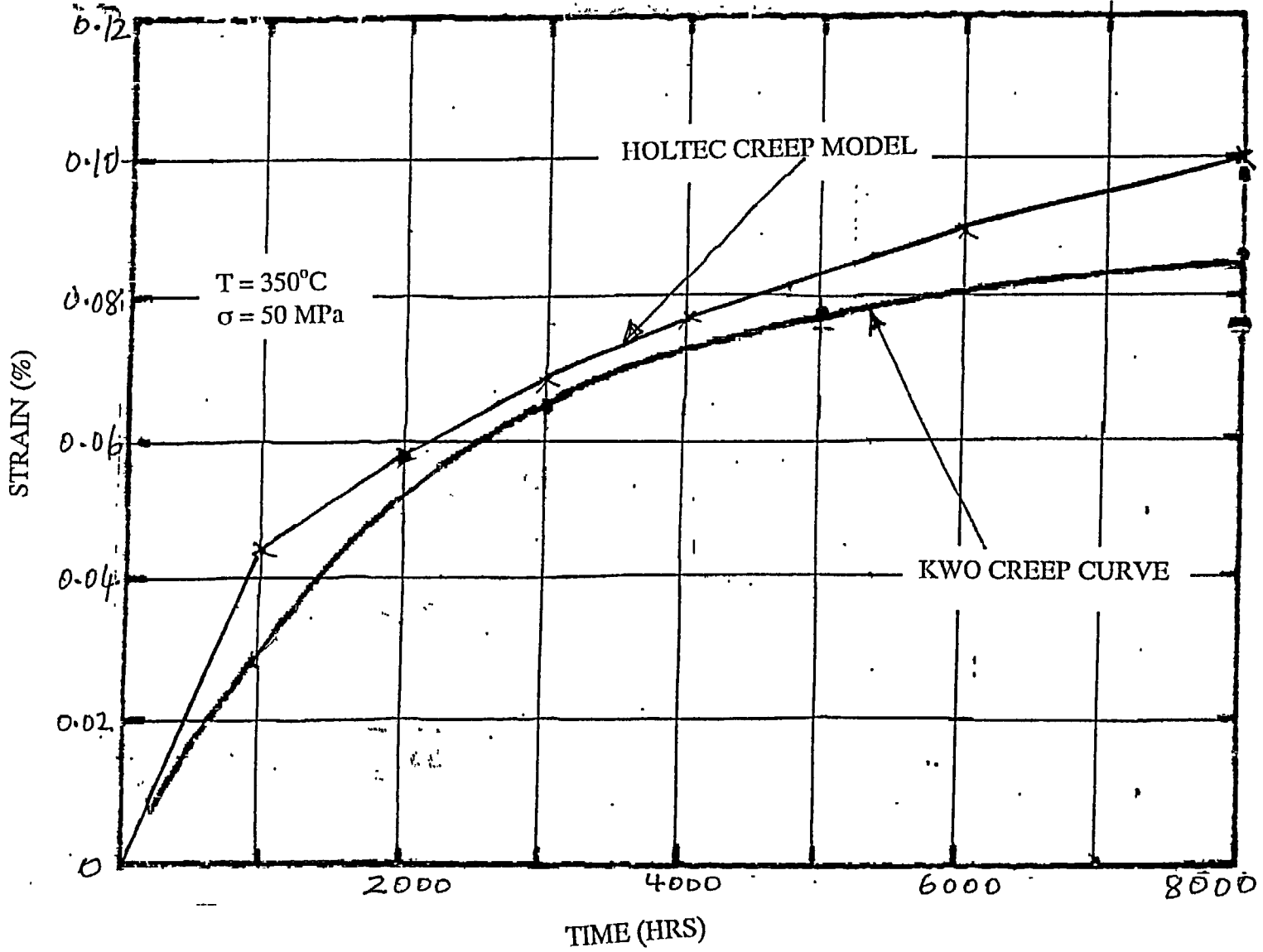


FIGURE 4.A.5: COMPARISON OF HOLTEC CREEP MODEL TO KASPAR ET. AL. CREEP CURVE FOR KWO IRRADIATED SAMPLES

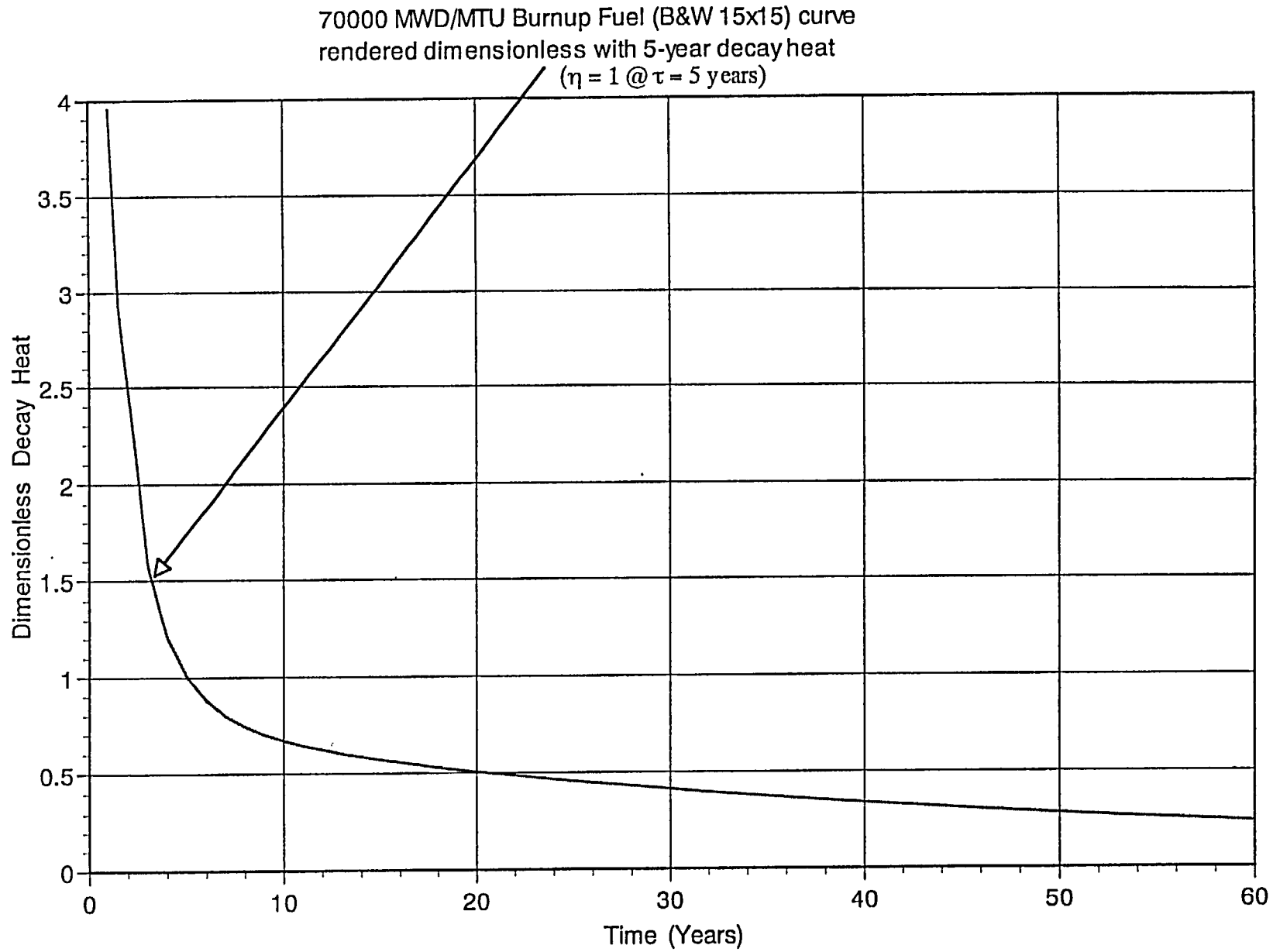


FIGURE 4.A.6: PWR FUEL DECAY HEAT VS. POST CORE DECAY TIME

70000 MWD/MTU Burnup Fuel (GE 7x7) curve
rendered dimensionless with 5-year decay heat
($\eta = 1$ @ $\tau = 5$ years)

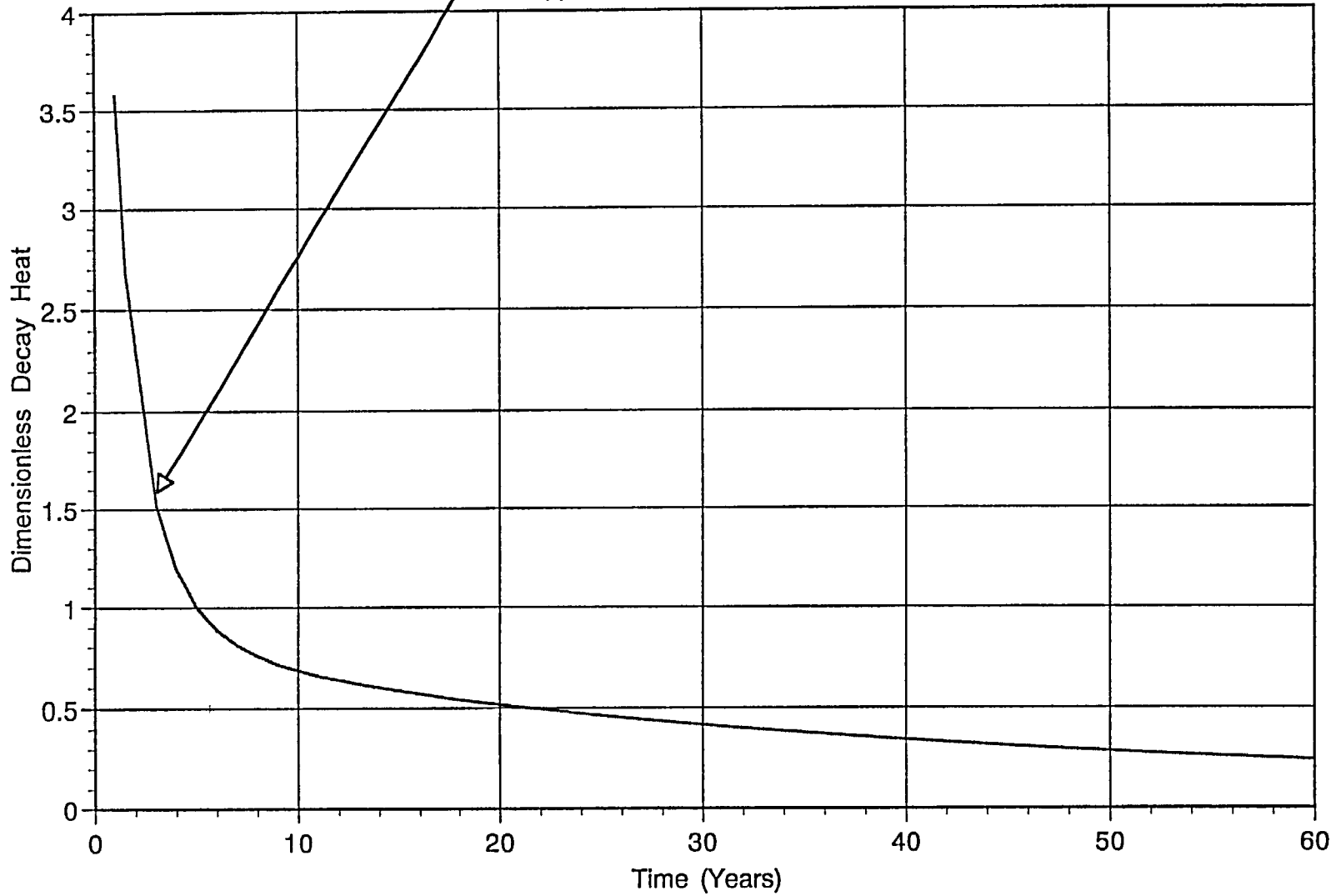


FIGURE 4.A.7: BWR FUEL DECAY HEAT VS. POST CORE DECAY TIME

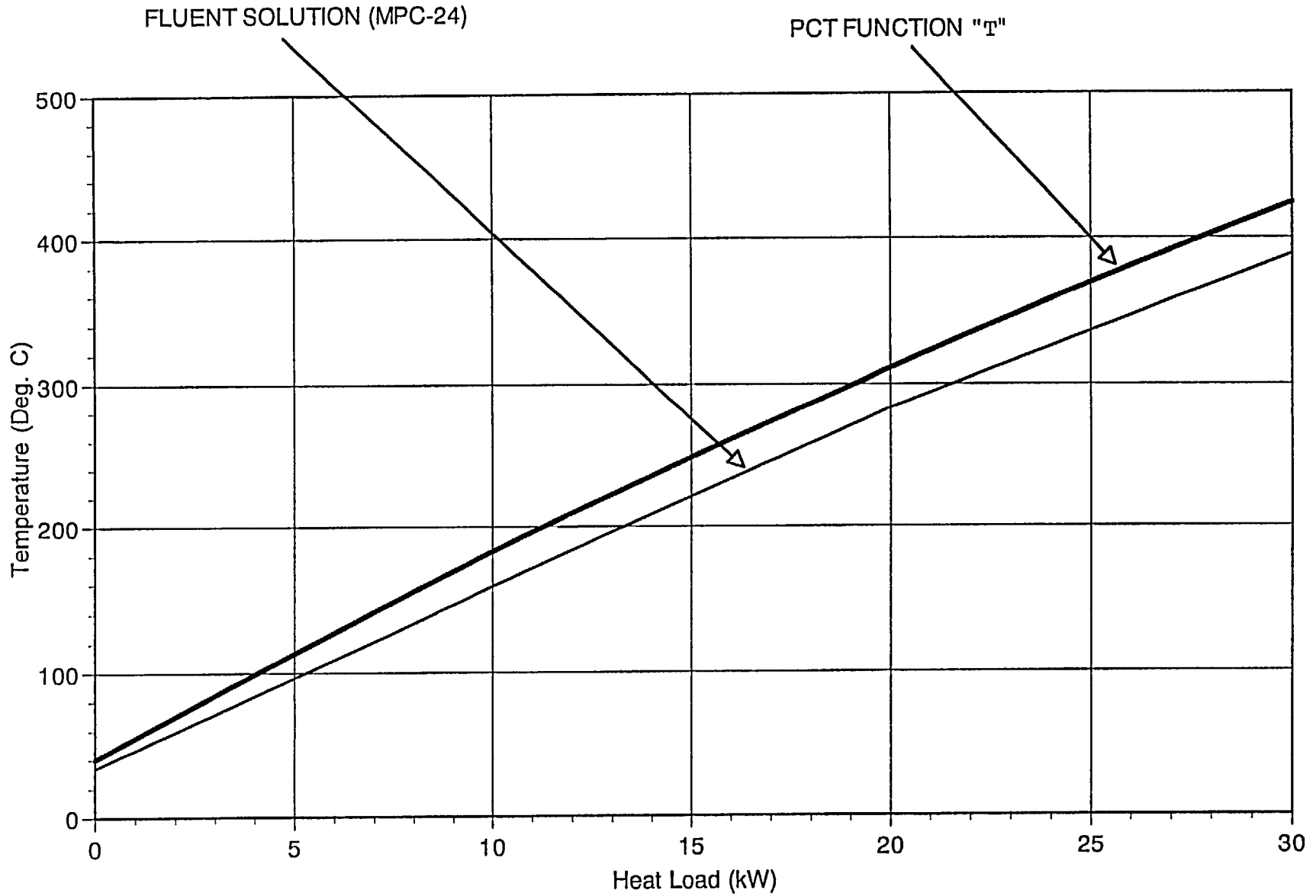


FIGURE 4.A8: PEAK CLAD TEMPERATURE VARIATION WITH MPC HEAT LOAD FOR PWR CANISTERS

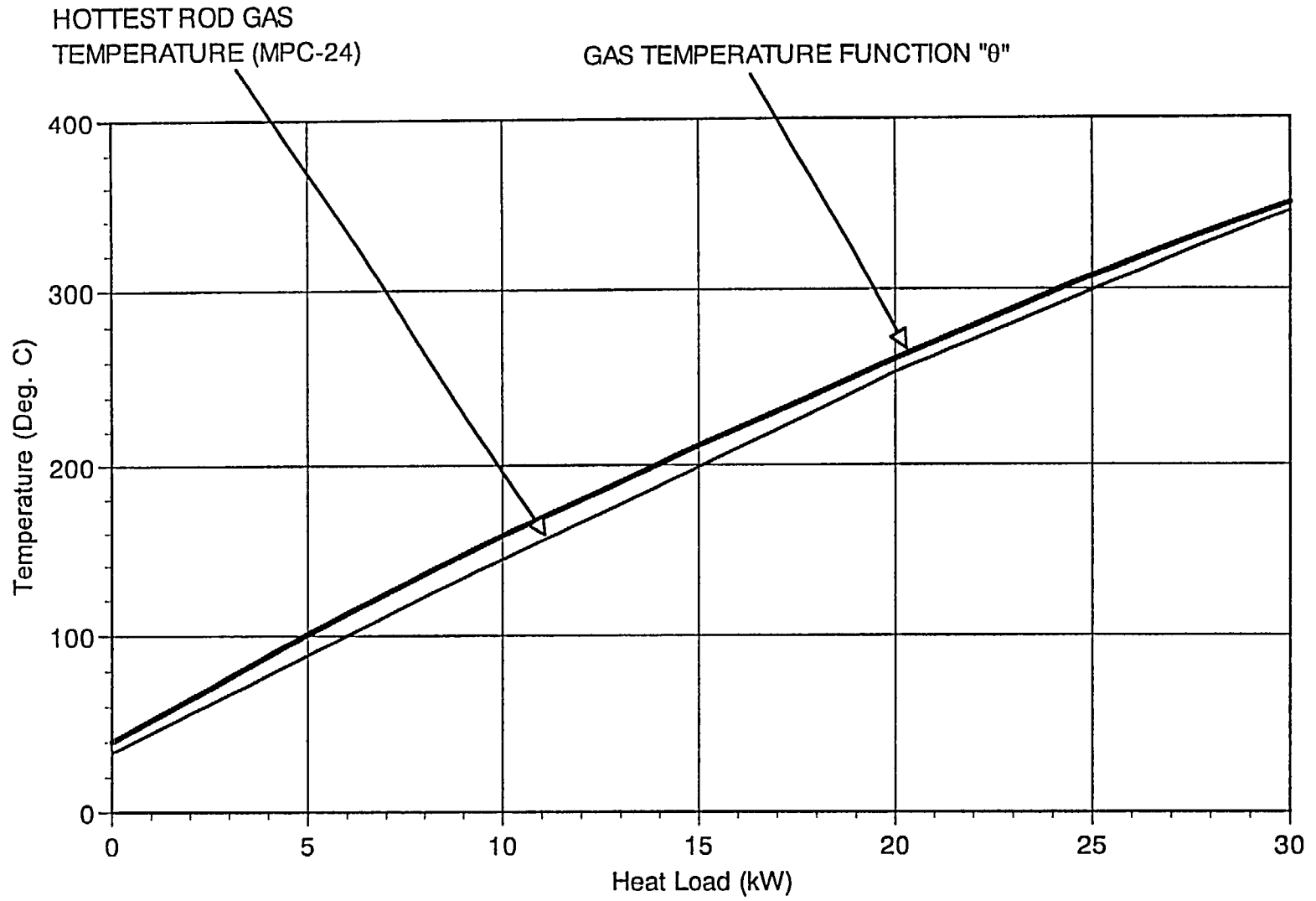


FIGURE 4.A.9: ROD GAS TEMPERATURE VARIATION WITH MPC HEAT LOAD (Q) FOR PWR CANISTERS

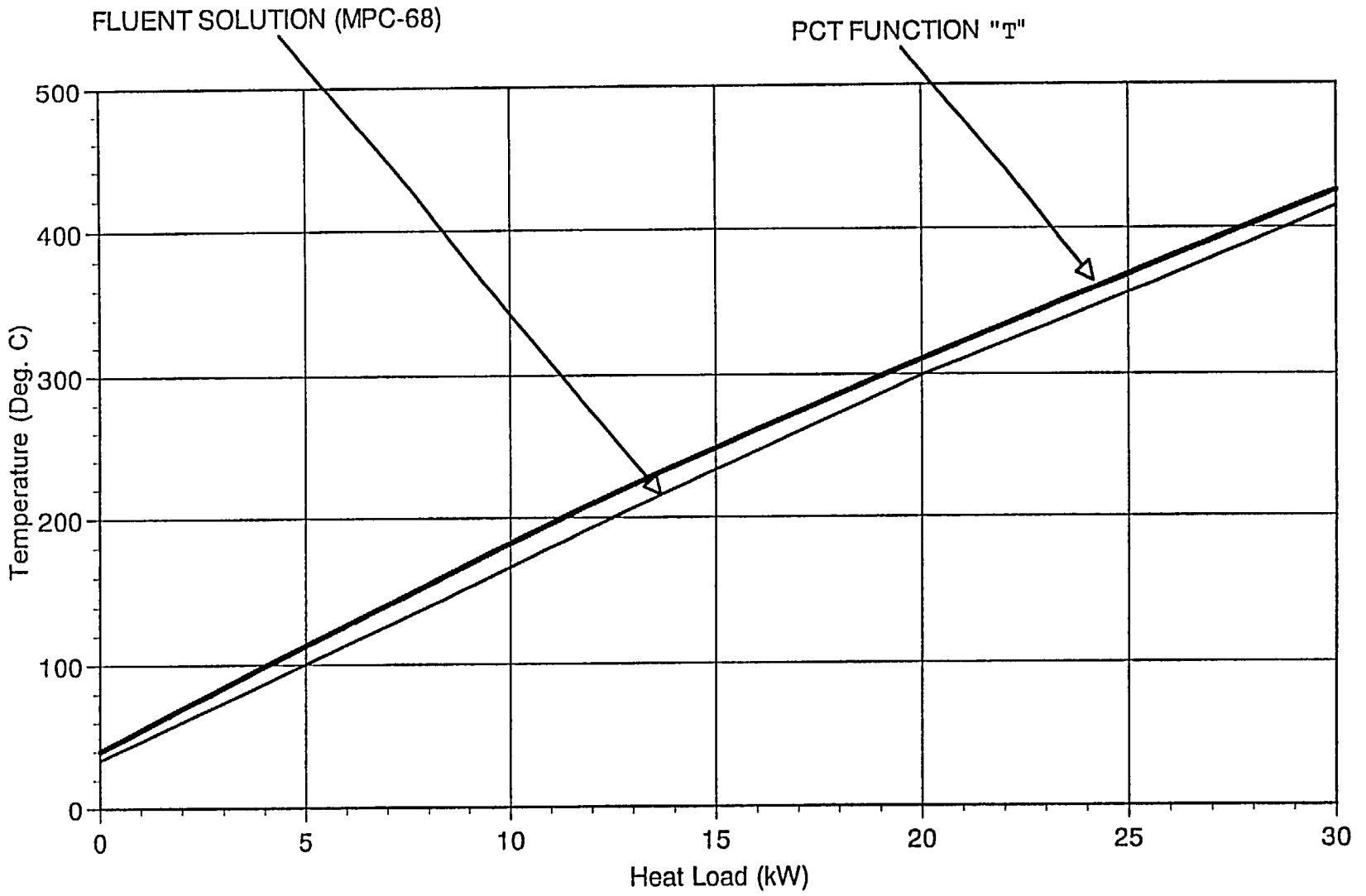


FIGURE 4.A.10: PEAK CLAD TEMPERATURE VARIATION WITH MPC HEAT LOAD FOR BWR CANISTERS

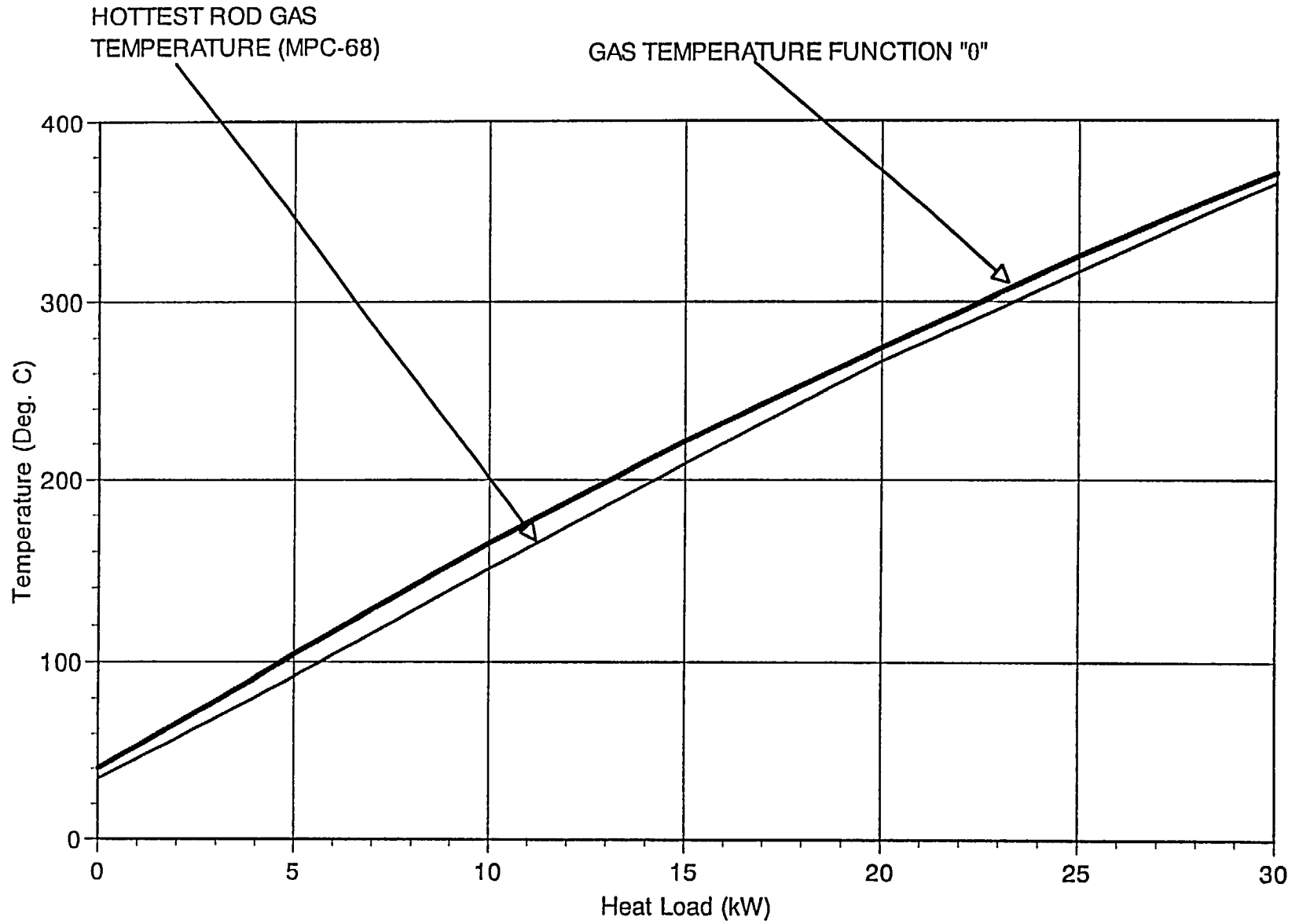
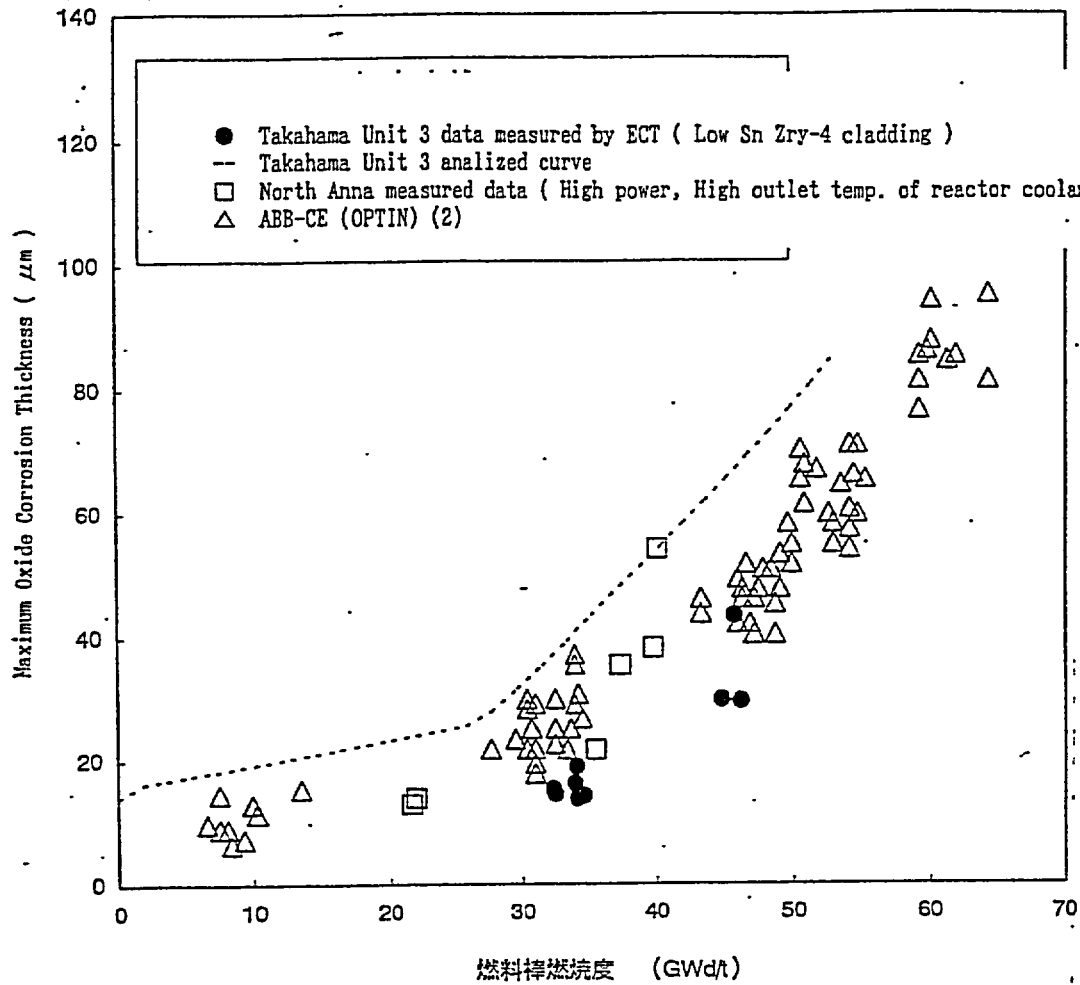


FIGURE 4.A.11: ROD GAS TEMPERATURE VARIATION WITH MPC HEAT LOAD (Q) FOR BWR CANISTERS



- (1) Kilp, G.R., et al.: "Corrosion experience with zircaloy and ZIRLO in operating PWRs", ANS/ENS Topical Meeting, Avignon, France, April, 1991.
 (2) Jourdain, P., et al., "Corrosion performance of optimised and advanced fuel rod cladding in PWRs at high burnups", Top fuel 97, BNES, 1997.

Oxide Corrosion Thickness vs Burn Up
 compared with other previous data

FIGURE 4.A.12: OXIDE CORROSION DATA

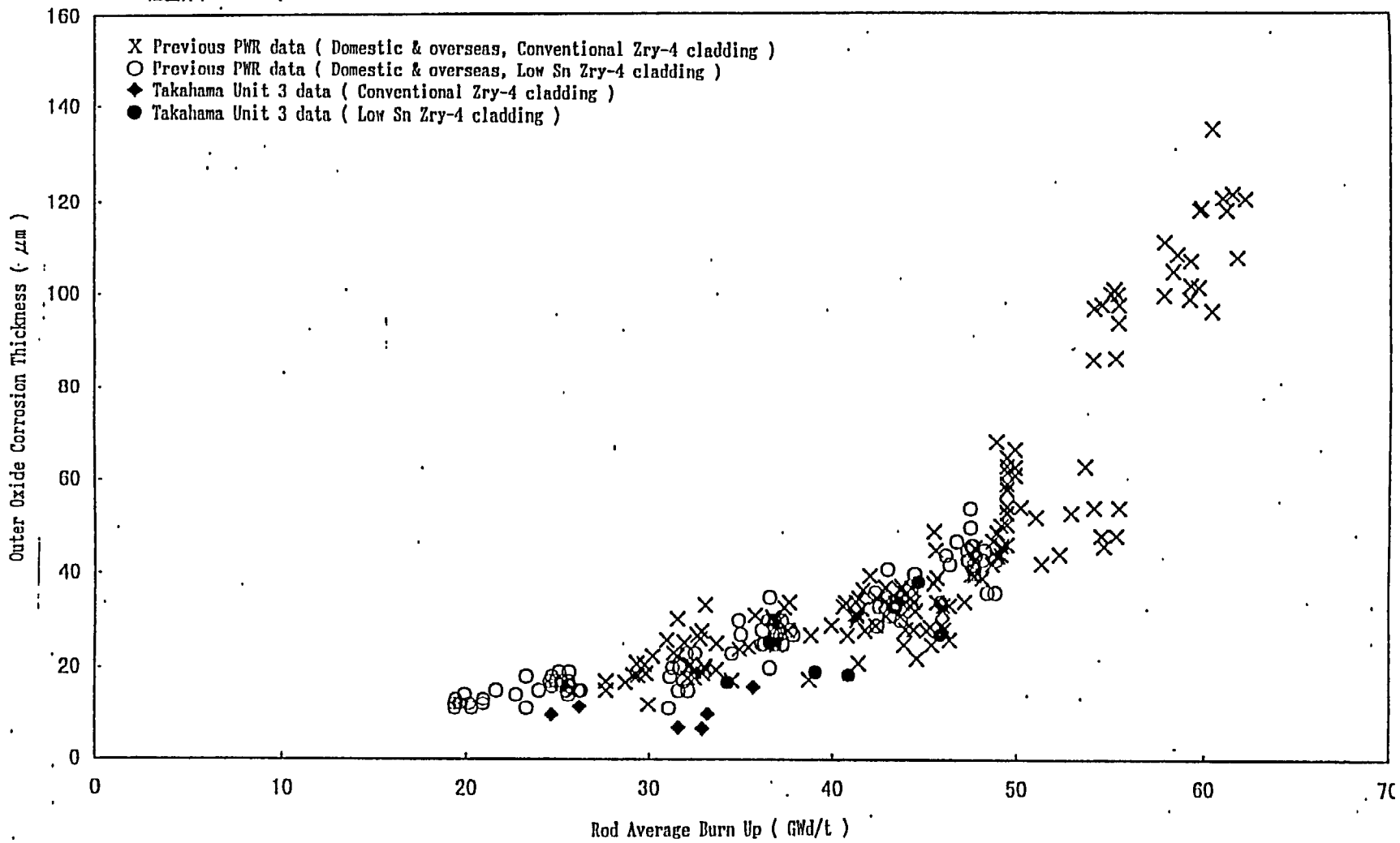


FIGURE 4.A.13: OXIDE CORROSION DATA

APPENDIX 4.B: CONSERVATISMS IN THE THERMAL ANALYSIS OF THE HI-STORM 100 SYSTEM

4.B.1. OVERVIEW OF CASK HEAT REMOVAL SYSTEM

The HI-STORM 100 overpack is a large, cylindrical structure with an internal cavity suited for emplacement of a cylindrical canister containing spent nuclear fuel (SNF). The canister is arrayed in an upright manner inside the vertically oriented overpack. The design of the system provides for a small radial gap between the canister and the cylindrical overpack cavity. One principal function of a fuel storage system is to provide a means for ensuring fuel cladding integrity under long-term storage periods (20 years or more). The HI-STORM 100 overpack is equipped with four large ducts near its bottom and top extremities. The ducted overpack construction, together with an engineered annular space between the MPC cylinder and internal cavity in the HI-STORM 100 overpack structure, ensures a passive means of heat dissipation from the stored fuel via ventilation action (i.e., natural circulation of air in the canister-to-overpack annulus). In this manner a large structure physically interposed between the hot canister and ambient air (viz. the concrete overpack engineered for radiation protection) is rendered as an air flow device for convective heat dissipation. The pertinent design features producing the air ventilation ("chimney effect") in the HI-STORM 100 cask are shown in Figure 4.B.1.

A great bulk of the heat emitted by the SNF is rejected to the environment (Q_1) by convective action. A small quantity of the total heat rejection occurs by natural convection and radiation from the surface of the overpack (Q_2), and an even smaller amount is dissipated by conduction to the concrete pad upon which the HI-STORM 100 overpack is placed (Q_3). From the energy conservation principle, the sum of heat dissipation to all sinks (convective cooling (Q_1), surface cooling (Q_2) and cooling to pad (Q_3)) equals the sum of decay heat emitted from the fuel stored in the canister (Q_d) and the heat deposited by insolation, Q_s (i.e., $Q_d + Q_s = Q_1 + Q_2 + Q_3$). This situation is illustrated in Figure 4.B.2. In the HI-STORM 100 System, Q_1 is by far the dominant mode of heat removal, accounting for well over 80% of the decay heat conveyed to the external environment. Figure 4.B.3 shows the relative portions of Q_d transferred to the environs via Q_1 , Q_2 , and Q_3 in the HI-STORM 100 System under the design basis heat load.

The heat removal through convection, Q_1 , is similar to the manner in which a fireplace chimney functions: Air is heated in the annulus between the canister and the overpack through contact with the canister's hot cylindrical surface causing it to flow upward toward the top (exit) ducts and inducing the suction of the ambient air through the bottom ducts. The flow of air sweeping past the cylindrical surfaces of the canister has sufficient velocity to create turbulence that aids in the heat extraction process. It is readily recognized that the chimney action relies on a fundamental and immutable property of air, namely that air becomes lighter (i.e., more buoyant) as it is heated. If the canister contained no heat emitting fuel, then there would be no means for the annulus air to heat and rise. Similarly, increasing the quantity of heat produced in the canister would make more heat available for heating of annulus air, resulting in a more vigorous chimney action. Because the heat energy of the spent nuclear fuel itself actuates the chimney action, ventilated overpacks of the HI-STORM 100 genre are considered absolutely safe against thermal

malfunction. While the removal of heat through convective mass transport of air is the dominant mechanism, other minor components, labeled Q_2 and Q_3 in the foregoing, are recognized and quantified in the thermal analysis of the HI-STORM 100 System.

Heat dissipation from the exposed surfaces of the overpack, Q_2 , occurs principally by natural convection and radiation cooling. The rate of decay heat dissipation from the external surfaces is, of course, influenced by several factors, some of which aid the process (e.g., wind, thermal turbulence of air), while others oppose it (for example, radiant heating by the sun or blocking of radiation cooling by surrounding casks). In this appendix, the relative significance of Q_2 and Q_3 and the method to conservatively simulate their effect in the HI-STORM 100 thermal model is discussed.

The thermal problem posed for the HI-STORM 100 System in the system's Final Safety Analysis Report (FSAR) is as follows: Given a specified maximum fuel cladding temperature, T_c , and a specified ambient temperature, T_a what is the maximum permissible heat generation rate Q_d , in the canister under steady state conditions? Of course, in the real world, the ambient temperature, T_a , varies continuously, and the cask system is rarely in a steady state (i.e., temperatures vary with time). Fortunately, fracture mechanics of spent fuel cladding instruct us that it is the time-integrated effect of elevated temperature, rather than an instantaneous peak value, that determines whether fuel cladding would rupture. The most appropriate reference ambient temperature for cladding integrity evaluation, therefore, is the average ambient temperature for the entire duration of dry storage. For conservatism, the reference ambient temperature is, however, selected to be the maximum yearly average for the ISFSI site. In the general certification of HI-STORM 100, the reference ambient temperature (formally referred to as the normal temperature) is set equal to 80°F, which is greater than the annual average for any power plant location in the U.S.*

The thermal analysis of the cask system leads to a computed value of the fuel cladding temperature greater than T_a by an amount C . In other words, $T_c = T_a + C$, where C decreases slightly as T_a (assumed ambient temperature) is increased. The thermal analysis of HI-STORM 100 is carried out to compute C in a most conservative manner. In other words, the mathematical model seeks to calculate an upper bound on the value of C .

Dry storage scenarios are characterized by relatively large temperature elevations (C) above ambient (650°F or so). The cladding temperature rise is the cumulative sum of temperature increments arising from individual elements of thermal resistance. To protect cladding from overheating, analytical assumptions adversely impacting heat transfer are chosen with particular attention given to those temperature increments which form the bulk of the temperature rise. In this appendix, the principal conservatisms in the thermal modeling of the HI-STORM 100 System and their underlying theoretical bases are presented. This overview is intended to provide a physical understanding of the large margins buried in the HI-STORM 100 design which are summarized in Section 4.4.6 of this FSAR.

* According to the U.S. National Oceanic and Atmospheric Administration (NOAA) publication, "Comparative Climatic Data for the United States through 1998", the highest annual average temperature for any location in the continental U.S. is 77.8°F in Key West, Florida.

4.B.2 CONSERVATISM IN ENVIRONMENTAL CONDITION SPECIFICATION

The ultimate heat sink for decay heat generated by stored fuel is ambient air. The HI-STORM 100 System defines three ambient temperatures as the environmental conditions for thermal analysis. These are, the Normal (80°F), the Off-Normal (100°F) and Extreme Hot (125°F) conditions. Two factors dictate the stipulation of an ambient temperature for cladding integrity calculations. One factor is that ambient temperatures are constantly cycling on a daily basis (night and day). Furthermore, there are seasonal variations (summer to winter). The other factor is that cladding degradation is an incremental process that, over a long period of time (20 years), has an accumulated damage resulting from an "averaged-out" effect of the environmental temperature history. The 80°F normal temperature stated in the HI-STORM 100 FSAR is defined as the highest annual average temperature at a site established from past records. This is a principal design parameter in the HI-STORM 100 analysis because it establishes the basis for demonstrating long-term SNF integrity. The choice of maximum annual average temperature is conservative for a 20-year period. Based on meteorological data, the 80°F is chosen to bound annual average temperatures reported within the continental US.

For short periods, it is recognized that ambient temperature excursions above 80°F are possible. Two scenarios are postulated and analyzed in the FSAR to bound such transient events. The Off-Normal (100°F) and Extreme Hot (125°F) cases are postulated as continuous (72-hour average) conditions. Both cases are analyzed as steady-state conditions (i.e., thermal inertia of the considerable concrete mass, fuel and metal completely neglected) occurring at the start of dry storage when the decay heat load to the HI-STORM 100 System is at its peak value with fuel emitting heat at its design basis maximum level.

4.B.3 CONSERVATISM IN MODELING THE ISFSI ARRAY

Traditionally, in the classical treatment of the ventilated storage cask thermal problem, the cask to be analyzed (the subject cask) is modeled as a stand-alone component that rejects heat to the ambient air through chimney action (Q_1) by natural convection to quiescent ambient air and radiation to the surrounding open spaces (Q_2), and finally, a small amount through the concrete pad into the ground (Q_3). The contributing effect of the sun (addition of heat) is considered, but the dissipative effect of wind is neglected. The interchange of radiative heat between proximate casks is also neglected (the so-called "cask-to-cask interactions"). In modeling the HI-STORM 100 System, Holtec International extended the classical cask thermal model to include the effect of the neighboring casks in a most conservative manner. This model represents the flow of supply air to the inlet ducts for the subject cask by erecting a cylinder around the subject cask. The model blocks all lateral flow of air from the surrounding space into the subject cask's inlet ducts. This mathematical artifice is illustrated in Figure 4.B.4, where the lateral air flow arrows are shown "dotted" to indicate that the mathematical cylinder constructed around the cask has blocked off the lateral flow of air. Consequently, the chimney air must flow down the annulus

* According to NOAA, the highest daily mean temperature for any location in the continental U.S. is 93.7°F, which occurred in Yuma, Arizona.

from the air plenum space above the casks, turn around at the bottom and enter the inlet ducts. Because the vertical downflow of air introduces additional resistance to flow, an obvious effect of the hypothetical enclosing cylinder construct is an increased total resistance to the chimney flow which, it is recalled, is the main heat conveyance mechanism in a ventilated cask. Throttling of the chimney flow by the hypothetical enclosing cylinder is an element of conservatism in the HI-STORM modeling.

Thus, whereas air flows toward the bottom ducts from areas of supply which are scattered in a three dimensional continuum with partial restriction from neighboring casks, the analytical model blocks the air flow completely from areas outside the hypothetical cylinder. This is illustrated in Figure 4.B.4 in which an impervious boundary is shown to limit HI-STORM 100 cask access to fresh air from an annular opening near the top.

Thus, in the HI-STORM model, the feeder air to the HI-STORM 100 System must flow down the hypothetical annulus sweeping past the external surface of the cask. The ambient air, assumed to enter this hypothetical annulus at the assumed environmental temperature, heats by convective heat extraction from the overpack before reaching the bottom (inlet) ducts. In this manner, the temperature of the feeder air into the ducts is maximized. In reality, the horizontal flow of air in the vicinity of the inlet ducts, suppressed by the enclosed cylinder construct (as shown in Figure 4.B.4) would act to mitigate the pre-heating of the feeder air. By maximizing the extent of air preheating, the computed value of ventilation flow is underestimated in the simulation.

4.B.4 CONSERVATISM IN RADIANT HEAT LOSS

In an array of casks, the external (exposed) cask surfaces have a certain "view" of each other. The extent of view is a function of relative geometrical orientation of the surfaces and presence of other objects between them. The extent of view influences the rate of heat exchange between surfaces by thermal radiation. The presence of neighboring casks also partially blocks the escape of radiant heat from a cask thus affecting its ability to dissipate heat to the environment. This aspect of Radiative Blocking (RB) is illustrated for a reference cask (shown shaded) in Figure 4.B.5. It is also apparent that a cask is a recipient of radiant energy from adjacent casks (Radiant Heating (RH)). Thus, a thermal model representative of a cask array must address the RB and RH effects in a conservative manner. To bound the physical situation, a Hypothetical Reflecting Boundary (HRB) modeling feature is introduced in the thermal model. The HRB feature surrounds the HI-STORM 100 overpack with a reflecting cylindrical surface with the boundaries insulated.

In Figures 4.B.6 and 4.B.7 the inclusion of RB and RH effects in the HI-STORM 100 modeling is graphically illustrated. Figure 4.B.6 shows that an incident ray of radiant energy leaving the cask surface bounces back from the HRB thus preventing escape (i.e., RB effect maximized). The RH effect is illustrated in Figure 4.B.7 by superimposing on the physical model reflected images of HI-STORM 100 cask surrounding the reference cask. A ray of radiant energy from an adjacent cask directed toward the reference cask (AA) is duplicated by the model via another ray of radiant energy leaving the cask (BB) and being reflected back by the HRB (BA'). A significant feature of this model is that the reflected ray (BA') initiated from a cask surface (reference cask)

assumed to be loaded with design basis maximum heat (hottest surface temperature). As the strength of the ray is directly proportional to the fourth power of surface temperature, radiant energy emission from an adjacent cask at a lower heat load will be overestimated by the HRB construct. In other words, the reference cask is assumed to be in an array of casks all producing design basis maximum heat. Clearly, it is physically impossible to load every location of every cask with fuel emitting heat at design basis maximum. Such a spent fuel inventory does not exist. This bounding assumption has the effect of maximizing cask surface temperature as the possibility of "hot" (design basis) casks being radiatively cooled by adjacent casks is precluded. The HRB feature included in the HI-STORM 100 model thus provides a bounding effect of an infinite array of casks, all at design basis maximum heat loads. No radiant heat is permitted to escape the reference cask (bounding effect) and the reflecting boundary mimics incident radiation toward the reference casks around the 360° circumference (bounding effect).

4.B.5 CONSERVATISM IN REPRESENTING BASKET AXIAL RESISTANCE

As stated earlier, the largest fraction of the total resistance to the flow of heat from the spent nuclear fuel (SNF) to the ambient is centered in the basket itself. Out of the total temperature drop of approximately 650°F (C=650°F) between the peak fuel cladding temperature and the ambient, over 400°F occurs in the fuel basket. Therefore, it stands to reason that conservatism in the basket thermal simulation would have a pronounced effect on the conservatism in the final solution. The thermal model of the fuel basket in the HI-STORM 100 FSAR was accordingly constructed with a number of conservative assumptions that are described in the HI-STORM 100 FSAR. We illustrate the significance of the whole array of conservatisms by explaining one in some detail in the following discussion.

It is recognized that the heat emission from a fuel assembly is axially non-uniform. The maximum heat generation occurs at about the mid-height region of the enriched uranium column, and tapers off toward its extremities. The axial heat conduction in the fuel basket would act to diffuse and levelize the temperature field in the basket. The axial conductivity of the basket, quite clearly, is the key determinant in how well the thermal field in the basket would be homogenized. It is also evident that the conduction of heat along the length of the basket occurs in an uninterrupted manner in a HI-STORM 100 basket because of its continuously welded honeycomb geometry. On the other hand, the in-plane transfer of heat must occur through the physical gaps that exist between the fuel rods, between the fuel assembly and the basket walls and between the basket and the MPC shell. These gaps depress the in-plane conductivity of the basket. However, in the interest of conservatism, only a small fraction of the axial conductivity of the basket is included in the HI-STORM 100 thermal model. This assumption has the direct effect of throttling the axial flow of heat and thus of elevating the computed value of mid-height cladding temperature (where the peak temperature occurs) above its actual value. In actuality, the axial conductivity of the fuel basket is much greater than the in-plane conductivity due to the continuity of the fuel and basket structures in that direction. Had the axial conductivity of the basket been modeled less conservatively in the HI-STORM 100 thermal analysis, then the temperature distribution in the basket will be more uniform, i.e., the bottom region of the basket would be hotter than that computed. This means that the temperature of the MPC's external surface in the bottom region is hotter than computed in the HI-STORM 100 analysis. It is a well-

known fact in ventilated column design that the lower the location in the column where the heat is introduced, the more vigorous the ventilation action. Therefore, the conservatism in the basket's axial conductivity assumption has the net effect of reducing the computed ventilation rate.

To estimate the conservatism in restricting the basket axial resistance, we perform a numerical exercise using mathematical perturbation techniques. The axial conductivity (K_z) of the MPC is, as explained previously, much higher than the in-plane (K_r) conductivity. The thermal solution to the MPC anisotropic conductivities problem (i.e. K_z and K_r are not equal) is mathematically expressed as a sum of a baseline isotropic solution T_o (setting $K_z = K_r$) and a perturbation T^* which accounts for anisotropic effects. From Fourier's Law of heat conduction in solids, the perturbation equation for T^* is reduced to the following form:

$$K_z \frac{d^2 T^*}{dz^2} = -\Delta K \frac{d^2 T_o}{dz^2}$$

Where, ΔK is the perturbation parameter (i.e. axial conductivity offset $\Delta K = K_z - K_r$). The boundary conditions for the perturbation solution are zero slope at peak cladding temperature location ($dT^*/dz = 0$) (which occurs at about the top of the active fuel height) and $T^* = 0$ at the bottom of the active fuel length. The object of this calculation is to compute T^* where the peak fuel cladding temperature is reached. To this end, the baseline thermal solution T_o (i.e. HI-STORM isotropic modeling solution) is employed to compute an appropriate value for $d^2 T_o / dz^2$ which characterizes the axial temperature rise over the height of the active fuel length in the hottest fuel cell. This is computed as $(-\Delta T_{ax} / L^2)$ where ΔT_{ax} is the fuel cell temperature rise and L is the active fuel length. Conservatively postulating a lower bound ΔT_{ax} of 200°F and L of 12 ft, $d^2 T_o / dz^2$ is computed as $-1.39^\circ\text{F}/\text{ft}^2$. Integrating the perturbation equation shown above, the following formula for T^* is obtained:

$$T^* = \left(\frac{\Delta K}{K_z} \right) \frac{d^2 T_o}{dz^2} L^2$$

Employing a conservative low value for the $(\Delta K / K_z)$ parameter of 0.15, T^* is computed as -30°F . In other words, the baseline HI-STORM solution over predicts the peak cladding temperature by approximately 30°F .

4.B.6 HEAT DISSIPATION UNDERPREDICTION IN THE MPC DOWNCOMER

Internal circulation of helium in the sealed MPC is modeled as flow in a porous medium in the fueled region containing the SNF (including top and bottom plenums). The basket-to-MPC shell clearance space is modeled as a helium filled radial gap to include the downcomer flow in the thermal model. The downcomer region, as illustrated in Figure 4.4.2, consists of an azimuthally varying gap formed by the square-celled basket outline and the cylindrical MPC shell. At the locations of closest approach a differential expansion gap (a small clearance on the order of 1/10 of an inch) is engineered to allow free thermal expansion of the basket. At the widest locations, the gaps are on the order of the fuel cell opening ($\sim 6''$ (BWR) and $\sim 9''$ (PWR) MPCs). It is heuristically evident that heat dissipation by conduction is maximum at the closest approach locations (low thermal resistance path) and that convective heat transfer is highest at the widest gaps locations (large downcomer flow). In the FLUENT thermal model, a radial gap that is large

compared to the basket-to-shell clearance and small compared to the cell opening is used. As a relatively large gap penalizes heat dissipation by conduction and a small gap throttles convective flow, the use of a single gap in the FLUENT model understates both conduction and convection heat transfer in the downcomer region. Furthermore, heat dissipation by the aluminum heat conduction elements, if used, is conservatively neglected in the thermosiphon models employed in the HI-STORM modeling.

Heat dissipation in the downcomer region is the sum of five elements, viz. convective heat transfer (C1), helium conduction heat transfer (C2), basket-to-shell contact heat transfer (C3), radiation heat transfer (C4) and aluminum conduction elements (if used) heat transfer (C5). In the HI-STORM thermal modeling, two elements of heat transfer (C3 and C5) are completely neglected, C2 is severely penalized and C1 is underpredicted. In other words the HI-STORM thermosiphon model has choked the radial flow of heat in the downcomer space. This has the direct effect of raising the temperature of fuel in the thermal solutions.

4.B.7 CONSERVATISM IN MPC EXTERNAL HEAT DISSIPATION TO CHIMNEY AIR

The principle means of decay heat dissipation to the environment is by cooling of the MPC surface by chimney air flow. Heat rejection from the MPC surface is by a combination of convective heat transfer to a through flowing fluid medium (air), natural convection cooling at the outer overpack surface, and by radiation heat transfer. Because the temperature of the fuel stored in the MPC is directly affected by the rate of heat dissipation from the canister external surface, heat transfer correlations with robust conservatisms are employed in the HI-STORM simulations. The FLUENT computer code deployed for the modeling employs a so called "wall-functions" approach for computing the transfer of heat from solid surfaces to fluid medium. This approach has the desired effect of computing heat dissipation in a most conservative manner. As this default approach has been employed in the thermal modeling, it is contextually relevant to quantify the conservatism in a classical setting to provide an additional level of assurance in the HI-STORM results. To do this, we have posed a classical heat transfer problem of a heated square block cooled in a stream of upward moving air. The problem is illustrated in Figure 4.B.8. From the physics of the problem, the maximum steady state solid interior temperature (T_{max}) is computed as:

$$T_{max} = T_{sink} + \Delta T_{air} + \Delta T_s$$

where,

T_{sink}	= Sink temperature (mean of inlet and outlet air temperature)
ΔT_{air}	= Solid surface to air temperature difference
ΔT_s	= Solid block interior temperature elevation

The sink temperature is computed by first calculating the air outlet temperature from energy conservation principles. Solid-to-air heat transfer is computed using classical natural convection correlation proposed by Jakob and Hawkins ("Elements of Heat Transfer", John Wiley & Sons, 1957) and ΔT_s is readily computed by an analytical solution to the equation of heat conduction in solids. By solving this same problem on the FLUENT computer code using the in-built "wall-

functions”, in excess of 100°F conservative margin over the classical result for T_{\max} is established.

4.B.8 MISCELLANEOUS CONSERVATISMS

Section 4.4.6 of the FSAR lists eleven elements of conservatism, of which certain non-transparent and individually significant items are discussed in detail in this appendix. Out of the balance of conservatisms, the one of notable mention is the conservatism in fuel decay heat generation stipulation based on the most heat emissive fuel assembly type. This posture imputes a large conservatism for certain other fuel types, which have a much lower quantity of Uranium fuel inventory relative to the design basis fuel type. Combining this with other miscellaneous conservatisms, an aggregate effect is to overestimate cladding temperatures by about 15°F to 50°F.

4.B.9 CONCLUSIONS

The foregoing narrative provides a physical description of the many elements of conservatism in the HI-STORM 100 thermal model. The conservatisms may be broadly divided into two categories:

1. Those intrinsic to the FLUENT modeling process.
2. Those arising from the input data and on the HI-STORM 100 thermal modeling.

The conservatism in Category (1) may be identified by reviewing the Holtec International Benchmark Report [4.B.1], which shows that the FLUENT solution methodology, when applied to the prototype cask (TN 24P) over-predicts the peak cladding temperature by as much as 79 °F. and as much as 37°F relative to the PNNL results (see Attachment 1 to Reference [4.B.1]) from their COBRA SFS solution as compared against Holtec’s FLUENT solution.

Category (2) conservatisms are those that we have deliberately embedded in the HI-STORM 100 thermal model to ensure that the computed value of the peak fuel cladding temperature is further over-stated. Table 4.B.1 contains a listing of the major conservatisms in the HI-STORM 100 thermal model, along with an estimate of the effect (increase) of each on the computed peak cladding temperature.

Table 4.B.1

Conservatism in the HI-STORM 100 Thermal Model

MODELING ELEMENT	CONSERVATISM [°F]
Long Term Ambient Temperature	2 to 30
Hypothetical Cylinder Construct	~5
Axial Heat Dissipation Restriction	30
MPC Downcomer Heat Dissipation Restriction	50
MPC External Heat Dissipation Under-prediction	50
Miscellaneous Conservatisms	15 to 50

4.B.9 REFERENCES

- [4.B.1] “Topical Report on the HI-STAR/HI-STORM Thermal Model and its Benchmarking with Full-Size Cask Test Data”, Holtec Report HI-992252, Rev. 1.

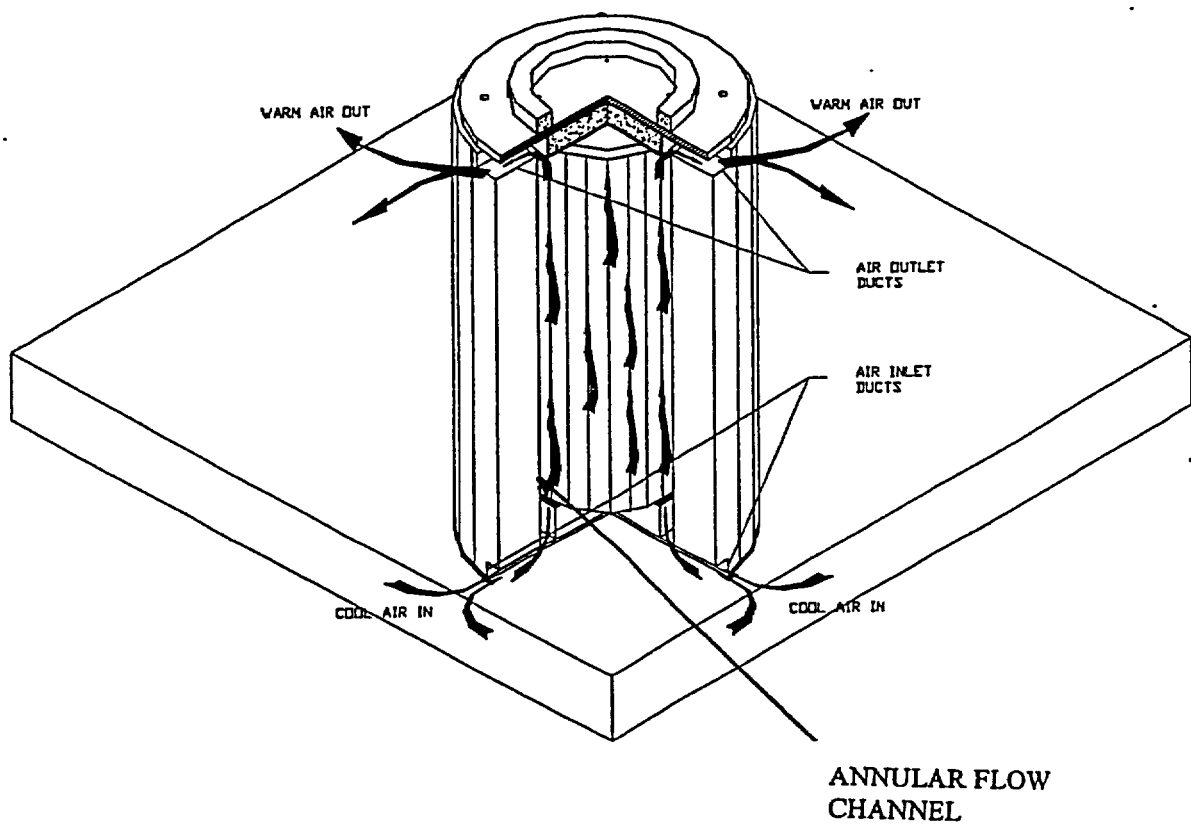


FIGURE 4.B.1: CUTAWAY VIEW OF A HI-STORM OVERPACK
STANDING ON AN ISFSI PAD

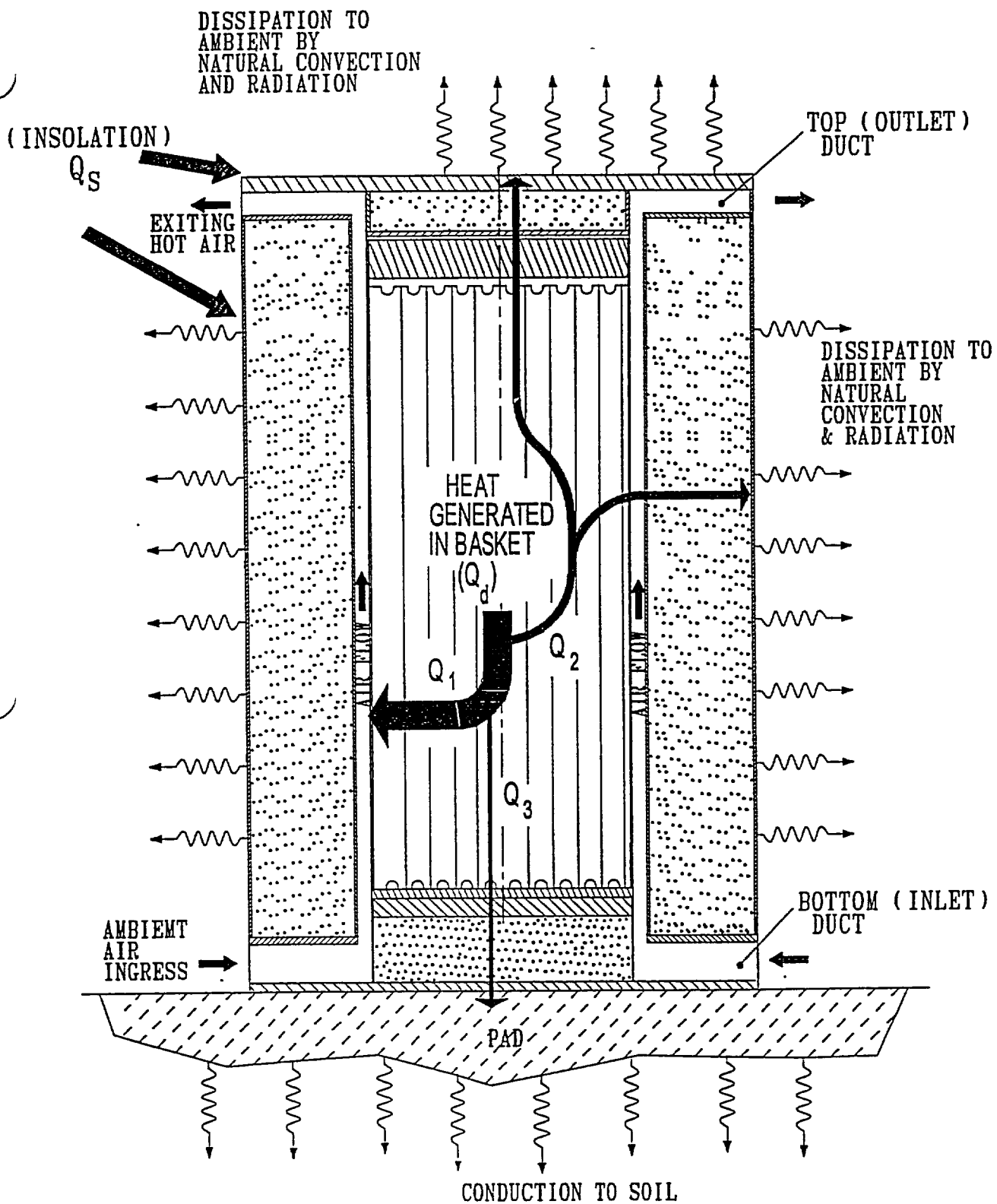


FIGURE 4.B.2: DEPICTION OF THE HI-STORM VENTILATED CASK HEAT DISSIPATION ELEMENTS

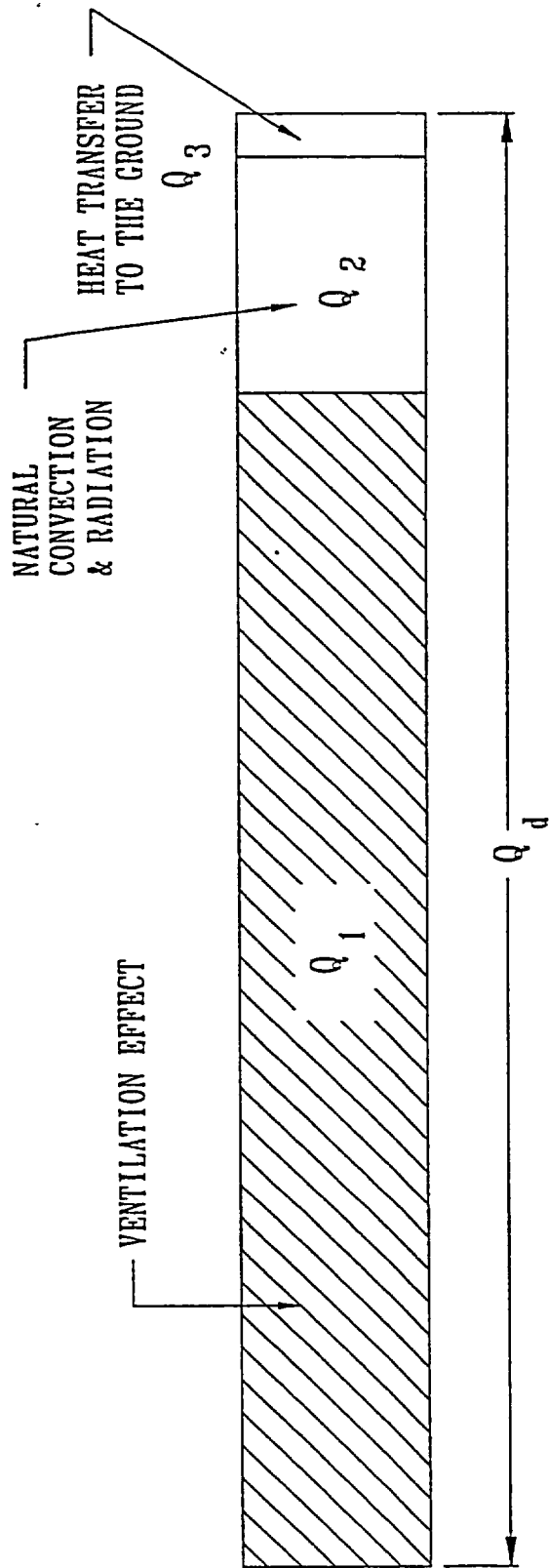


FIGURE 4.B.3: RELATIVE SIGNIFICANCE OF HEAT DISSIPATION ELEMENTS IN THE HI-STORM 100

LEGEND:  IMPERVIOUS BOUNDARY

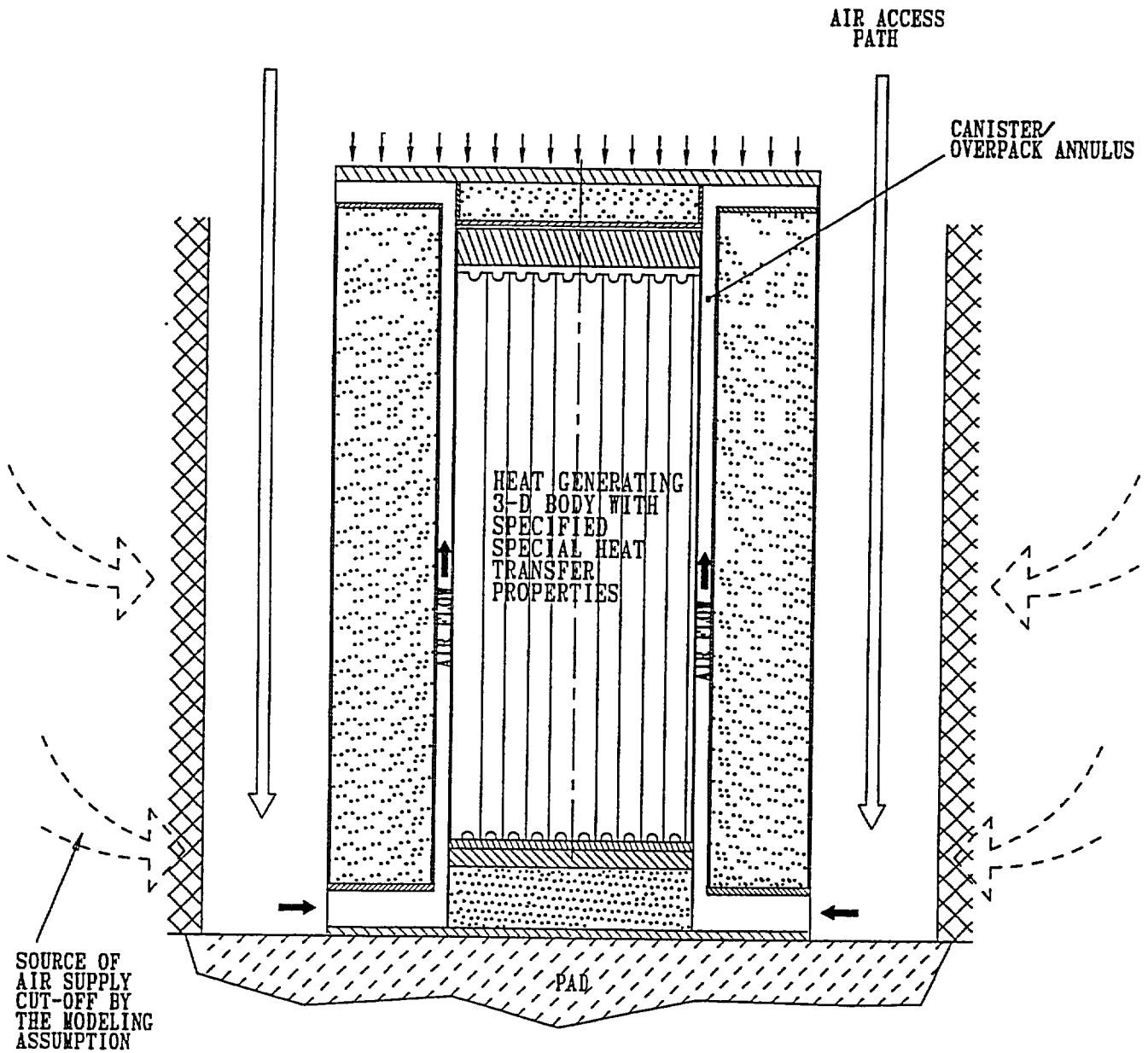


FIGURE 4.B.4: AIR ACCESS RESTRICTIONS IN THE HI-STORM THERMAL MODEL

REVISION 1

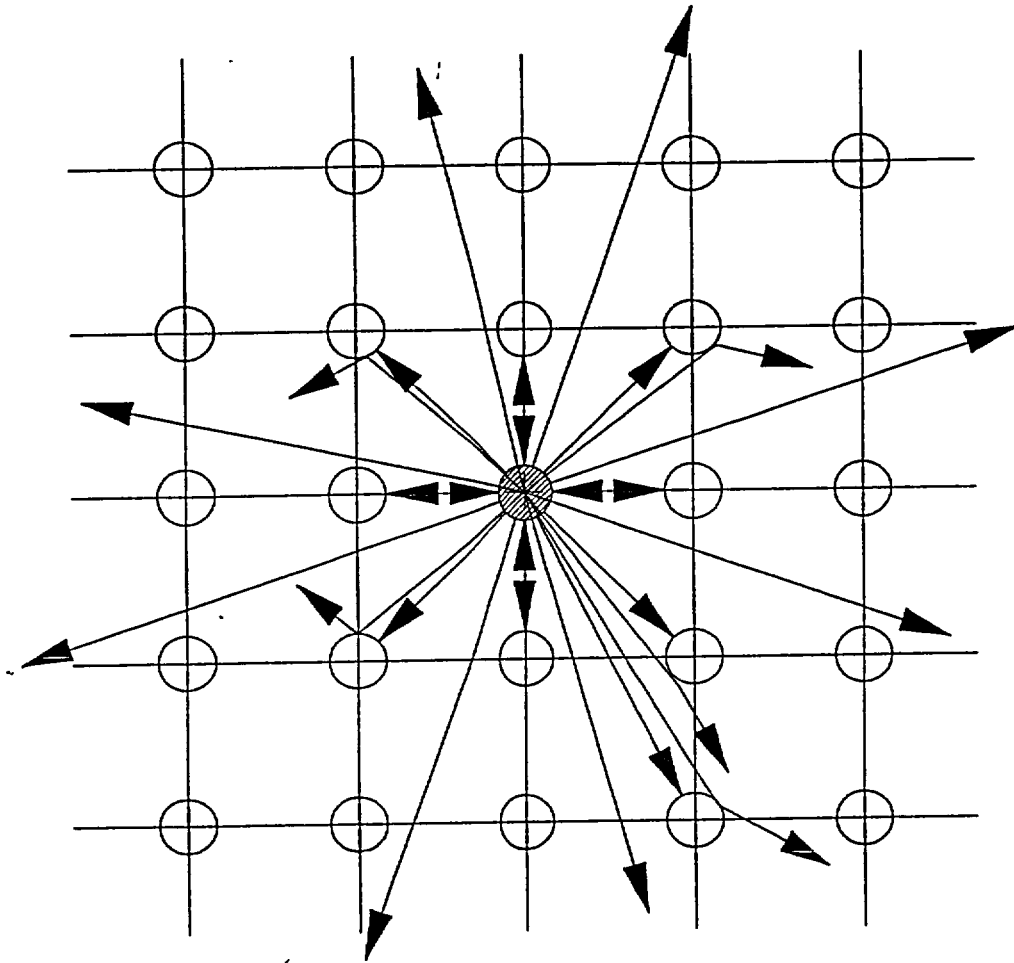


FIGURE 4.B.5: IN-PLANE RADIATIVE COOLING OF A HI-STORM CASK IN AN ARRAY

REVISION 1

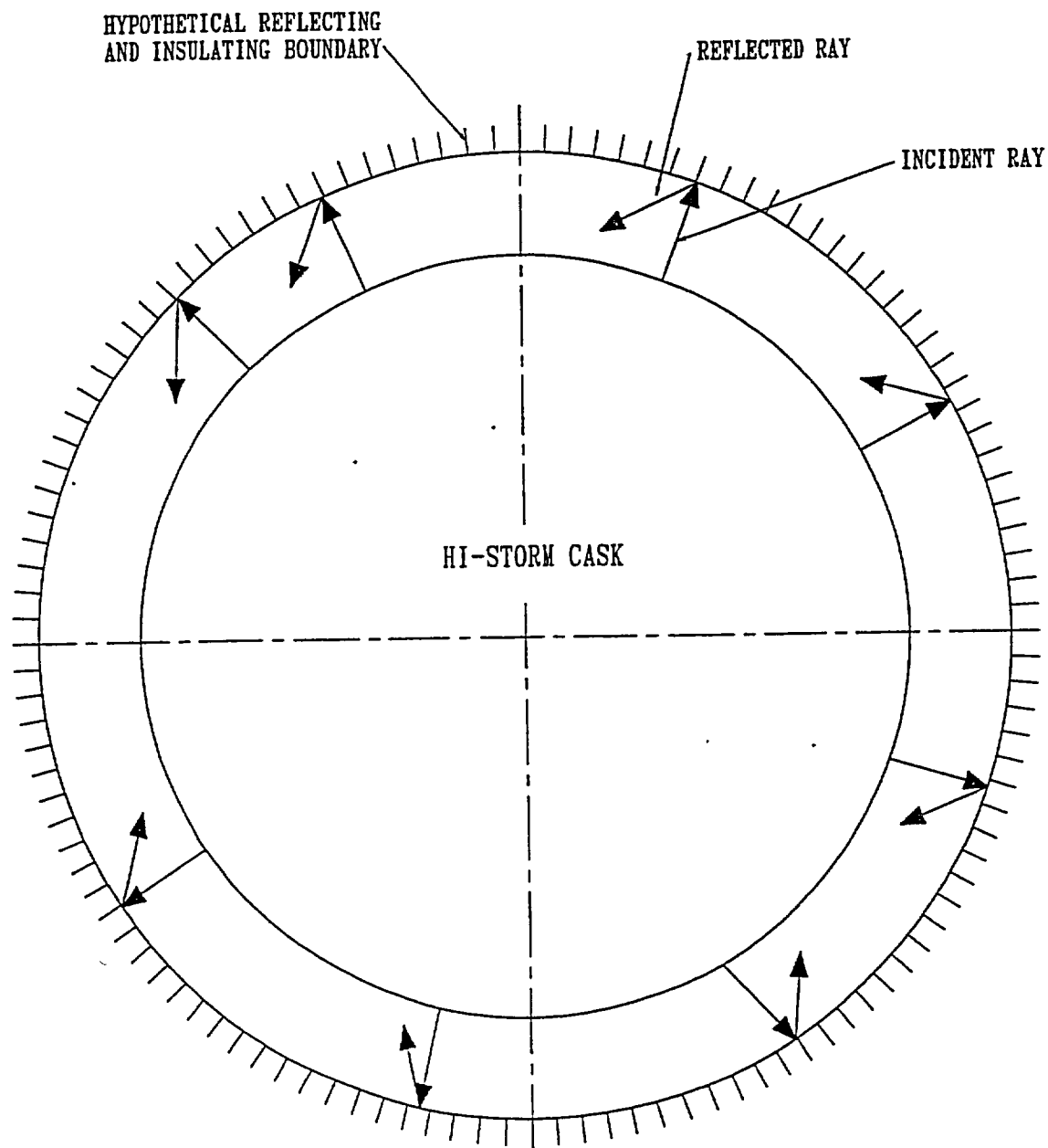


FIGURE 4.B.6: IN-PLANE RADIATIVE BLOCKING OF A HI-STORM CASK BY HYPOTHETICAL REFLECTING BOUNDARY

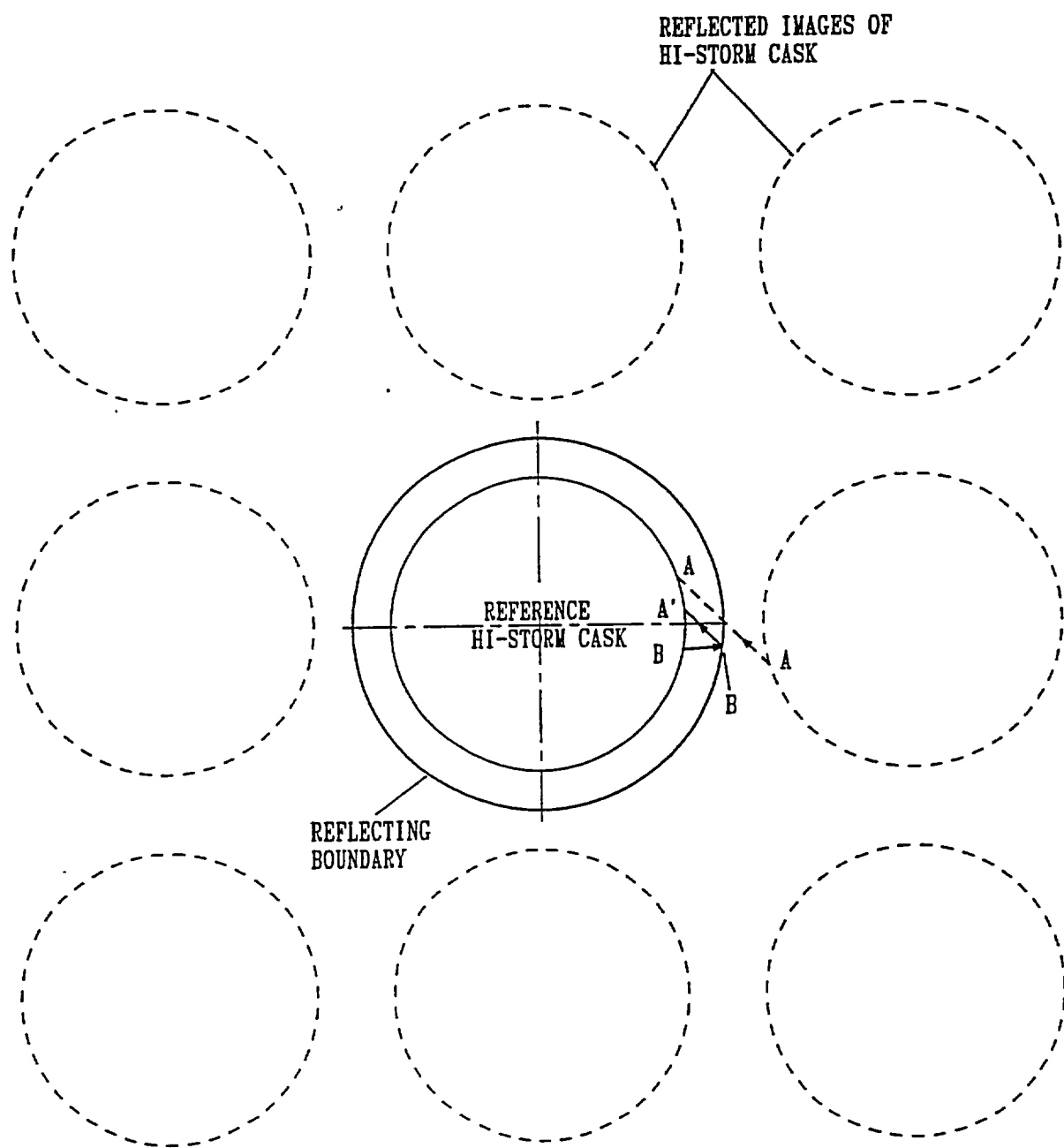


FIGURE 4.B.7: RADIATIVE HEATING OF REFERENCE HI-STORM CASK BY SURROUNDING CASKS

REVISION 1

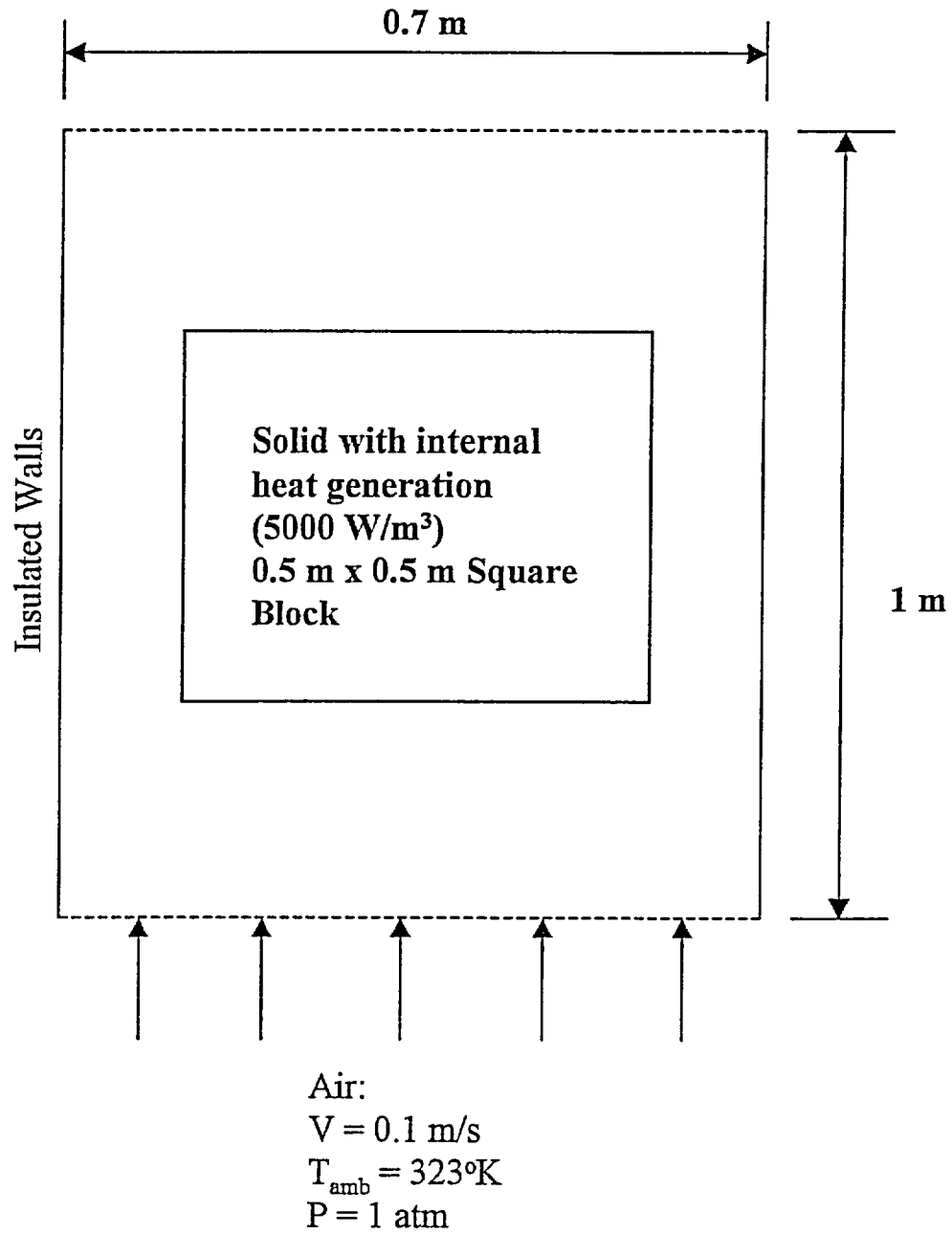


FIGURE 4.B.8: A CLASSICAL THERMAL SCENARIO: AIR COOLING OF A HEATED SQUARE BLOCK